energy&fuels

pubs.acs.org/EF Review

Inherent Metal Elements in Biomass Pyrolysis: A Review

Paola Giudicianni,*[,‖] Valentina Gargiulo,[‖] Corinna Maria Grottola, Michela Alfè, Ana Isabel Ferreiro, Miguel Abreu Almeida Mendes, Massimo Fagnano, and Raffaele Ragucci

Cite This: *Energy Fuels* 2021, 35, 5407−5478 Read Online

ACCESS | Metrics & More | Article Recommendations

ABSTRACT: One of the main drawbacks of using biomass as pyrolysis feedstock consists of the huge variability of the different biomass resources which undermines the viability of downstream processes. Inherent inorganic elements greatly contribute to enhance the compositional variability issues due to their catalytic effect (especially alkali and alkaline earth metals (AAEMs)) and the technical problems arising due to their presence. Due to the different pretreatments adopted in the experimental investigations as well as the different reactor configurations and experimental conditions, some mechanisms involving interactions between these elements and the biomass organic fraction during pyrolysis are still debated. This is the reason why predicting the results of these interactions by adapting the existing kinetic models of pyrolysis is still challenging. In this work, the most prominent experimental works of the last 10 years dealing with the catalytic effects of biomass inherent metals on the pyrolysis process are reviewed. Reaction pathways, products distributions and characteristics, and impacts on the products utilization are discussed with a focus on AAEMs and on potential toxic metallic elements in hyperaccumulator plants. The literature findings are discussed in relation to the applied laboratory procedures controlling the concentration of inherent inorganic elements, their capability of preserving the chemical integrity of the main organic components, and the ability of resembling the inherent inorganic elements in the raw biomass. The goal is to reveal possible experimental inconsistencies and to provide a clear scheme of the reaction pathways altered by the presence of inherent inorganics. This analysis paves the way for the examination of the proposed modifications of the existing models aiming at capturing the effect of inorganics on pyrolysis kinetics. Finally, the most relevant shortcomings and bottlenecks in existing experimental and modeling approaches are analyzed and directions for further studies are suggested.

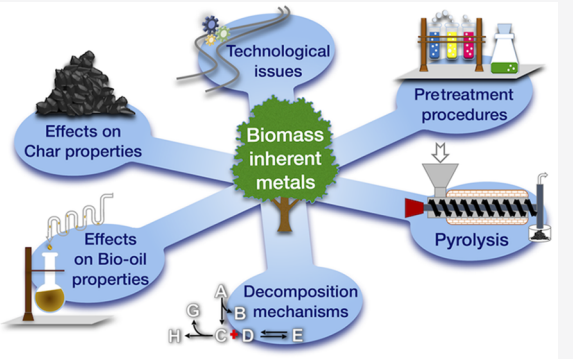

1. INTRODUCTION

Pyrolysis consists of a complex network of reactions occurring when biomass is heated in the absence of molecular oxygen. Pyrolysis products can be grouped into three categories, condensable vapors (also known as bio-oil or pyrolysis liquid), permanent gases, and a carbon-rich solid residue (also known as charcoal or char) in the following referred as the condensable fraction, gas and char, respectively. In the text, the term bio-oil is used to refer to the condensable fraction obtained under the fast pyrolysis conditions defined in Section 2.

Significant attention was given to the condensable fraction, more specifically to bio-oil and char. The condensable fraction could have in the near future a strategic importance as a substitute for fossil fuels in stationary applications,[1] as a precursor of transport biofuels, and as a source of chemicals.[2] Likewise, char has a huge potential for diverse applications such as fuel for power generation, fertilizers, an adsorbent matrix for environmental applications or process gas cleaning, a reducing agent in blast furnaces, catalysts, raw materials for supercapacitors, and fillers in composites.[3] Thus, there is every reason for biobased products from pyrolysis to contribute to carbon footprint reductions in the energy and transportation fuel production sectors and in the fossil-based materials market.

However, biomass is often criticized for indirect land use change (ILUC). In this context, different sources of residual biomass (such as maintenance operations of city and forest greenery, residues from agricultural and industrial sectors) as well as biomass from marginal soils (such as contaminated soils) may mitigate ILUC issues. This approach is also consistent with the growing trend toward circular economic models in which the main target is to create production chains that promote the valorization of waste and byproducts from production processes.

Among the lignocellulosic residues, a wide array of materials can be considered as feedstock for the pyrolysis process, such as wood, agricultural crops, grass, fruit and cereals husks, and fruit

Received: November 30, 2020
Revised: February 23, 2021
Published: March 18, 2021

https://doi.org/10.1021/acs.energyfuels.0c04046
Energy Fuels 2021, 35, 5407−5478

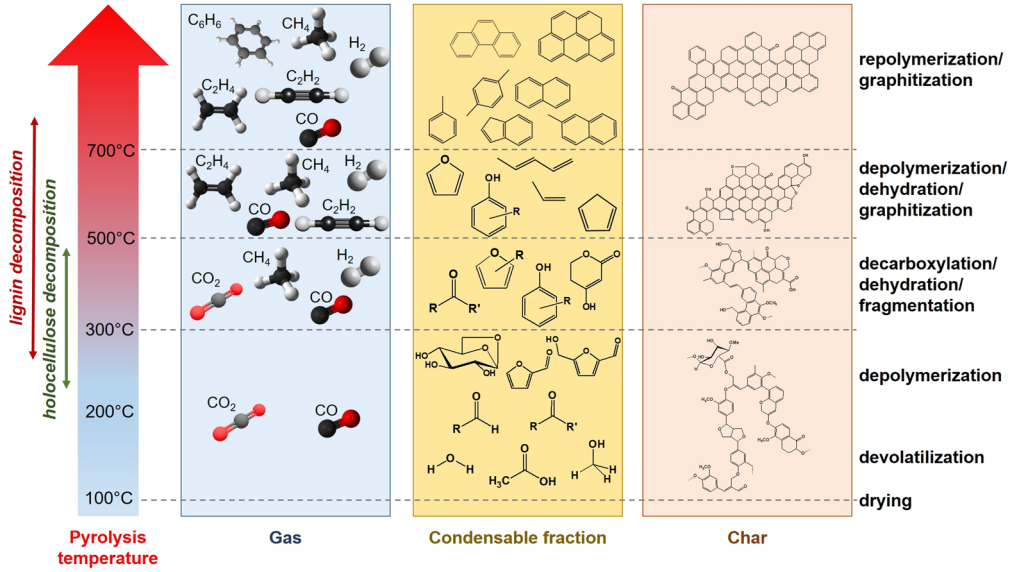

Figure 1. Schematic representation of the evolution of the pyrolysis products as the severity of heat treatment increases.

shell or pits. One of the most relevant concerns in using these residues is the variability of their chemical−physical characteristics, which hinders the possibility of producing a fuel or a material with reliable properties. Both inorganic and organic phases in the biomass exhibit a relevant variation in composition[4−6] so that it is hard to understand to which extent the pyrolysis products properties are affected by specific operating parameters or feedstock characteristics. To address these issues, basic studies of the mechanisms involved in pyrolysis of single biomass organic components and mixtures of them were conducted,[7] and numerical predictive models were elaborated adopting different approaches.[8]

The role of inherent (or intrinsic) inorganic elements[4] received great attention since they showed a catalytic activity in promoting some decomposition pathways.[9] Among the inorganic elements, alkali and alkaline earth metals (AAEMs) were the most studied given their abundance in the lignocellulosic biomass.[5] Their presence affects significantly the chemical composition and the physical properties of the pyrolysis products, sometimes compromising their further utilization[1,10] or upgrading.[11] There are specific cases in which the presence of other inorganic elements may also play a role. This is the case, for example, of some agricultural residues such as cereal straw and rice husks rich in Si[12] or hyperaccumulator plants grown on contaminated soils enriched with heavy metals (HMs). HMs, which are usually neglected due to their overall low level of concentration, exhibited a clear role in catalytic upgrading of biomass pyrolysis assisted by zeolite-based catalysts[13] but also raised environmental issues due to their transfer to the condensable fraction or their retention in the char.[14,15]

The analyses of the literature showed that different experimental procedures were used for studying the role of inherent inorganic elements in pyrolysis, thus hampering the correct comprehension of their catalytic activity and making challenging the comparison among the available data and the use of these data for validating the predictive numerical models. It is irrefutable that the use of experimental data to build robust numerical models allows achieving high effectiveness in optimizing the operating conditions of the pyrolysis process and accuracy in testing its limits.

The aim of this review is to summarize the recent literature on the effect of inherent inorganic elements on biomass pyrolysis, with a focus on AAEMs and some trace metals which represent the major source of pollution in contaminated soils (Pb, Cd, Cu, and Zn).

Section 2 provides an overview of the main transformations occurring in the biomass during pyrolysis. The main characteristics of the pyrolysis products, namely, the condensable fraction, char, and gas, are presented. Section 3 describes the typical composition of lignocellulosic biomass with a focus on the inorganic elements content and distribution among the different lignocellulosic biomass categories. Section 4 reviews the laboratory procedures for controlling AAEMs elements concentration and highlights their effectiveness, the capability of preserving the chemical integrity of the main organic components, and the ability of resembling the inherent inorganic elements in the raw biomass. Section 5 discusses the recent experimental studies dealing with the catalytic effect of AAEMs and the most abundant HMs on the pyrolysis process, in terms of reaction pathways and products composition. Section 6 is devoted to the description of the technical problems encountered during pyrolysis and product use and the most studied pretreatments able to reduce ash problems in biomass utilization. Some considerations related to the economics of specific pretreatments were also provided. Section 7 reviews the most widely applied modeling approaches for catching the effects of inherent metals on pyrolysis kinetics. Finally, the most relevant shortcomings are highlighted in Section 8 in order to prepare a systematic framework for further developments of this research area.

2. BIOMASS PYROLYSIS: AN OVERVIEW

During pyrolysis, as temperature increases, primary biomass degradation causes the formation of condensable volatiles, while the formation of gas (mainly CO, CO_2, and CH_4) is limited; the condensable fraction yield increases with temperature up to about 500 °C. At this temperature, most of the volatile species have been released and may undergo secondary degradation

https://doi.org/10.1021/acs.energyfuels.0c04046
Energy Fuels 2021, 35, 5407−5478

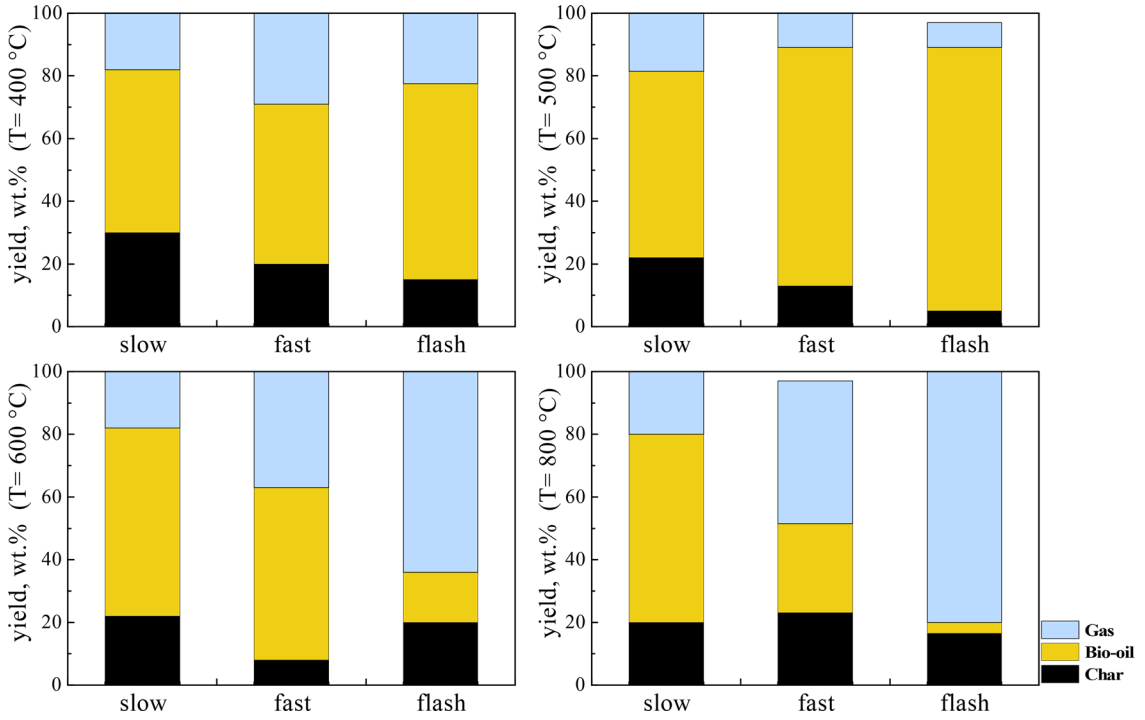

Figure 2. Pine wood pyrolysis products distribution as a function of temperature and heating rate. The experimental data refer to slow pyrolysis at T = 400, 600, and 800 °C,[32] fast pyrolysis at 400 and 600 °C,[33] flash pyrolysis at 400 °C,[34] slow pyrolysis at T = 500 °C,[35] fast and flash pyrolysis at T = 500 °C,[36] flash pyrolysis at 600 and 800 °C,[37] and fast pyrolysis at 800 °C.[38]

reactions that produce gas (mostly CO, CO_2, CH_4, and H_2) and low molecular weight (LMW) condensable species. Under conditions where the secondary reactions are relevant (prolonged vapors residence time at high temperature), the condensable fraction yield reaches a maximum, while the gas yield increases significantly. In the meantime, the solid residue, whose structure and chemistry have been greatly altered by the thermal treatment, evolves toward a porous carbonaceous structure with a reduced oxygen content (primary char). The vapors still entrapped in the porous char matrix, depending on the temperature and the residence time, may undergo polymerization reactions producing a solid product called secondary char whose structure and chemical composition is much more similar to that of carbon coke than that of primary char.[16] Figure 1 represents qualitatively the evolution of the pyrolysis products as the severity of heat treatment increases.

At a low heating rate, the char yield from woody biomass, typically, decreases from about 40 to 20 wt % as temperature increases from 400 to 700 °C, whereas the decay curve is shifted to higher values for biomass characterized by a high ash content such as herbaceous biomass and agricultural residues, sludges,[17] and macroalgae.[18] Microalgae are targeted as a source of lipids for algal oil including the production of biofuels;[19] therefore, their use in pyrolysis is less attractive.

At a high heating rate, the char yield decreases in favor of the production of gas and the condensable fraction. For temperatures lower than 500 °C, high heating rates correspond, on average, to higher temperatures at which primary decomposition occurs. In these conditions, devolatilization is promoted at the expense of char-forming reactions.[20] If a high heating rate is applied at temperatures exceeding 500 °C, the activities of the secondary reactions are enhanced, thus promoting gas production and even secondary char formation if the temperature is sufficiently high (about 700 °C[21]). Two opposing driving forces concur in determining the formation of secondary char in these conditions: (1) Higher average temperatures inside the particles enhance the activity of the repolymerization reactions promoting the production of secondary char. (2) Conversely, the disruptive devolatilization induced by the higher heating rate creates a more open char structure that favors an easier escape of volatiles and reduces the extent of reactions forming secondary char given the reduced residence time of the volatiles inside the char pores.[22]

Pressure indirectly affects the progress of secondary reactions by changing the vapors residence time. The short vapor residence time induced by subatmospheric pressure conditions is the basic idea behind the development of the vacuum pyrolysis experimental facility at Université Laval in Québec, Canada.[23] Limited data are presented in the literature on the effect of pressure on char yield highlighting the concomitant effect of pressure and the carrier gas flow rate on the formation of secondary char.[24−29]

Optimal ranges of temperature, heating rate, and gas residence time have been defined for the maximization of both char and condensable fraction yields, thus leading to the identification of slow/conventional pyrolysis as the appropriate process for char production and fast pyrolysis as the most suitable process for the maximization of bio-oil. With a certain degree of approximation, it is possible to indicate the characteristics of these processes based on the operating temperature, heating rate, and residence time of the vapors and solids in the reaction chamber:[30,31]

- Slow pyrolysis is characterized by low heating rates (~0.1−1 °C/s) and a solid residence time variable from a few minutes to a few hours.
- Conventional pyrolysis is characterized by moderate heating rates (up to 200−300 °C/min), reaction

https://doi.org/10.1021/acs.energyfuels.0c04046
Energy Fuels 2021, 35, 5407−5478

Table 1. Fast Pyrolysis Plants with Capacity Higher than 10 kg/h in 2020[46]

Owner/Location	TRL	Feedstock	Type of reactor	ref
CanmetEERGY/CA	1−3	wood residues	fluidized bed, ablative reactor	47
Ensyn/CA	6−7, 8	forest residues	circulating transported bed	48
Fraunhofer UMSICHT/DE	1−3	sewage sludge, waste residues, wood residues, industrial biomass residues, biowaste fractions, other agricultural residues, animal excrements	screw reactor	49
Iowa State University/US	1−3	corn stover and woody waste	fluidized bed	50
Universidad de Concepciòn/CL	1−3	n.a.	fluidized bed	51
University of Idaho/US	1−3	waste streams	screw reactor	52
National Renewable Energy Laboratory/US	1−3	n.a.	entrained flow reactor	53
Alternative energy Solutions Ltd./NZ	4−5	n.a.	n.a.	46
BTG/NL	4−5	n.a.	rotating cone	54
G4 Insight/US	4−5	forestry residues	n.a.	46
Green Fuel Nordic/FI	4−5	lignocellulosic biomass	n.a.	46
Mississipi State University/US	4−5	n.a.	screw reactor	55
Renewable Oil International LLC/US	4−5	n.a.	screw reactor	48
RISE ETC/SE	4−5	lignocellulosic biomass	ablative cyclone reactor	56
RTI International/US	4−5	n.a.	bubbling fluidized bed	48
University of Science and Technology of China/CN	4−5	n.a.	n.a.	46
USDA-ARS-ERRC/US	4−5	lignocellulosic biomass	fluidized bed	55
Karlsruhe Institute of Technology/DE	4−5, 6−7	agricultural residues	twin screw reactor	48
BTG-Btl/NL	4−5, 8	agricultural residues, sludge, animal excrements	rotating cone	54
Valmet/FI	6−7	forest residues	circulating fluidized bed	48
Versa Renewables LCC/US	6−7	lignocellulosic biomass	n.a.	
Fortum/FI	6−7, 8	forest residues	circulating fluidized bed	48
Ensyn//CA	6−7, 8	forest residues	circulating transported bed	48
Red Arrow/US	8	n.a.	circulating transported bed, circulating fluidized bed	48
Twence/NL	9	forest residues	rotating cone	57

temperatures from 400 to 550 °C, and a solid residence time of several minutes (up to 10 min).

- Fast pyrolysis is characterized by high heating rates (∼100−1000 °C/s), a very short residence time of hot vapors (∼1 s), and temperatures between 400 and 550 °C.
- Flash pyrolysis is characterized by very high heating rates (>1000 °C/s) and high reaction temperatures (900−1300 °C).

As an example, in Figure 2, the yields of products obtained from pine wood pyrolysis at different temperatures under slow, fast, and flash pyrolysis conditions are reported.

2.1. Condensable Fraction. The chemistry of the condensable fraction is very complex, and it is the result of the composite nature of the biomass and the severity (time−temperature relationship) of the thermal treatment to which the biomass is exposed. The number of species identified is in the order of 300 and can be grouped in primary, secondary, and tertiary products[39] whose relative contents can be manipulated by changing the thermal conditions of the process as well as their residence time in the reaction environment. As represented in Figure 1, in the optimal conditions for its yield maximization, the condensable fraction is mainly made up of acids, alcohols, aldehydes, esters, ketones, phenols, guaiacols, syringols, sugars, furans, alkenes, and aromatics.[39] A variable amount of water may be produced during pyrolysis even though multiple condensation stages (fractionated condensation) allow controlling the water content in the condensable fraction.[1] The cracking severity lowers the molecular weight distribution of the components in the resulting condensable fraction and produces more gas. At very high temperatures, dehydrogenation/aromatization reactions can eventually lead to larger polynuclear aromatic hydrocarbons that may condense into polycyclic aromatic hydrocarbons (PAH).[39]

Lehto et al.[1] reported the typical ranges of the main physical and chemical properties of the bio-oil: it has an acidic nature and is characterized by high values of density, viscosity, and surface tension, all physical properties that depend on the water content. The high oxygen content makes the bio-oil immiscible with fossil-based oils and reduces its calorific value by less than half compared to that of mineral oils. Moreover, as a result of its heterogeneous composition, the bio-oil is not as stable as conventional petroleum fuels; in particular, its components can react to each other to form larger water-insoluble molecules.[1,40−42] Finally, a non-negligible fraction of suspended solids is also detected in the bio-oils causing a significant impact on the storage phases and on bio-oil utilization.[43−45]

Due to these peculiar characteristics and the scarcity of pyrolysis plants operating on an industrial scale, bio-oils have not yet found a wide diffusion on the energy market. Few companies have today initiatives in pursuing commercial-scale bio-oil production plants. Table 1 summarizes some of the currently operational fast pyrolysis reactors with capacities higher than 10 kg/h.[46] Only a few of them are at a precommercial/commercial technology readiness level (TRL). They differ for the method employed for heat transfer, but basically, two types of rectors are adopted to achieve fast heating rates, namely, fluidized bed

https://doi.org/10.1021/acs.energyfuels.0c04046
Energy Fuels 2021, 35, 5407−5478

reactors and screw reactors. The former resulted in a lower performance with high ash herbaceous biomass (e.g., corn stover) due to bed fouling, which prevented steady reactor operation.

Over the years, the selective production of platform chemicals such as hydrocarbons, phenols, anhydrosugars, other oxygenates, and recently, nitrogen-containing compounds through biomass catalytic fast pyrolysis (CFP) has been extensively studied to overcome the obstacles that prevented the utilization of bio-oils as fuel in internal combustion engines and to promote the takeoff of a fast pyrolysis-based biorefinery. High costs and technical problems related to catalysts make the chemical routes less feasible and affordable.

Process design, from feedstock adaptation to reactor configuration, is another factor to be considered due to the need of reducing heat and mass transfer resistance to guarantee high products yields. Energy intensive pretreatments such as drying, deashing, and grinding[58] and technological barriers to the scale-up of the most diffused reactor configurations (fluidized beds, rotating cone, microwave heating reactors) burden the economics of the whole CFP-based biorefinery.

2.2. Char. Char can be considered as a multiphase system composed of a carbon network and a mineral phase. Low temperature char can contain condensed vapors occluding partly the porosity of the solid matrix.[59] The addition of organic vegetable matter to poorly productive soils in order to improve their physical−chemical characteristics was a well-known practice in ancient times.[60] Nowadays, the deep knowledge of the chemical and physical characteristics of char is leading to the exploration of many routes for valorizing the char potential for diverse applications.[3]

The relative contents of organic and mineral phases and their composition varies with the process operating variables, namely, temperature, heating rate, pressure, and gas and solid residence times. A detailed description of the effects of these variables on the char characteristics is out of the scope of this review and is available in ref 10. Pyrolysis temperature affects the chemical and physical characteristics of the char more than the other variables. The C and O contents of biomass typically range between 50 and 40 wt % on a dry ash free basis, whereas the H content varies between 5 and 7 wt %. The most significant changes during char production occur in the temperature range of 200−400 °C, where C and O contents are in the range of 70−80 and 10−30 wt %, respectively.[10] The char produced at temperatures lower than 300 °C is the result of dehydration and depolymerization reactions of hemicellulose and the cleavage of the glycosidic linkages between the sugars of cellulose; therefore, it is mainly composed of oligosaccharides in an amorphous phase with a high concentration of free radicals as result of the competition between the mechanism of devolatilization and the reactions of dehydration. The removal of acid groups as temperature increases determines a strong increase of pH from mild acid to basic values in the temperature range between 200 and 400 °C. Hydroxyl groups are at first concentrated and then released determining the nonmonotonous trend of the cation exchange capacity (CEC).[61] Carboxyl, carbonyl, and methoxyl groups decrease up to the complete falling off at temperatures in the range of 600 °C−700 °C. Above 600 °C, typical pH values are in the range of 8−10.[10] At temperatures higher than about 700 °C, charring reactions occur, determining the growth of graphene layers and the removal of heteroatoms, thus increasing the char aromaticity. At these temperatures, chars may reach C and O contents of higher than 95% and lower than 5%, respectively, whereas the H content decreases to less than 2% or even below 1% for very high treatment temperatures.[10] Data collected in ref 10 show an unclear correlation between the pyrolysis temperature and the N content of the char.

The mineral phase is very stable, except for some inorganic elements in volatile compounds (Section 5.3). As a consequence of this thermal stability, the ash yield is almost independent of the temperature, while its content increases almost linearly due to the devolatilization of the organic fraction.[62] The increase of the pH of the char toward alkaline values with temperature is mainly due to the concentration of inorganic elements in the alkaline form.

The textural characteristics of char evolve as the pyrolysis temperature increases changing the relative weight of the micro-, meso-, and macroporosity,[63] including pores with diameters smaller than 2 nm, between 2 and 50 nm, and greater than 50 nm, respectively. Devolatilization, repolymerization of entrapped condensable species, graphitization, and ash sintering phenomena occur, thus resulting in a nonmonotonous trend of the char specific surface area with temperature. A maximum in the range of of 300−500 m^2/g at temperatures varying between 500 and 700 °C was observed depending on the original biomass type and heating rate.[10]

It is worth noting that given the different chemical characteristics of the biomass types, in order to produce high quality chars with reliable properties, the composition of the feedstock must be properly controlled. Nevertheless, even though the correlations between the process operating variables and the char yield could be predicted with a good level of accuracy,[64] the prediction of the effects of the same variables and, above all, of the intrinsic properties of the feedstock on the morphological characteristics is still a critical issue.

2.3. Gas. The pyrolysis gas is composed mainly of CO and CO_2, while H_2 and CH_4 are present in limited amounts. Traces of light hydrocarbons, typically C_2 and C_3, can be also detected. In the literature, the trends of the gaseous species yields, at least the most abundant ones such as CO, CO_2, and CH_4, were studied as a function of process temperature and heating rate. In addition, when the complete gas composition was provided, the heating value of the gas was also reported. The review papers by Di Blasi[21] and Neves et al.[65] reported a wide collection of this type of data.

For temperatures below about 500 °C, primary decomposition reactions produced mostly CO and CO_2, with yields weakly increasing as a function of temperature. Overall, CO and CO_2 yields at about 500 °C were in the ranges of 2−15 and 5−15 wt %,[65] respectively. Narrower ranges were reported in ref 21, namely, 2−7 and 3−9 wt % for CO and CO_2, respectively. At intermediate temperatures, around 400 °C there was a slight production of CH_4 and H_2; however, their production became relevant at temperatures higher than 500 °C and was concomitant with a rapid increase in CO yield ranging between 20 and 40 wt % at around 800 °C, while CO_2 yield only slightly increased to about 20 wt % at 800 °C.[65] At the same time, higher yields were also observed for the other minor species, such as CH_4 and H_2 (8 and 1 wt %, respectively, at T = 800 °C[65]). The trends of the gaseous species yields suggested that both CO and CO_2 were produced by primary degradation of the biomass; however, CO, as well as CH_4, H_2, and the other light hydrocarbons were formed from the secondary degradation of volatiles formed during the primary degradation. The low heating value was found to have a linear dependence on the pyrolysis temperature, increasing from 1 to about 18 MJ/kg as

https://doi.org/10.1021/acs.energyfuels.0c04046
Energy Fuels 2021, 35, 5407−5478

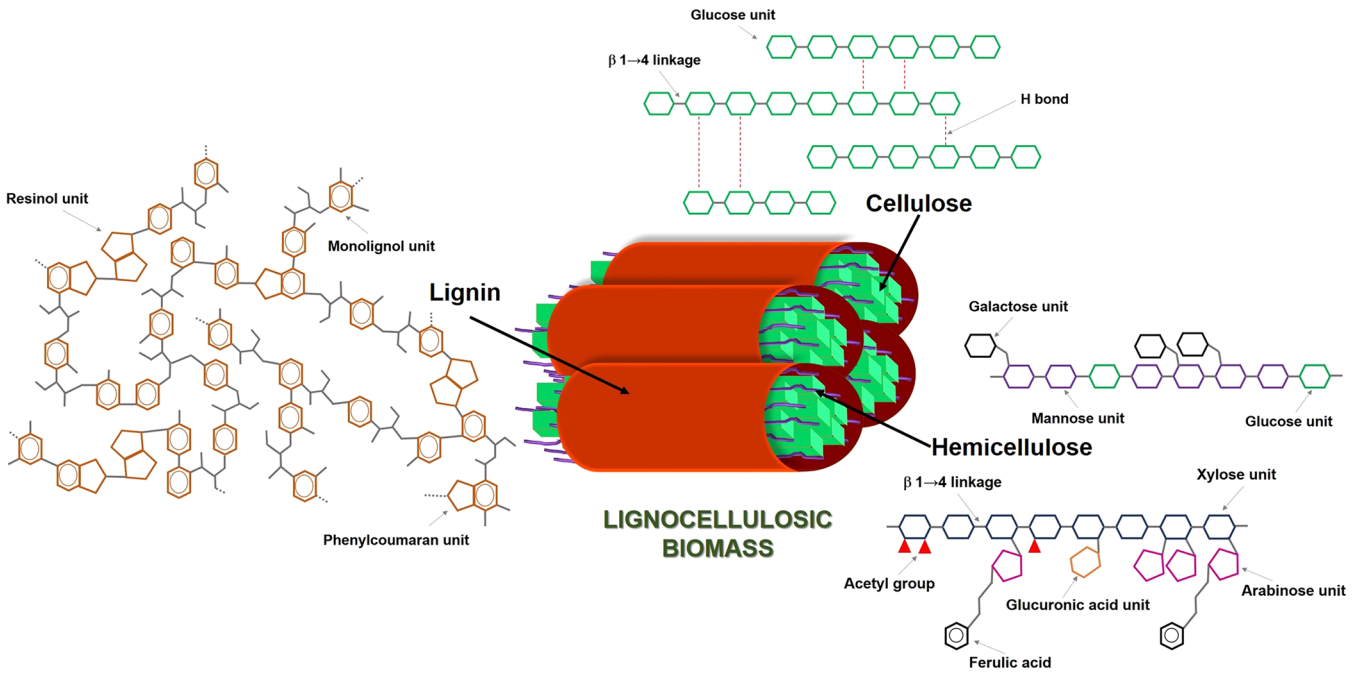

Figure 3. Schematic representation of main components of cell wall of lignocellulosic biomass.

the temperature increased from 300 to 900 °C.[65] At low temperatures, the heating rate did not induce significant changes in gas species yields, whereas at higher temperatures, if associated with sufficiently long gas residence times, it induced higher yields of secondary species.[21]

Few data concerning the influence of pressure on the composition of the gas phase resulting from cellulose pyrolysis were reported by Mok and Antal[24] in the pressure range of 1−6 atm. These data have purely qualitative value since the mass balance on carbon closes at 60%. An increase in pressure corresponded to a reduction in gas and carbon yields; in particular, the yield of CO_2 increased, while the yields of the other gas species decreased.

3. LIGNOCELLULOSIC FEEDSTOCK FOR PYROLYSIS

The feasibility of a pyrolysis-based biorefinery is strictly dependent on its capability of being flexible with respect to the biomass source. Depending on the geographical context and the territorial development, biomass species may have very different chemical and physical characteristics.

Many databases collecting peer-reviewed data reported elemental and proximate analyses of several biomasses.[4,66] The analysis of these databases shows a considerable variability in the contents of C, H, N, S, O, volatile matter, fixed carbon and ash, and ash composition. The variability is reduced if biomass species are grouped in families or subfamilies, and some common traits can be observed for woody and herbaceous families, the latter further divided into grasses, straws, and fruit husks/shells subfamilies.[4]

However, the elemental, proximate, and ash analyses provide only bulk properties that are not sufficient to describe adequately the impact of biomass heterogeneity on pyrolysis products quality and plant performance. A more reliable approach is to describe biomass in both engineer (proximate and ultimate analyses) and biologist (biochemical analysis) languages and to consider it as a composite made up of many components constituting the plant cell wall. Organic components and inorganic elements evolve differently during thermal treatment, and they can interact with each other producing a nonlinear combination of effects that determine the properties and yields of the pyrolysis products.[67,68]

In this section, an overview of the main constituents of terrestrial lignocellulosic biomass, namely, woody and herbaceous biomass, is presented together with minor components that, although present in low amounts, can play a relevant role in determining pyrolysis products yields and properties. A detailed description of the biomass inherent inorganic elements and of the factors affecting their amount and speciation is also provided.

3.1. Organic Components. The main components of the lignocellulosic cell wall are cellulose, hemicellulose, and lignin, and they are schematized in Figure 3.

Cellulose is a linear macromolecular polysaccharide consisting of cellobiose units linked by β-1,4-glycosidic bonds to form long chains with a high degree of polymerization (DP) (average DP comprised between 9000 and 10,000[69]). Given its high DP, it is not soluble in water. Numerous hydrogen bonds due to the high content of hydroxyl groups confer to cellulose a strong crystalline structure. It is abundant in the secondary wall of the plant cells and less so in the primary cell wall. The degree of crystallinity varies, but on average, it is around 70% in wood.

Hemicelluloses are found in both primary and secondary cell walls and are composed of short branched polysaccharides chains (500−3000 sugar units) cross-linked to other cell wall constituents. Hemicelluloses have a heteropolymeric structure made up mainly by six-carbon sugars as mannose, galactose, glucose, and 4-O-methyl-D-glucuronic acid and the five-carbon sugars as xylose and arabinose. Most of the sugars within the hemicellulose backbone are linked through β-1,4-glycosidic bonds. In many cases, the hydroxyl groups in the ring structure are replaced by methoxyl and acetoxyl groups. Hemicelluloses, usually, are named according to the main sugar unit type, so they are divided into four general groups: xylans, mannans, xyloglucans, and mixed-linkage β-glucans.[70] Hemicellulose

https://doi.org/10.1021/acs.energyfuels.0c04046
Energy Fuels 2021, 35, 5407−5478

accounts for about one-third of total biomass dry weight, and it is present along with cellulose in almost all terrestrial plant cell walls. The hemicellulose distribution varies in softwoods and hardwood. Galacto-glucomannan and glucomannan prevail in softwood, while xylans are present in lower amounts. Hardwood and herbal plants hemicellulose consists mainly (more than 90%) of 4-O-methyl-D-glucurono-D-xylan units, whereas the (glucurono)-arabino-xylan unit is the dominant form in annual plants, like straw and grass.[70]

Lignin is a natural biopolymer making up to 10−25 wt % of plant biomass. It is a complex, dense, amorphous, secondary cell wall racemic heteropolymer embedding the cellulosic microfibrils, and it is responsible for the cell wall structural rigidity. Lignin is composed of p-hydroxyphenyl (H), guaiacyl (G), and syringyl (S) monomers (monolignols) produced from p-coumaryl, coniferyl, and sinapyl alcohols, respectively. The three hydroxycinnamyl alcohol monomers are characterized by a different degree of methoxylation increasing from 0 to 2 in the order of p-coumaryl, coniferyl, and sinapyl alcohols. In the lignin network, the different monomeric units are bonded together through C−O−C bonds (α or β-O-4 ether linkages) or C−C linkages (5−5′, β−5′, β−β, and β−1). The proportion of the three monolignols differs among different regions in the cell wall, among cell types, and among plant species. G units predominate in gymnosperm lignins, and G and S units predominate in angiosperms, while grass lignin is composed of H, G, and S units.[71]

Usually, cellulose, hemicellulose, and lignin account for more than 90% of the entire lignocellulosic biomass; however, other species should be considered such as pectin, extractives, and inorganics.

Pectin is a heteropolysaccharide mostly containing galacturonic acid intercalated with L-rhamnose units bearing side chains. H ions of the carboxylic functional group are replaced at different substitution degrees with methyl groups.

Extractives are organic biomass components accounting for 5%−30% of biomass dry weight, and they can be extracted with water and organic solvents. Indeed, they are typically classified as hydrophilic or hydrophobic depending on their solubility in polar or nonpolar solvents, respectively. Extractives compositions vary significantly species to species; in particular, there are variations according to the family, genera, and species and even to the biomass location, part, age, and to the season. Polyphenols are the most abundant hydrophilic extractives, whereas hydrophobic extractives (more abundant in softwoods) are mainly composed of terpenes and fatty acids.[72]

The relative content of the above-mentioned components depends not only on the type of biomass or plant organ but also on the specific constrains of the growing site and the harvesting time as revealed by the available databases reporting the components analyses of many examples of the same species.[5,66,73]

Cellulose content is higher in herbaceous and agricultural residues, woody stems, stalk, fibers, and lower in bark, leaves, woody twigs, and pits. Conversely, hemicellulose and lignin show the opposite trend, and they are typically more abundant in woody plants than in herbaceous and agricultural residues. Hemicellulose is predominant in hardwood and in annual plants, and lignin is predominant in softwood and perennial plants. Pit and shells contain high concentrations of lignin. A nontrivial trend was found for lignin concentration in stems and leaves; higher concentrations were found in leaves and young shoots of woody biomass than in stems, whereas the opposite trend was found for grasses.[74] Finally, extractives are more abundant in agricultural residues than in woody plants, especially hardwoods where extractives are concentrated in bark and leaves.

3.2. Inorganics in Lignocellulosic Biomasses. In addition to the organic fraction, biomass often contains variable levels of inorganic elements. Different areas of the scientific literature dealt with the classification and behavior of inorganic elements, in particular, in the field of botanical science, for the study of plant physiology, and in the field of chemical and engineering sciences, for the study of the behavior of inorganic elements in several biomass conversion processes. Since the interest in these elements has different motivations, their classification follows completely different approaches.

Kirkbey[75] provided an overview of the "essential mineral elements"[76] in higher plants defined as essential elements in completing the plant lifecycle, not replaceable by another element, and participating directly in plant metabolism. They are classified as macronutrients and micronutrients according to the concentration needed for plant's life. Besides C, H, and O forming the organic molecules, macronutrients comprise N, S, P, K, Ca, and Mg, whereas Fe, Mo, B, Cu, Mn, Zn, Ni, and Cl are considered micronutrients, and their concentration ranges from 0.1 to 200 mg/kg.[77] Macronutrients and micronutrients are grouped in four classes according to their biochemical behavior and physiological functions. N and S belong to the first group and are mainly involved (together with C, H, and O) in the formation of the organic building blocks of the plant (amino acids, proteins, enzymes, and nucleic acids). S is absorbed as sulfate by the plant roots and transported to the leaves where it is transformed and incorporated into the protein structure of the plant.[78] P, B, and Si, constituting the second group, are typically present in the form of esters and participate in energy transfer reactions. The third group comprises K, Na, Ca, Mg, Mn, and Cl which are mostly involved in establishing electrochemical potential. Finally, the fourth group is formed by Fe, Cu, Zn, and Mo which contribute in facilitating the electron transport. Actually, Co, Na, and Si, together with other inorganic elements, such as Al and Se, cannot be included in the category of the "essential mineral elements", but are considered only beneficial for plants since they are not required by all plants but can promote plant growth and may be essential for particular taxa.[79]

On the other hand, since lignocellulosic biomass was widely studied as a solid fuel, the thermo-chemical behavior of the inorganic elements was studied in the combustion system to limit slagging, bed agglomeration, fouling, and corrosion. The chemical form of the inorganic elements is decisive in understanding the phenomena occurring during ash formation under an oxidizing atmosphere, as well as under the reducing conditions typical of the pyrolysis process. Moreover, the chemical speciation is also responsible for the mobility of the inorganic elements in water and soil. Many inorganic characterization procedures and indices retrieved from coal ash know-how revealed to have poor reliability as indicators of the behavior of inorganic elements in ash formation.[80] In contrast, the approach proposed by Benson and Holm[81] for a low-grade coal based on sequential extractions proved to be very useful in identifying the chemical form of inorganic elements also in biomass. Four groups of inorganic elements were identified based on their solubility in different leaching solutions expressing the type of association of inorganic elements in the plant tissues: dissolved salts, organically bound matter, included mineral matter, and excluded mineral matter.[82] Dissolved salts are typically found as ions (K^+, Na^+, Ca^{2+}, Cl^-, HPO_4^{2-}, SO_4^{2-},

https://doi.org/10.1021/acs.energyfuels.0c04046
Energy Fuels 2021, 35, 5407−5478

Table 2. Inorganic Elements Content in Different Types of Biomass

	N (wt %)	S (wt %)	P (mg/kg)	K (mg/kg)	Ca (mg/kg)	Mg (mg/kg)	Na (mg/kg)	Al (mg/kg)	Fe (mg/kg)	Si (mg/kg)	ref
Woody biomass											
Ash tree	0.5681	0.1713	1566	7026	6801	184	3928	1232	285	n.a.	87
Drupe tree	0.0499	0.2	669	2007	4407	458	49	151	93	n.a.	88
Olive branches	1.7711	n.a.	1695	7436	5701	657	87	155	115	n.a.	88
Olive tree prunings	0.59	0.07	650	3000	11,000	850	72	1000	1300	36,000	89
Olive tree prunings	0.59	0.07	650	3000	11,000	850	72	1000	1300	36,000	66
Willow	0.5269	0.1341	1870	8057	12,820	321	3698	6646	987	n.a.	87
Willow	0.47	0.041	467	1610	4603	335	110	150	31	725	90
Willow	0.6	0.02	1215	3242	4961	667	n.a.	86	38	99	66
Pine	0.09	n.d.	n.a.	137	1241	213	23	n.a.	7.5	n.a.	91
Beech	0.09	n.d.	n.a.	813	1204	380	6	n.a.	22.9	n.a.	
Beech powder (<250 μm)	0.022	0.02	90	1150	3100	370	8	48	47	170	66
Beech chips	0.15	0.02	104	1331	2964	503	36	26	99	242	66
Birch	n.a.	n.a.	130	1000	1100	180	3	0.4	6	1	66
Spruce pellets	0.0900	n.d.	7	354	712	352	90	53	26	84	66
Spruce logging residues	n.a.	0.03	290	1500	10,100	450	54	230	670	2000	66
Spruce chips	0.08	0.01	52	352	924	124	21	64	44	256	66
Fir	0.27	n.d.	54	657	893	144	18	56	25	255	66
Red oak (sawdust)	0.03	0.01	18	444	241	78	32	49	64	303	66
Eucalyptus	0.37	0.05	348	2467	5231	488	n.a.	91	14	103	66
Eucalyptus	0.14	0.03	n.a.	1378	1328	n.a.	359	n.a.	n.a.	n.a.	66
Eucalyptus	n.a.	0.0956	1720	5709	14,250	212	11,140	1142	280	n.a.	87
Grape vines	1.070	0.08	4117	33,506	6738	30	234	87	72	555	66
Aspen	n.a.	0.01	320	1400	4200	490	17	10	30	n.a.	
Poplar	n.a.	0.1156	1150	3523	8642	276	2400	1040	302	n.a.	87
Poplar	0.23	0.05	788	1900	4122	852	9	210	n.a.	526	66
Poplar[a]	n.a.	0.0079	38	1597	2554	417	233	3	–	–	14
Herbaceous biomass											
Reed	n.a.	0.2	652	10,695	1014	125	87	106	114	n.a.	87
Corn stalks	n.d.	0.0564	2127	32	4686	5924	6463	1911	518	13400	12
Grass plant	1.2190	0.2	1193	6048	6055	1088	961	1724	587	–	88
Thistle	1.19	0.11	1100	9600	14,000	1900	4400	930	640	7700	89
Reed canary grass	1.39	0.115	1510	1685	2795	627	79	396	276	4062	90
Straw											
Bagasse	0.4	0.0060	284	2682	1518	6261	93	n.a.	125	17340	12
Rice straw	0.4	0.0221	752	5402	4772	6283	5106	n.a.	205	174,510	12
Wheat straw	0.1	0.0787	214	28,930	7666	4329	7861	2455	132	44,440	12
Wheat straw	1.3504	n.a.	831	11,870	14,110	1670	303	1482	1468	n.a.	88
Wheat straw[a]	n.a.	n.a.	305	10,435	1509	570	128	114	54	n.a.	14
Wheat straw[a]	n.a.	0.0409	372	13,629	1723	842	37	72	62	n.a.	14
Wheat straw	0.6	0.1	500	11,000	2500	750	150	150	200	8500	92
Barley straw[a]	n.a.	0.0492	753	10,757	3441	1205	661	64	54	n.a.	14
Winter barley straw	n.a.	n.a.	n.a.	9000	4000	n.a.	n.a.	n.a.	n.a.	2900	93
Spring barley straw	n.a.	n.a.	n.a.	8600	4300	n.a.	n.a.	n.a.	n.a.	4600	93
Rye straw	n.a.	n.a.	n.a.	97,000	2700	n.a.	n.a.	n.a.	n.a.	3500	93
Winter rape straw	n.a.	n.a.	n.a.	78,000	11,600	n.a.	n.a.	n.a.	n.a.	400	93
Shells											
Ground nut shell	0.8	0.0299	278	17,690	12,970	3547	467	3642	1092	10,960	12
Coconut shell	n.d.	0.0035	94	1965	1501	389	1243	73	115	256	12
Walnut shell[b]	n.a.	0.0790	691	5202	9081	1283	554	n.a.	3095	n.a.	94
Almond shell[b]	n.a.	0.0288	383	6714	1570	500	165	n.a.	1641	n.a.	94
Pine nut shell[b]	n.a.	0.0652	716	2201	728	905	193	n.a.	1318	n.a.	94
Husks											
Millet husk	0.1	0.0317	1267	3860	6255	11,140	1427	n.a.	1020	150,840	12
Rice husk	0.6	0.0163	337	9061	1793	1612	132	n.a.	533	220,690	12

https://doi.org/10.1021/acs.energyfuels.0c04046
Energy Fuels 2021, 35, 5407−5478

Table 2. continued

	N (wt %)	S (wt %)	P (mg/kg)	K (mg/kg)	Ca (mg/kg)	Mg (mg/kg)	Na (mg/kg)	Al (mg/kg)	Fe (mg/kg)	Si (mg/kg)	ref
Husks											
Rice husks	0.3	0.03	500	11,000	2500	400	70	70	80	98,500	92
Coffe husk	0.266	0.09	1000	12,500	5000	1300	n.a.	n.a.	176	n.a.	95
Others											
Coir pith	0.7	0.0467	1179	26,283	3126	8095	10,564	1653	837	13,050	12
Corn cob	n.d.	0.0015	445	9366	182	1693	141	n.a.	24	9857	12
Coconut coir	0.2	0.0064	47	2438	477	532	1748	148	187	2990	12

[a]As received. [b]Data based on ash composition and yield.

Table 3. Ash contents of Different Plant Parts of Woody and Herbaceous Species

	Trunk/stems (wt %, db)	Trunkbark (wt %, db)	Twig (wt %, db)	Leaf (wt %, db)	ref
Albizzia l.	1.1	6.9	2.1	3.24	97
Syzygium f.	1	7.1	2.3	4	97
Pterospermum l.	0.9	7.8	3.1	3.8	97
Premna b.	1.9	9.3	4.1	11.6	97
Populus n.	2.9	n.a.	2.1	17.9	88
Arundo d.	4.9	–	–	12.5	88
Arundo d.	3.2	–	–	11.3	86
Cynara c.	6.8	–	–	11.7	86
Miscanthus s.	1.9	–	–	6.2	86
Panicum v.	2.6	–	–	7.6	86
Fiber s.	4.1	–	–	8.1	86
Sweet s.	5	–	–	8.2	86

and $Si(OH)_3O^-$) in the fluid matter inside the plants. Inorganic elements in the fluid matter are translocated from the soil to the plant, and due to the water evaporation during the translocation especially in hot weather, or after plant harvesting, they accumulate as precipitated salts according to the water solubility order (phosphates < carbonates< sulfates < chlorides < nitrates). Their chemical form is responsible of the high mobility during water leaching.

Cations (K^+, Na^+, Ca^{2+}, Mg^{2+}, Fe^{3+}, and Al^{3+}) and covalently bonded S, P, and Cl are bound the organic species of the plants tissues. Organically associated elements, mostly in the form of oxalates, can undergo complex transformations during the thermal treatment of biomass thus resulting in inorganic matter in the residues after incineration.[14]

Included mineral matter comprises discrete inorganic particles typically containing Ca, Mg, and Si. Finally, excluded mineral matter includes aluminosilicates (rich in K, Na, Ca, and Fe), feldspars, or quartz deriving from soil contamination. According to the definition reported by Vassilev et al.,[4] the inorganic elements belonging to the last two classes cannot be considered to be inherent (or intrinsic). They divided inorganic elements into authigenic and technogenic types. The natural mineral phase originated by biogenic processes during plant growth or by natural processes after plant death is classified as authigenic, whereas fine mineral particles introduced into the plant by water suspension or adhering to external plant surfaces and pores are classified as detrita.[15] The mineral phase of anthropogenic origin introduced to the biomass during its collection, transportation, or transformation is defined as technogenic. Typically, authigenic minerals are more mobile and reactive than technogenic inorganics.

Silicates have both authigenic (opal), detrital, and technogenic occurrences (different forms of quartz and aluminosilicates). Fe, Al, Na, and Ti oxides and hydroxides typically present in the soil have a low water solubility; therefore, their presence in the biomass is limited and has mostly a detrital or technogenic origin. Sulfur is bonded both in organic and inorganic forms as sulfate that has mostly an authigenic origin. Conversely, phosphorus is present mainly as phosphates and can have an authigenic or technogenic origin due to specific biomass processing practices (e.g., phosphates fertilizer in agriculture). Low mobility carbonates in lignocellulosic biomass can have a detrital origin, whereas highly mobile chlorides can have an authigenic occurrence (halite, sylvite, K, Ca, and Bi chlorides) or can occur as additives during processing of natural biomass. Alkali metals are typically present in the form of salts and to a lesser extent in the form of organic salts; conversely, alkaline earth metals are typically bound to the organic matrix. Nitrates can have an authigenic or technogenic origin being added as fertilizers to natural biomass.

Overall, the inorganic elements content results in a highly variable relation with several factors such as plant species, plant organs, element seasonal cycling, soil characteristics, storage time, harvesting and drying, or milling postprocessing. Data from proximate analysis collected for 72 species among woody and herbaceous biomass estimated an ash content in the range of 0.1−20 wt %.[4] Table 2 lists literature data on the content of the most abundant inorganic elements in different types of biomass.

3.2.1. Plant Species and Tissues and Growing Conditions. The main factors modifying the mineral content of vegetal biomass are genotype, plant tissue, and growing conditions.[83−86] The variability of the concentration of the most abundant inorganic elements in different types of biomass and different plant organs is evident in the data reported in Tables 2 and 3, respectively.

The data reported in Table 2 are consistent with the data reported in ref 5 for collecting the ash composition of 72 varieties of biomass among woody and herbaceous biomass.[4] N,

https://doi.org/10.1021/acs.energyfuels.0c04046
Energy Fuels 2021, 35, 5407−5478

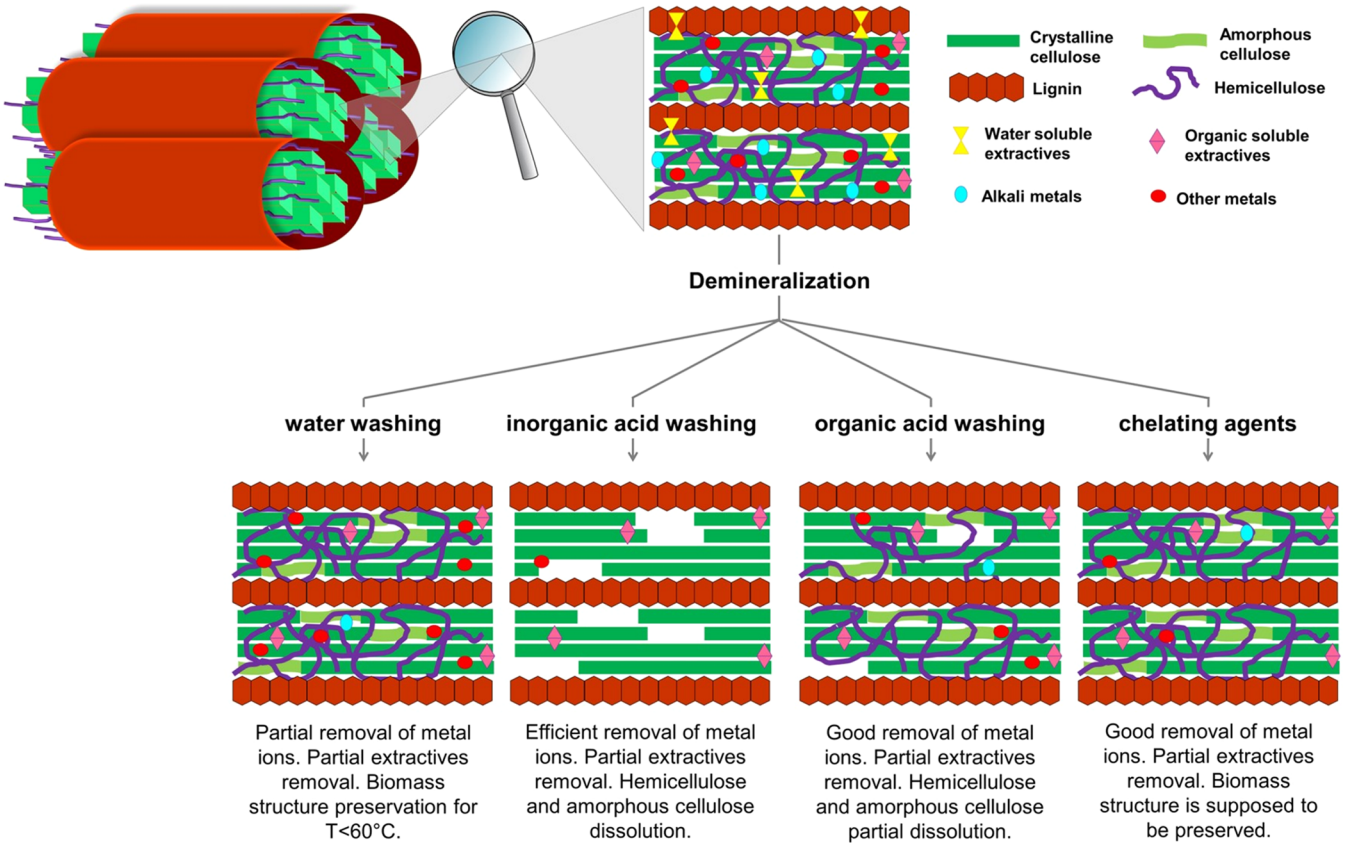

Figure 4. Biomass demineralization procedures and their effects on the organic matrix.

Si, Ca, and K are the most abundant elements; more specifically, wood and herbaceous biomass, except reed, are enriched in Ca, whereas the other biomasses, mainly straws, contain more Si and K than wood. The S content is higher in herbaceous biomass that in wood. P is more abundant in the herbaceous and woody biomass and in husks than in straws, and high amounts of Al can be also detected in wood. Cl, not reported in Table 2, has an average concentration in plant shoots of about 0.01 wt % of dry matter.[75] Depending on the use of Cl containing fertilizer and on the salt concentration in the soil, the Cl content can exceed 1 wt % of dry matter and depends more on crop management and soil type than on the type of plant.[96] It is worth noting that in some cases (e.g., poplar) the same species show very different contents of inorganic elements, suggesting that other factors contribute to the inorganic elements contents in plants.

In Table 3, the ash contents of different plant parts of some woody and herbaceous biomasses are reported.

According to the data reported in Table 3, among the different plant parts, bark shows higher ash content than wood, and leaves show the highest ash content for both woody and herbaceous species.

Size reduction also affects the content of inorganics; it was found that inherently small and grindable inorganic constituents, such as ash, tended to accumulate in the finer fraction.[98]

3.2.2. Soil Characteristics. Considering that the most sustainable strategy is to cultivate biomass crops for renewable energy production in marginal lands (e.g., contaminated, salinized, or arid lands) with the aim to reduce competition for land with food crops, it is important to verify if the environmental constraints of such soils could affect biomass mineral composition.

Drought treatments determined a lower ash content in biomass crops, maybe for the reduction of uptake of minerals by roots due to the reduction of transpiration and thus of root water absorption, while salt stress increased ashes,[99,100] due to the higher accumulation of Cl^-, SO_4^-, and Na^+.[101]

Also soil fertility affects biomass composition; nitrogen fertilization increases ash content,[102] while limestone addition improves ash melting behavior, since it improves the formation of high temperature melting calcium potassium phosphates, thus preventing the formation of potassium-rich phosphate and silica melt.[103]

Regarding the mineral composition of plants grown in contaminated soils (e.g., in phytoremediation plants), it depends on the presence of potential toxic elements (PTEs) in a bioavailable form that can be assessed by chemical methods[104] or by biological methods.[105,106]

The tree species most used for phytoremediation are poplar, willow, and eucalyptus, while among the herbaceous crops giant reed, miscanthus, and brassica spp are the most used.[107]

The most accumulated PTEs in woody biomasses are As, Cd, Cu, Pb, Zn, and Hg with some differences among and within the species[108] due to the affinity of different genotypes to specific PTEs.[107] They are typically present in the biomass at trace levels, but their concentration can increase to higher levels depending on plant type and within the plant on the considered organ. While hyperaccumulators are characterized by values of a bioaccumulation factor higher than 1[109] (PTEs concentration in plant tissue > contaminated media), the energy crops are characterized by a fast growth rate and high biomass production with lower values of the bioaccumulation factor.[110] Poplar, among the phytoremediation plants, accumulated high amounts

https://doi.org/10.1021/acs.energyfuels.0c04046
Energy Fuels 2021, 35, 5407−5478

Table 4. Effect and Removal Efficiency of Different Demineralization Pretreatments on Biomass Samples

Biomass	Leaching agent	Leaching agent concentration	T (°C)	Time (h)	Ash removal efficiency[a]	Results	Drawbacks	ref
poplar wood chips	H_2O		25	96	25	Treatment did not change carbohydrate or lignin contents. K and P contents were reduced by 88% and 76%, respectively. Si content was unchanged.	Amount of extractives is reduced by pretreatment.	129
	H_2SO_4	0.05 M	80	3	70	Treatment did not change the lignin content. Treatment removed minerals more effectively than the neutral wash. Contents of Ca, Mg, Mn, and Zn were also reduced. Si content was unchanged.	Amount of extractives is reduced by pretreatment. Applied conditions favored a partial xylan removal.	
pine wood	H_2O		50	4	44.4	K, Na, and P were easy to remove (>80% of removal efficiency). Removal of Mg, Fe, and Al was lower, and it followed the order of Mg > Fe > Al. Ca was the element poorly removed.	Mass loss was 7%.	115
	HNO_3	1%	50	2	88.9	HNO_3 ensured the highest removal efficiency. All the investigated inorganics were easily removed with the exception of Fe and Al exhibiting a removal efficiency of ~60%.	Mass loss was 7.8%.	
	CH_3COOH	1%	50	2	77.8	Results indicated that Na, K, Mg, and P were completely removed. Ca exhibited a removal of ~70% and Fe and Al of less than 60%.	Mass loss was 8%.	
pine wood	synthetic condenser liquid	pH 2.1	90	2	99	AAEMs content is reduced by 97%. Mass loss was nearly the sum of AAEMs and water and ethanol extractives in raw biomass.		126
Douglas fir and hybrid poplar	H_2O		121 (in autoclave)	0.5	66.7 (D. fir), 22.9 (H. pop)	Significant reductions in amount of ash and extractives in both woods were detected. Reductions in contents of Ca, Mg, Na, and K in both woods were detected.	Extractives were leached out. Reductions of hemicellulose and soluble lignin fractions were detected for both woods. Hot water treatments facilitated hemicellulose hydrolysis.	130
	H_2SO_4	12 mM	25	3	46.7 (D. fir), 46.1 (H. pop)	Significant reductions in amounts of ash and extractives in both woods were detected.	Extractives were leached out.	

https://doi.org/10.1021/acs.energyfuels.0c04046
Energy Fuels 2021, 35, 5407−5478

Table 4. continued

Biomass	Leaching agent	Leaching agent concentration	T (°C)	Time (h)	Ash removal efficiency[a]	Results	Drawbacks	ref
						Greater reductions of Ca, Mg, Na, and K contents were detected for both woods compared to water washing.	Reductions of hemicellulose and soluble lignin fractions were detected for both woods.	
poplar wood powder	H_2O		90	2	28.6	Contents of holocellulose and lignin did not significantly change. Inorganic species contents did not significantly change. Demineralization effects of water were negligible.		131
	HCl	2 M	60	6	84.3	K, Mg, and Ca contents decreased in a significant way.	Holocellulose content decreased from 81.8 to 70.0 wt %. Hemicellulose (xylan) and pectic materials were hydrolyzed.	
	HF	3 wt %	25	1	82.9	Contents of holocellulose and lignin did not significantly change. K, Mg, and Ca contents decreased in a significant way. HF washing did not cause easy chemical degradation and ensured efficient inorganic constituents removal.		
willow (Salix) wood	HCl	n.a.	n.a.	n.a.	99	Demineralization process successfully removed mineral content of biomass.	Hemicellulose content moved from 19.4 to 3.5 wt %.	132
beech wood	CH_3COOH	0.3, 1.0, 5.0, 10.0 wt %	30, 60, 90	0.5 up to 2	range 59−99	Ca and Mg removal efficiencies significantly decreased with reduction of acetic acid concentration, while for K only a slight decrease was noticed. For Na, leaching efficiencies up to 96% were achieved for all tested concentrations. Reduction of residence time to 30 min as well as decrease of temperature to 30 °C had no significant influence on leaching efficiency for high concentrations (5 and 10 wt %).		133
	H_2O		20, 50	2, 24	range 21-43	At room temperature, ash removal increased gradually with duration of treatment, moving from 25% at 2 h up to 32% at 24 h. At 50 °C, treatment duration did not significantly affect ash removal.		

https://doi.org/10.1021/acs.energyfuels.0c04046
Energy Fuels 2021, 35, 5407−5478

Table 4. continued

Biomass	Leaching agent	Leaching agent concentration	T (°C)	Time (h)	Ash removal efficiency[a]	Results	Drawbacks	ref
beech wood	HNO_3	0.1%, 1%	20, 50	2, 4	range 70-95	At low acid concentrations, treatment duration and higher temperature allowed for higher ash removal efficiencies. HNO_3 was much more effective than acetic acid. K, Na, and P were easy to remove and exhibited over an 80% removal rate. Removal of Mg, Fe, and Al was lower, following the order Mg > Fe > Al. Ca removal reached the highest value with HNO_3 treatment.	Mass loss was always below 10%.	115
	CH_3COOH	0.1%, 1%	20, 50	2, 4	range 50-75	Treatment duration did not seem to greatly influence the results. Increasing temperature aided in achieving higher ash removal when the acid concentration was low. K, Na, and P were easy to remove and exhibited over an 80% removal rate with any of the applied conditions. Removal of Mg, Fe, and Al was lower, following the order Mg > Fe > Al. Ca was the element mostly affected by treatment conditions, and its removal by AcOH was higher compared to that obtained with H_2O.	Mass loss was always below 10%.	
oak wood	H_2O		50	4	57.1	K, Na, and P were completely removed. Mg removal reached a value of ~30%. Ca, Fe, and Al were removed with a very low efficiency.	Mass loss was 10.6%.	115
	HNO_3	1%	50	2	85.7	HNO_3 was the reagent ensuring highest removal efficiency. AAEMs were easily removed. Fe and Al exhibited a removal efficiency around 60% and 25%, respectively.	Mass loss was 10.4%.	
	CH_3COOH	1%	50	2	71.4	Na, K, Mg, and P were completely removed. Ca exhibited a removal around 35%, and Fe and Al values below 20%.	Mass loss was 9.8%.	

https://doi.org/10.1021/acs.energyfuels.0c04046
Energy Fuels 2021, 35, 5407−5478

Table 4. continued

Biomass	Leaching agent	Leaching agent concentration	T (°C)	Time (h)	Ash removal efficiency[a]	Results	Drawbacks	ref
moso bamboo	H_2SO_4	3 wt %	25	2	54.1	Large portion of inorganics could be removed by acid washings.	Negative effects on chemical structure of moso bamboo followed the order: HCl > HNO_3 > H_2SO_4 > HF.	134
	HCl	3 wt %	25	2	76.4	K, Fe, and Na contents were below detection limits in washed samples.	Acid washings could promote depolymerization of cellulose or/and hemicellulose.	
	HF	3 wt %	25	2	69.5	Efficiency of four acids followed the order: HCl > HNO_3 > HF > H_2SO_4.		
	HNO_3	3 wt %	25	2	70.9			
candlenut wood	H_2O		30, 60, 90	3	6.4, 28.6, 29.3	Ash contents decreased, and volatile matter contents increased with all the treatments.	As water temperature rised, relative energy loss increased, indicating that a loss of organic matter occured.	135
						Amounts of K, S, and Cl decreased greatly.		
						Ash removal efficiencies increased with increasing process temperature.		
Swedish softwood sawdust (spruce/pine mixture)	CH_3COOH	5, 10 wt %	85	0.5, 1, 1.5	11.4 and 77.1 for 0.5 h, 28.6 and 67.1 for 1 h, 57.1 and 74.3 for 1.5 h	Most of AAEMs were removed after 30 min of treatment. No reduction of Si content was observed.		122
						Removal of inorganic matter was enhanced by the higher acidity.		
						No significant dissolution of volatile fraction occured for all investigated conditions.		
pine bark	H_2O		20	48	8.6	Water leaching was ineffective for inorganic matter removal.		136
	CH_3COOH	3, 5 M	20	48	38.4, 48.4	Reduction of total inorganic matter increased with acid concentration increasing.		
						Removal efficiency was low compared to results achieved with H_2SO_4.		
						Acetic acid removed more inorganics than HCl and HNO_3 at same pH level.		
	HCl	0.05, 0.1, 0.5 M	20	48	14.3, 67.4, 72.4	Reduction of total inorganic matter increased with acid concentration increasing.	Mass loss with 0.5 M HCl solution was 18%.	
						HCl efficiencies for single inorganic species were Al (66%), Ca (90%), Fe (66%), K (92%), Mg (98%), Na (100%), and S (25%).		

https://doi.org/10.1021/acs.energyfuels.0c04046
Energy Fuels 2021, 35, 5407−5478

Table 4. continued

Biomass	Leaching agent	Leaching agent concentration	T (°C)	Time (h)	Ash removal efficiency[a]	Results	Drawbacks	ref
	H_2SO_4	0.5 M	20	48	89.6	Total inorganic matter was reduced by more than 80%, reaching the highest value of removal efficiency among different conditions tested.		
	HNO_3	0.5 M	20	48	35.5	Total inorganic matter was reduced by more than 30% after 48 h leaching, a value quite low compared to HCl and H_2SO_4 treatments.		
Chinese fir waste	HCl	2 wt %	30	3	85.3	Ash content decreased markedly after all chemical pretreatments, especially after HCl and HCOOH treatments.	Water-soluble extractives were removed.	118
	H_3PO_4	2 wt %	30	3	75.8	Acid pretreatments exhibited a more significant effect on reducing ash content than that of alkaline solutions.	Mass loss occured in all the cases.	
	HCOOH	2 wt %	30	3	82.1	Acids showed more obvious removal effects on Ca and Mg than that of alkaline solutions.	All chemical pretreatments promoted decomposition of hemicellulose, cellulose, and lignin in different extents.	
	CH_3COOH	2 wt %	30	3	70.5	Cellulose crystallinity increased in following the order: KOH > HCl > NH3 > CH_3COOH > H_3PO_4 > CHCOOH.	Alkaline compounds favored removal of lignin and hemicellulose rather than acids.	
	NH_3	2 wt %	30	3	65.3			
	KOH	2 wt %	30	3	73.7			
miscanthus	H_2O		50	4	22.6	K, Na, and P were removed with an efficiency of >70%. Removal of Mg reached a value of ∼40%. Ca, Fe, and Al were removed with an efficiency between 20% and 55%.	Mass loss was 4.4%.	115
	HNO_3	1%	50	2	38.7	HNO_3 ensured highest removal efficiency. All AAEMs and P were removed with an efficiency over 80%, while Fe and Al had a removal efficiency of ∼60%.	Mass loss was 4.9%.	
	CH_3COOH	1%	50	2	29	Na, K, Mg. and P were removed with an efficiency of >80%. Ca, Fe, and Al removals were characterized by values between 50% and 75%.	Mass loss was 4.7%.	
eucalyptus	H_2O		50	4	40	Ash removal was low. K, Na, and P were removed with an efficiency of >80%.	Mass loss was 10.6%.	115

https://doi.org/10.1021/acs.energyfuels.0c04046
Energy Fuels 2021, 35, 5407−5478

Table 4. continued

Biomass	Leaching agent	Leaching agent concentration	T (°C)	Time (h)	Ash removal efficiency[a]	Results	Drawbacks	ref
						Mg and Fe removals reached a value around 50%.		
						Ca and Al were removed with a lower efficiency (<10%).		
	HNO_3	1%	50	2	72	Even if HNO_3 was the reagent ensuring the highest removal efficiency, the deashing process was overall not very successful.	Mass loss was 10.9%.	
						AAEMs and P were removed with an efficiency of >70%.		
						Fe and Al exhibited a removal efficiency of ∼30%.		
	CH_3COOH	1%	50	2	44	Ash removal was quite low.	Mass loss was 10.8%.	
						Na, K, Mg, and P were removed with an efficiency of >80%.		
						Ca, Fe, and Al removals were characterized by values between 0% and 40%.		
giant reed, switchgrass, and cardoon leaves	H_2O		80	2	62.5, 65.9, 27	Good reduction of ash content was achieved, except for cardoon leaves.		137
						Good removal of K, P, S, and Cl was achieved, while contents of other metals and Si were unchanged.		
switchgrass	H_2O		20	48	40.8	Most inorganic elements (K and Na) were removed.		136
	CH_3COOH	0.5 M	20	1, 8, 48	47.6, 47.6, 48.4	Acid treatment improved inorganic matter reduction significantly.	Acid leaching led to large mass losses because a portion of cellulose and hemicellulose was leached out.	
						Leaching time and acid type did not show a clear influence on inorganic matter reduction.		
	HCl	0.01 M	20	1, 48	46.2, 47.3	After 1 h, almost all acid-soluble elements were leached out.		
switchgrass	EDTA	10 g/L		0.083, 0.167, 0.250, 0.333	range 56.5−87.3	Extraction treatments with acetic acid and citric acid showed few differences depending on extraction time.	Mass loss ranged from 4.7% to 8.0% for all extraction conditions except for H_2SO_4, treatment characterized by a significant mass loss (up to 32.9% after 20 min).	128
	citric acid	10 g/L		0.083, 0.167, 0.250, 0.333	range 52.5−64.5	Treatment with H_2SO_4 allowed for significant ash removal already at 5 min.	During the extraction with H_2SO_4, a larger amount of holocellulose was hydrolyzed.	
	CH3COOH	10 g/L		0.083, 0.167, 0.250, 0.333	range 54.3−62.8	With EDTA, an increase of ash removal was detected with increasing reaction time.	Use of EDTA poses some environmental issues since EDTA is characterized by a high environmental persistence.	

https://doi.org/10.1021/acs.energyfuels.0c04046
Energy Fuels 2021, 35, 5407−5478

Table 4. continued

Biomass	Leaching agent	Leaching agent concentration	T (°C)	Time (h)	Ash removal efficiency[a]	Results	Drawbacks	ref
	H_2SO_4	10 g/L		0.083, 0.167, 0.250, 0.333	range 54.7−70.8	Treatment with EDTA allowed for highest reduction in ash among all treatments tested (87.3% after 20 min of reaction). All treatments allowed for K removal between 95.5% and 99.4%. EDTA, citric acid, and H_2SO_4 were able to remove Ca with a high efficiency (removal between 95.6% and 99.6%), while acetic acid removed a maximum of 81.4% Ca at a higher extraction time. Concerning Mg removal, all treatments exhibited good performances (removal between 95.5% and 99.6%). Si removal after EDTA treatment was significantly higher than after other treatments, reaching 75.2% after 20 min of reaction.		
Jose tall wheatgrass	H_2O		22	2	47.2	Water leaching removed both inorganic and organic fractions (extractives).	Extractives were significantly removed, leading to a mass loss up to 15%.	113
sweet sorghum stalk	HCl	0.1 mL/L	25	4	46.7	Contents of all metallic species decreased. K removal was around 99.53%, while those of Ca, Mg, Cu, Na, Mn, and Fe were in the range of 71%−95%. For Zn, a very low removal (9.35%) was detected. Contents of cellulose and hemicellulose increased to 38.45% and 35.85 wt % from 33.78 and 30.14 wt %, respectively, while the lignin content did not change.	Extractives content decreased from 24.37% to 12.88%.	138
palm kernel shell (PKS), palm empty fruit bunches (EFB), and palm mesocarp fiber (PMF)	H_2SO_4	2 M	25	48	~64.7 (PKS), ~58.6 (EFB), ~22.6 (PMF)	HCl, H_2SO_4, HNO_3, and $HClO_4$ were very efficient in reduction of Ca and Mg contents.	Pretreatment with diluted HF slightly affected the chemical structure of EFB and PMF.	120
	HCl	2 M	25	48	71.8 (PKS), ~61.4 (EFB), ~26.2 (PMF)	HF led to a higher Si reduction.	In HCl-leached PKS, some contents of hemicellulose and probably cellulose were dissolved.	
	HNO_3	2 M	25	48	~70.5 (PKS), ~61.4 (EFB), ~25 (PMF)		After acid pretreatment, surface porosity of samples increased.	

https://doi.org/10.1021/acs.energyfuels.0c04046
Energy Fuels 2021, 35, 5407−5478

Table 4. continued

Biomass	Leaching agent	Leaching agent concentration	T (°C)	Time (h)	Ash removal efficiency[a]	Results	Drawbacks	ref
	HF	2 M	25	48	~35 (PKS), 93.9 (EFB), 83.9 (PMF)			
	$HClO_4$	2 M	25	48	~70.5 (PKS), ~57.1 (EFB), ~26.2 (PMF)			
sugarcane bagasse (SCB) and trash (SCT)	H_2O		25	1	31.6, 20.8	High Na and K removals were obtained after leaching of both biomass samples. Mg was poorly extractable from both biomass matrices at 25 °C (36% and 40% for SCT and SCB, respectively). Use of water corresponded to smaller mass losses.		124
	citric acid	0.192 kg dm^{-3}	25	1	42.1, 30.2	High K removal was obtained for both biomass samples. Removal of Na reached highest values among all tested conditions. Removal of Mg was over 90%, except for SCB (78%). Chelating effect of citric acid warranted removals of K, Na, Al, Fe, Si, and Mg to a level comparable to stronger mineral acids. Weak acidic nature did not induce extensive organic components hydrolysis. Its use led to smaller mass losses.		
	HCl	0.182 kg dm^{-3}	25	1	42.1, 32.1	High Na and K removals were obtained after leaching both biomass samples with HCl and H_2SO_4. Mg removal was >90%.	HCl and H_2SO_4 contributed to elimination of inorganics, but induced mild hydrolysis of hemicelluloses.	
	H_2SO_4	0.501 kg dm^{-3}	25	1	42.1, 32.1			
bagasse	synthetic condenser liquid	pH 2.1	90	2	<5	AAEMs contents were reduced by 91%. Under used leaching conditions, hardly any loss of hydrolyzable sugars or lignin occurred. Mass loss was nearly identical to the sum of AAEMs and water and ethanol extractives in biomass.		126
rice straw	HF	3 wt %	25	1	93.1	K, Mg, Na, Fe, Zn, and P were significantly reduced.		139

https://doi.org/10.1021/acs.energyfuels.0c04046
Energy Fuels 2021, 35, 5407−5478

Table 4. continued

Biomass	Leaching agent	Leaching agent concentration	T (°C)	Time (h)	Ash removal efficiency[a]	Results	Drawbacks	ref
						Ca and Si were not easily removed. Structural and compositional properties of material were unchanged.		
rice straw	H_2O		25	2	33.3	After deionized water leaching, most K and Na were removed.	C/H ratio slightly decreased suggesting that only a little fraction of organic components was removed after the treatment with H_2O and AcOH.	116
						Ca, Mg, and Fe were scarcely removed.		
	CH_3COOH	5%	25	2	47.1	AcOH had hardly any adverse effect on treated biomass. AcOH ensured higher removal efficiency for K and Na than H_2O.		
	HCl	5%	25	2	50.7	Amounts of Ca, Mg, and Fe had different degrees of decline after acid leaching (decline increased with acidity of leaching agent). Ca and Mg were almost completely removed after the treatment with inorganic acids.	C/H ratio decreased, suggesting that a fraction of organic components was removed. HCl might potentially introduce undesirable Cl into treated biomass, contaminating final products.	
	H_2SO_4	5%	25	2	46		C/H ratio decreased, suggesting that a fraction of organic components was removed. H_2SO_4 might potentially introduce undesirable S into treated biomass, contaminating final products. H_2SO_4 leaching had the most significant effect on biomass structure since it dissolved hemicellulose and cellulose. H_2SO_4 leaching could erode fibrous structure of biomass, and a large number of micropores and mesopores can be generated.	
	HNO_3	5%	25	2	54.7		C/H ratio decreased, suggesting that a fraction of organic components was removed. HNO_3 might potentially introduce undesirable N into treated biomass, contaminating final products.	
	H_3PO_4	5%	25	2	47.7		C/H ratio decreased, suggesting that a fraction of organic components was removed. H_3PO_4 might potentially introduce undesirable P into treated biomass, contaminating final products.	

https://doi.org/10.1021/acs.energyfuels.0c04046
Energy Fuels 2021, 35, 5407−5478

Table 4. continued

Biomass	Leaching agent	Leaching agent concentration	T (°C)	Time (h)	Ash removal efficiency[a]	Results	Drawbacks	ref
rice straw	aqueous phase bio-oil	pH 2.9	50	2	38.3	Na, K, Ca, and Mg were removed with an efficiency of over 90%. High removal efficiency could be related to predominant presence of acetic acid in the bio-oil. Presence of phenols in bio-oil helped in AAEMs removal.		140
rice straw	H_2O		30, 60, and 90	3	8.22, 17.6, 30.1	Ash contents decreased, and volatile matter contents increased for all treatments. Amounts of K, S, and Cl decreased greatly. Removal efficiencies of ash increased with increasing process temperature.	As water temperature rised, relative energy loss increased, indicating that a loss of organic matter occured.	135
rice husk	H_2O		25	2	13.7	Demineralization efficiencies for single metals were K 92.0%, Na 84.7%, Ca 10.2%, and Mg 40.2%.		141
	HCl	5%	25	2	17.9	Demineralization efficiencies for single metals were K 99.7%, Na 90.4%, Ca 86.3%, and Mg 98.8%		
rice husk	HCl	2 M	25	2	4.3	HCl removed mainly AAEMs in ash, but did not remove Si. Removal efficiencies of K, Ca, Na, and Mg were all >90% and comparable to those of H_3PO_4 and HF.		142
	HF	2 M	25	2	98.1	Ash content reduced to 0.24% due to Si removal. Na is almost completely removed, and K is removed more than 96%. Removal efficiencies of Mg and Ca were not as significant as those of K and Na.		
	H_3PO_4	2 M	25	2	4.8	Ash content reduced slightly. H_3PO_4 mainly removed AAEMs but not Si. Na was almost completely removed, and K was removed more than 96%, while removal efficiencies of Mg and Ca were >88% and >72%, respectively.		
wheat straw	HCl	1.4 M	25	2	97	Acidic treatment removed a large quantity of AAEMs, leading to	Biomass fibrous structures have been eroded during treatments, leading to	143

https://doi.org/10.1021/acs.energyfuels.0c04046
Energy Fuels 2021, 35, 5407−5478

Table 4. continued

Biomass	Leaching agent	Leaching agent concentration	T (°C)	Time (h)	Ash removal efficiency[a]	Results	Drawbacks	ref
						high demineralization efficiencies.	development of pores, increased specific surface area, and total pore volume.	
	HF	1.4 M	25	2	93.1	HCl, due to its strong acidity, showed the highest demineralization efficiency, leading to efficiency values of 77.42%, 89.13%, 65.09%, and 87.96% for K, Ca, Na, and Mg removals, respectively.	Acidic treatments can dissolve hemicellulose, cellulose, and lignin.	
	HCl+HF	1.4 M	25	2	87.3			
wheat straw	HCl	0.2, 0.4, and 0.6 M	25−27	2	48.3, 70, 80.4	High ash reduction was obtained.	Demineralization process with HCl and HNO_3influenced the elemental composition.	144
						Highest ash removal was achieved with highest acid concentration.	C/H ratio decreased, suggesting that a fraction of organic components was also removed during demineralization process with HCl and HNO_3.	
							After treatments, biomass surface became spongy and fluffy.	
	HNO_3	0.2, 0.4, and 0.6 M	25−27	2	61.1, 75, 72.1	High ash reduction was obtained but slightly lower than that achieved with HCl.		
						HNO_3 seemed more effective in desulphurization compared to HCl and NaOH.		
	NaOH	0.2, 0.4, and 0.6 M	25−27	2	64, 60.8, 51.1	High ash reduction was obtained in all explored conditions.	C/H ratio decrease was higher for 0.2 M NaOH compared to other samples.	
						Best result was achieved with lowest concentration (0.2 M).	After treatment with 0.2 M NaOH, the surface seemed to be diffused and eroded.	
							Alkaline solution dissolved the hemicellulose structure.	
wheat straw	H_2O		30, 60, and 90	3	56.8, 60.4, 69.7	After treatment, ash contents decreased, and volatile matter contents increased.	As water temperature rised, relative energy loss increased, indicating that a loss of organic matter occured.	135
						Amounts of K, S, and Cl greatly decreased.		
						Removal efficiencies of ash increased with increasing water temperature.		
wheat straw	CH_3COOH	5%	25	2	22	Leaching efficiency of AcOH was comparable to that of H_2SO_4.	H/C ratio decreased.	119
							AcOH led to some changes in biomass surface chemical functional groups.	

https://doi.org/10.1021/acs.energyfuels.0c04046
Energy Fuels 2021, 35, 5407−5478

Table 4. continued

Biomass	Leaching agent	Leaching agent concentration	T (°C)	Time (h)	Ash removal efficiency[a]	Results	Drawbacks	ref
	H_2SO_4	5%	25	2	20	H_2SO_4 exhibited a quite low deashing efficiency.	Slight increase in H/C was observed, possibly due to reduction of carbonaceous matter.	
							H_2SO_4 led to significant changes in chemical structure of treated biomass.Acidic solution dissolved hemicelluloses first, then cellulose, and has little effect on lignin.	
							Biomass surface was eroded, folds disappeared, and interspaces were created.	
	mixture of all acids	5%	25	2	64	Acid mix had highest deashing efficiency.	H/C ratio decreased.	
wheat straw	synthetic condenser liquid	pH 2.1	90	2	66.7	AAEMs content reduced by 97%.		126
						Under used conditions, any loss of hydrolyzable sugars or lignin occurred.		
						Mass loss was nearly the sum of AAEMs and water and ethanol extractives in raw biomass.		
barley straw	H_2O		50	4	42	K, Na, and P were removed with an efficiency of >80%.	Mass loss was 12.8%.	115
						Removals of Mg, Ca, Fe, and Al reached efficiency values between 20% and 50%.		
	HNO_3	1%	50	2	54.5	HNO_3 was the reagent ensuring highest removal efficiency.	Mass loss was 14.5%.	
						AAEMs and P were removed with an efficiency of >80%.		
						Fe was removed with a removal efficiency of ∼60% and Al with a very low value (<10%).		
	CH_3COOH	1%	50	2	50	Na, K, Mg, and P were removed with an efficiency above 80%.	Mass loss was 14.1%.	
						Ca, Fe, and Al removals were between 50% and 75%.		
corn stalk	H_2O		30, 60, and 90	3	38.9, 47.5, 57.5	Ash contents decreased, and volatile matter contents increased.	As water temperature rised, relative energy loss increased, indicating that a loss of organic matter occured.	135
						Amounts of K, S, and Cl decreased greatly.		
						Removal efficiencies of ash increased with increasing water temperature.		

https://doi.org/10.1021/acs.energyfuels.0c04046
Energy Fuels 2021, 35, 5407−5478

Table 4. continued

Biomass	Leaching agent	Leaching agent concentration	T (°C)	Time (h)	Ash removal efficiency[a]	Results	Drawbacks	ref
cotton stalk	H_2O		30, 60, and 90	3	61.5, 60.1, 63.8	Ash contents decreased, and volatile matter contents increased. Amounts of K, S, and Cl decreased greatly. Removal efficiencies of ash increased with increasing water temperature	As water temperature rised, relative energy loss increased, indicating that a loss of organic matter occured.	135
hay	synthetic condenser liquid	pH 2.1	90	2	83.3	AAEMs content reduced by 97%. Under used leaching conditions, hardly any loss of hydrolyzable sugars or lignin occurred. Mass loss corresponded to sum of the AAEMs and water and ethanol extractives in biomass.		126
corn stover	H_2O			2	53	Water leaching removed both inorganic and organic fractions (extractives).	Leaching removed a substantial fraction of extractives	113
corn stover	sodium citrate	0.05, 0.1, and 0.25 g/g	130 (2.7 bar)	2	67.5, 74, 72	With increase of concentration, overall ash content decreased K and Cl were removed almost completely by using lowest sodium citrate concentration (0.05 g/g). More than 95% of both S and Al were removed by using highest sodium citrate concentration (0.25 g/g). 75% of total Si was removed. Cellulose and hemicellulose were not degraded, while lignin content was slightly reduced.	Extractable inorganics, protein content, and total extractives were significantly reduced. Sodium can be recovered as a by-product.	127
	formic acid	0.1 g/g	130 (2.7 bar)	2	<1	With the exception of formic acid, each treatment was effective at removing corn stover structural ash.		
	oxalic acid	0.1 g/g	130 (2.7 bar)	2	7	Formic and oxalic acids proved to be the least effective reagents due to their limited binding capacity.		
	citric acid	0.1 g/g	130 (2.7 bar)	2	21			

[a]Calculated in accordance with the formula reported by Karnowo et al.[145]

https://doi.org/10.1021/acs.energyfuels.0c04046
Energy Fuels 2021, 35, 5407−5478

of Cd, Cu, Pb, and Zn, with concentrations higher in leaves than in trunks.[111] Willow accumulated more Cd in twigs and leaves, Pb in roots and twigs, and Zn in twigs.[112]

4. LABORATORY PROCEDURES CONTROLLING INORGANICS CONCENTRATION

4.1. Biomass Demineralization. Different approaches are reported in the literature for the removal of inorganic matter from biomass: water washing,[113−117] mineral acid leaching,[115−121] organic acid leaching,[115,118,119,122−126] and treatment with chelating agents.[127,128] Their effects on the inorganics removal and on the transformations induced into the organic matrix are summarized in Figure 4.

These chemical treatments can be performed at near ambient temperature but also at higher temperatures (up to 80−250 °C), in batch or continuous (solid−liquid extraction under reflux) modes, and also under pressure (hydrothermal conditions[127]). The degree of metal removal as well as the mass reduction of the original biomass associated with each process is found to be different and dependent mainly on the temperature, biomass composition, reaction time, and acid−base properties of the reagents.[113−128]

In Table 4, a selection of the results about the demineralization of different kinds of biomass published in the last 10 years is reported. For each biomass, the demineralization conditions applied (demineralized agent, concentration, time, and temperature), removal efficiency of the treatment, main results, and drawbacks of the treatment are summarized.

Water washing results in a less effective approach as compared to acid leaching procedures because it dissolves only water-soluble constituents (alkali metals, sodium and potassium ions to a more extent), alkaline earth metals (magnesium ions more than calcium ions), chlorine, sulfur, and phosphorus.[113−117] Moreover, the water washing is ineffective in Si removal; indeed, as reported in Table 4 for biomass rich in Si like rice husk, its content in the washed materials is almost the same of the raw one.

The ash removal efficiency of water washing is highly variable (Table 4); indeed, in the case of woody biomass types, at room temperature, values between 20% and 30% can be reached, while in the case of agricultural wastes also values up to 60% can be reached. Ash removal by water washing benefits from increased treatment temperature and washing time, although the rate of ash removal was very slow after a certain time.[115] Water washing can promote extractive leaching, and if it is performed at temperatures below 60 °C, negligible alterations of biomass structure occur.[113−117] On the contrary, when the temperature is higher, the partial dissolution of structural components is noticed. As matter of fact, Das and Sarmah[121] reported the dissolution of soluble lignin and hemicellulose in a sample of Douglas fir and hybrid poplar treated at 120 °C for half an hour.[121]

Ash removal by mineral acid leaching has been performed using different kinds of acids (HCl, HF, HNO_3, H_2SO_4, $HClO_4$, H_3PO_4) at different concentrations (from 0.1 up to 10 wt %) and temperatures.[115−121] In all the cases, the chemical treatment induced an effective removal of metals (alkali metals, alkaline earth metals, and also heavier metals as Fe, Al, Si, Mn), and in some cases, induced removal up to 95% with respect to the total ashes.[115−121] In general, the acid treatment allows for a more efficient ash removal, because the solubility of some ash-forming compounds is higher at lower pH.[129] However, on the basis of the results reported in Table 4, some differences in the ash removal efficiencies among the most used mineral acids can be highlighted. HCl and HNO_3 exhibit a removal efficiency of greater than 70% for woody biomass types, between 30% and 70% for energy crops, and between 10% and 50% for agricultural wastes. H_2SO_4 allows for a removal efficiency of greater than 50% for woody biomass types and bark and less than 50% for agricultural wastes. HF when used with a concentration between 3 and 10 wt %[121] reaches a removal efficiency of greater than 80% for woody biomass types and greater than 90% for agricultural wastes. In addition, HF is also the acid that is more efficient in the removal of Si; indeed, in the case of rice husk, HF allows for the reduction of SiO_2 up to 50%.[142]

Overall, the performed experiments indicate that metal leaching is enhanced by the higher acidity of the extraction medium[119] and by the high temperature, but those conditions correspond to a non-negligible mass reduction of the original biomass.[122] Indeed, after treatment with mineral acids, the biomass composition is significantly altered. The inorganic matter is mostly removed as well as other soluble LMW components (extractives, tannins). The hemicellulose is hydrolyzed due its amorphous and branched structure, and the cellulose partially depolymerized (amorphous cellulose dissolution).[115−121] Among the different inorganic acids, the use of H_2SO_4 and HCl cause the greater alteration of biomass composition, while HF causes the lowest (Table 4).

To overcome the problems related to the alteration of biomass component structure, leaching with organic acid has been widely proposed.[115,118,119,122−128] Formic, acetic, citric, and tartaric acids have been used to demineralize different kinds of biomasses showing good metal removal efficiencies.[124,127] Solutions containing up to 10 wt % of acetic acid allowed for the reduction of ashes between 50% and 90% in woody biomass, and the dissolution of the volatile fraction is limited or negligible.[118,122] Citric acid, indeed, warranted a metal removal level comparable to the stronger mineral acids, without inducing extensive components dissolution or hydrolysis, thereby keeping the biomass mass loss limited to a minimum and comparable to that of water washing.[124] On the basis of the good results achieved by using an acetic acid aqueous solution, different authors (Table 4) proposed also to use, as the leaching agent, the aqueous liquid derived from lignocellulosic biomass pyrolysis which is, basically, an aqueous solution containing organic acids, with acetic acid being the most abundant one. The proposed approach effectively removed metals present in the raw biomass (ash removal efficiency above 70%, Table 4) without the use of external chemicals limiting hemicellulose hydrolysis.[125,126,140]

Concerning the use of chelating agents for biomass demineralization, Reza et al.[127] demonstrated that the use of the conjugate base of citric acid can reduce the problem of hemicellulose hydrolysis and can favor metal removal taking advantage of the chelating properties of the organic anion. In their work, corn stover demineralization was performed in the presence of different concentrations of sodium citrate at 130 °C and 2.7 bar, leading to a reduction of ash content up to 66% just with the lowest reagent concentration (5 wt %).[127]

Edmunds et al.[128] explored the possibility to use ethylenediaminetetraacetic acid (EDTA) as the chelating agent, and they found that in the case of switchgrass the use of EDTA under microwave-assisted heating allowed for the highest reduction of ash among all the tested treatments (citric acid, acetic acid, sulfuric acid, and distilled water). Indeed, after an extraction time of 20 min with EDTA, an ash reduction around 87% was detected. Moreover, EDTA was able to remove more Si

https://doi.org/10.1021/acs.energyfuels.0c04046
Energy Fuels 2021, 35, 5407−5478

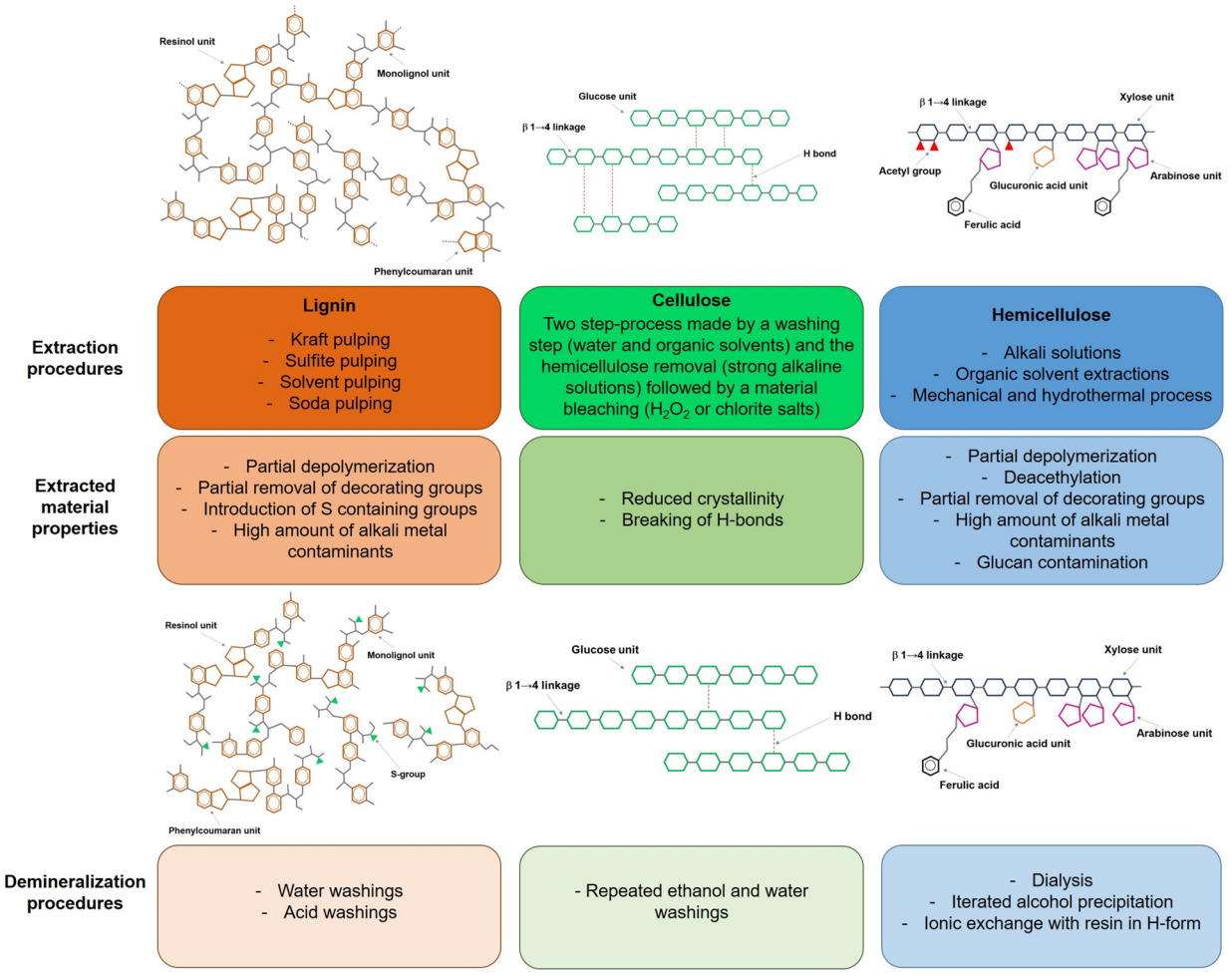

Figure 5. Typical extraction and demineralization procedures of main organic components of lignocellulosic biomass and schematic representation of modifications occurring to organic components as a consequence of extraction procedures.

compared to the other tested chemicals, without significant degradation of the structural components of biomass.[128]

In the end, it is worth noting that some authors proposed also alkali solutions as possible leaching agents for ash removal from biomass (Table 4), but even if they are very efficient in the removal of AAEMs and also of Si, their use leads to a severe alteration of biomass structure and composition.

4.2. Isolation and Demineralization of Cellulose, Hemicellulose, and Lignin. The main biomass organic components, namely, cellulose, hemicellulose, and lignin, have been studied in the literature under slow and fast pyrolysis conditions. In most cases, the material used for the experimentations was a commercial sample selected as a reference compound for the pure biomass component. Sometimes, the components were extracted from a raw biomass and then demineralized following different procedures. Figure 5 reports a list of the typical extraction and demineralization procedures.

Commercial samples typically sourced from Sigma-Aldrich and Avicel are the most common types of cellulose used in pyrolysis studies.[146,147] However, cellulose extraction from raw biomass has been performed to obtain a material that is more representative of the component in the original biomass.[147−149] Cellulose extraction, usually, is carried out through a two-step process. At first, the biomass is milled to a specific dimension and washed with distilled water to remove soluble impurities and then with other solvents to separate extractive fractions, while the second step consists of a series of chemical treatments to remove hemicellulose and lignin fractions[147−149] (bleaching procedure). The procedure allows for the isolation of a material containing residual traces of inorganic species[147] (between 0.1 and 2.45 wt %) that can influence its pyrolytic behavior. Patwardhan et al.[150] determined that the presence of sodium below 0.05 wt % can affect the levoglucosan production.[150] Cellulose extracted from raw biomass lost most of its crystallinity.[149,151] Indeed, in most cases, after the extraction process, an acid hydrolysis with concentrated H_2SO_4 or HNO_3 or HCl is usually performed to isolate crystalline cellulose.[151]

Hemicelluloses are the second most abundant polysaccharides in nature after cellulose, constituting about 20%−30% of the total mass of annual and perennial plants,[70,152] but their heterogeneous composition, branched structure, and amorphous nature make their isolation very difficult.[153] Moreover, because of the partial degradation during extraction, most properties of the native material are unknown. In addition, since hemicellulose properties vary considerably, depending on the botanic origin of the raw biomass and of the isolation procedures, it is quite impossible to identify a model macromolecule that successfully represents all the chemical and structural variations of this component. Commercially available xylans from beechwood and birchwood have often been used as a proxy for hardwood hemicellulose,[154,155] and in

https://doi.org/10.1021/acs.energyfuels.0c04046
Energy Fuels 2021, 35, 5407−5478

rare cases, commercially available glucomannans have been used as softwood proxy hemicellulose.[156−158] These factors contributed to the limited number of literature data about pyrolysis of hemicellulose compared to cellulose.

Extraction procedures for the isolation of hemicellulose from different biomasses and agricultural wastes include alkali or organic solvent extractions and mechanical or hydrothermal processes.[153,159−161] Currently, the alkali method is widely accepted and applied since it allows for the isolation of hemicellulose with a high DP and with a high yield.[161] Unfortunately, as a drawback, such a method induces some alterations into the polysaccharide structure. In the case of hemicellulose extracted from hardwood, for example, the strong alkaline conditions favor the dissolution of ester bonds leading to the removal of decorating groups as acetyl groups, hydrocinnamic groups, and ferulic groups.[153] Moreover, such strong conditions favor the cleavage of the glycosidic linkages between the glucuronic acid units and the xylose-based backbone.[162] To limit the structural alteration of hemicellulose, procedures based on the use of organic solvents as dimethyl sulfoxide (DMSO) or other inorganic reagents have been proposed.[153,159,160] Concerning the isolation methods based on mechanical and hydrothermal processes, they lead in most cases to the isolation of mixtures of oligosaccharides with a high degree of depolymerization, and glucan contamination can occur as well.[163]

The standard hemicellulose isolation techniques based on alkali extraction, moreover, lead to a significant amount of mineral residues in the final product (up to 5−10 wt % of ashes), which should be further purified. Some authors[164,165] proposed dialysis instead of washing with distilled water as a purification option. This procedure was applied to hemicellulose from switchgrass resulting in the reduction of the total ashes from 1.3 wt % of the extracted material to less than 0.1 wt %.[164] To reduce the content of residual mineral matter, an iteration of a process based on dissolution in water or in a solution of HCl in methanol followed by alcohol precipitation (with ethanol or methanol) and filtration was proposed.[166,167] Wang et al.[167] obtained a reduction of 98% of the ash content of a commercial xylan sample. Comparable results were obtained by Giudicianni et al.[154] by dissolving commercial beechwood xylan in distilled water and inducing the removal of the Na ions through a cationic exchange resin (Dowex in H-form). The change in the pH from 4.4 of the starting suspension to 2.2 of the eluate clearly testified to the exchange between the protons of the sulfonate groups of the resin in H-form and metal ions complexed with the carboxylate groups in the polysaccharide.[154]

Lignin can be extracted from a raw biomass, but actually, the available lignins are mainly byproducts of pulping chemical processes. When the lignin is isolated from the pulping liquor, it is named technical lignin. There are four processes for the extraction of lignin from pulping liquor classified as sulfur or sulfur-free processes (kraft pulping, sulfide pulping, soda pulping, and solvent pulping), and as consequence, there are four different types of technical lignins (kraft lignin, lignosulfate lignin, soda lignin, organosolv lignin). The lignin properties (molecular weight, content of phenolic hydroxyl, carboxyl and sulfur containing groups, hydrophilicity and hydrophobicity, presence of contaminants) are dependent on the pulping process applied.[168]

As a consequence of the extraction procedure, in addition to other inherent metals, lignin is bonded to a non-negligible amount of alkali metals (K and Na). Lignin demineralization is performed by acid treatments (acid washing), using preferentially H_2SO_4 acid, that is widely recognized as very efficient in removing ashes. Starting from a basic pH lignin suspension (ranging from 6.8[169] to 9.5,[170] depending on the quality of the raw lignin), H_2SO_4 (concentrated or 1N) is progressively added at room temperature until the pH decreased to ∼1[169,170] or 2−2.5[171−173] allowing for lignin precipitation. The pH decrease leads the organic bound Na ions on the lignin structure to be gradually replaced by H ions. The precipitated lignin is recovered after washing with distilled water. As a consequence of this acid treatment, structural and chemical−physical changes are introduced in the lignin structure: a reduction of the amount of hydroxyl groups, an increase of phenol to the aliphatic hydroxyl ratio, and a concomitant increase of the number of CO functions, as well as the elimination of carbonates eventually present.[170] The acid treatment of the lignin also produces cross-linking.[170]

In the case of lignin with low mineral impurities (as the lignin extracted by using the organosolv process), a washing with dilute HCl acid (0.1 N) for 15 min, followed by washings with deionized water, was also found effective to cut the ashes to less than 0.1 wt %.[174,175]

A demineralization procedure consisting of washings with a HF aqueous solution at 3 wt % at room temperature has been also proposed by Giudicianni et al.,[176] as it has been demonstrated that HF does not induce chemical degradation of the polymer.[117] The HF treatment is found to be more effective compared to water washing in reducing K and Na ions contents of the raw lignin (ashes <0.07 wt %).[176]

4.3. Biomass Doping to Mimic Inherent Inorganics.

Another approach to study and understand the effects of metal ions on biomass pyrolysis (catalytic activities and effects on the products properties) is based on the preparation of samples starting from a raw or a demineralized biomass purposely doped with increasing concentrations of a metal salt.[177] Usually, the concentrations of the loaded dopants depend on the final goal of the biomass doping process. When the goal is the study of the catalytic effect of a single metal ion or of a mixture of inorganics, concentrations comparable to those naturally occurring in a real biomass are explored.[177] When the goal is the production of activated carbons, the concentrations of the dopant agents are really high, reaching a mass ratio around 4.[178,179] When the goal is the preparation of engineered carbon-based materials enriched in metallic species or heteroatoms, the dopant concentrations are variable, and usually, they are between those reported for the previous cases.[180−183] Since the aim of this work is to review the effects of inherent minerals naturally occurring in biomass, the results related to biomass doping with mineral concentrations above those naturally occurring in a real biomass are not considered.

Dry mixing, wet impregnation, and cation exchange are the most common doping methods. The first method, which consists of the physically mixing of the selected metal salt or oxide and the dry biomass,[184] is mainly used in catalytic pyrolysis processes, and metal oxides are used as metal sources.[184] The wet impregnation method is the most common and consists of obtaining the doped biomass sample by water evaporation after soaking it in a salt solution at a defined concentration.[117,185−189] Chlorides, carbonates, nitrates, acetates, and phosphates are the main types of salts used as metal sources due to their low cost, availability, and high solubility.[117,185−189] The anion exchange method exploited the presence of exchangeable metals in biomass bound at hydroxyl and/or phenolic groups in the form

https://doi.org/10.1021/acs.energyfuels.0c04046
Energy Fuels 2021, 35, 5407−5478

Table 5. Advantages and Shortcomings of the Most Common Doping Methods

Doping method	Doping agent	Positive aspects	Drawbacks	ref
Dry mixing	oxides, chlorides, carbonates, hydroxides, nitrates	low cost and rapid procedure; high conentrations achievable	loose interaction between metal and biomass	132, 184
Wet impregnation	chlorides, nitrates, sulfates, carbonates	easy and low cost procedure; good availability of doping agents; defined final concentration; high conentrations achievable	disposal issues; presence of counterions; removal of extractives and other water-soluble components (depending on the procedure applied); changes in cellulose crystallinity; alteration of gas composition as consequence of counterion evolution during pyrolysis	117, 185, 186, 188, 189, 192−194
Ionic exchange	chlorides, nitrates, sulfates, carbonates	tight interaction between metal ions and biomass components; punctual insertion of metal ions within biomass structure	time-consuming; disposal issues; limited achievable concentration of dopant; removal of extractives and other water-soluble components	132, 177, 190

of cations or as a salt, and it uses soluble metal salts as for wet impregnation.[190] All these methods allow to include metal ions or salt in the biomass artificially. To obtain a natural introduction of metal ions into the biomass, a procedure based on the contact between the biomass and the salt solution in a fixed bed column is proposed by Martín-Lara et al.[191] to mimic biosorption, namely, a remediation process for pollutant removal and/or recovery from wastewater by inactive biomass.[191]

In Table 5, a list of possible advantages and shortcomings of the three doping methods are listed.

The wet impregnation method as well as the ion exchange method can induce some changes in the biomass structure and composition. If the aqueous solution used to introduce the metal ions into the biomass is removed by filtration, for example, leaching of water-soluble biomass components can occur, especially when the counterions have non-negligible acid−base properties.[177] Water-soluble extractives and alkali metals, for example, are easily leached out during the doping procedure, but also hemicellulose decomposition and cellulose alteration can take place, leading to a non-negligible change in the organic matter content (Table 4). Safar et al.[194] demonstrated that as consequence of rubber wood impregnation with K_2CO_3 a decrease of cellulose crystallinity occurred, likely due to the transformation of the cellulose structure from crystalline to amorphous due to weakening of H-bonds operated by K^+.[194] An appropriate control of pH around the biomass point of zero charge allows limiting the drawbacks related to the use of aqueous solutions.[192,193]

The use of salts in wet impregnation and ion exchange methods induces the presence in the aqueous medium of both cations, and anions and the acid−base properties of the anions have to be considered due to their possible effect on the biomass structure and thus on the pyrolytic biomass behavior.[177,192] Moreover, some counterions could be thermally decomposed during pyrolysis altering the composition of the pyrolysis gas products (production of CO_2).

5. EFFECT OF INHERENT METALS ON PYROLYSIS PROCESS

The role of inherent metals, especially AAEMs, in biomass pyrolysis has been extensively studied for many types of lignocellulosic biomass, and it is known to be relevant to the onset temperature of thermal decomposition and to the competition between different decomposition pathways. The recent understandings on the decomposition pathways of the main biomass organic components are presented first to pave the way for the discussion on the catalytic effect of the major inherent metals on pyrolysis product yields and characteristics. The discussion is subsequently extended to lignocellulosic biomass pyrolyzed under different operating conditions. Besides AAEMs, the effect of trace metals which are recognized as PTEs is addressed too in order to provide a guide to the pyrolytic conversion of biomass from phytoremediation treatments.

5.1. Effect of AAEMs on Cellulose Decomposition.

Complex chemical pathways for primary cellulose pyrolysis were developed starting from the well-known Broido−Schafizadeh (B−S) mechanism. In the B−S model, after the formation of active cellulose, two competing reactions were considered: the heterolytic cleavage of the glycosidic bond producing levoglucosan and the homolytic cleavage followed by ring opening to form light species, permanent gases, and char. A side charring reaction was also considered. Recent advancements in computational technology and chemistry provided insights into the reaction steps at the molecular level, at least for glucose-based compounds and short-chain oligomers.[8] Glycosidic bond cleavage was recognized to be the prominent pathway in determining the yields of the major products of cellulose pyrolysis, i.e., levoglucosan, LMW species, and furans. Three different mechanisms were proposed for the glycosidic bond cleavage which initiates the reaction steps leading to the production of levoglucosan: homolytic, heterolytic, and concerted mechanisms. Zhang et al.[195] found that the homolytic mechanism leading to the anydroglucose radical and then to levoglucosan and furaldehyde was preferred to the heterolytic mechanism in terms of activation energy. However, different pathways for the concerted mechanism were proposed, and all of them were found to be favored with respect to the homolytic and heterolytic ones. These results were obtained using small glucose-based compounds, such as methyl β-D-glucoside,[196] cellobiose,[197] and methyl cellobiose,[198] but also two-chain glucose hexamers containing interchain hydrogen bonds which resemble more closely a real cellulose fibril.[196] The contraction of glucopyranose to a glucofuranose ring was another pathway to be considered for the production of levoglucosan precursors; such a pathway is in competition with the formation of hydroxymethylfurfural (HMF) and formic acid precursors, a mechanism less favored because of the higher energy barrier.[199] A concerted cleavage of the glyosidic bond was proposed also for the formation of levoglucosenone,[200] and it was preferred to the pathway passing through the levoglucosan intermediate due to its high energy barrier.[197] The formation of furans and light oxygenates, such as hydroxyacetaldehyde, is initiated by the homolytic cleavage of the glycosidic bond rather than through a heterolytic or concerted mechanism. Ring opening is pivotal in the production of LMW species. Independently of the different proposed mechanisms,[201] this pathway is preferred to the

https://doi.org/10.1021/acs.energyfuels.0c04046
Energy Fuels 2021, 35, 5407−5478

levoglucosan route only at high temperature[202] and after dehydration reactions.

When a real cellulosic matrix is considered, additional factors affect the pyrolysis products distribution and the onset temperature of the thermal decomposition: the presence of crystalline and amorphous regions, the existence of intramolecular hydrogen bonds, and the DP. The cellulose crystalline region exhibits higher thermal stability than the amorphous region due to its packed structure.[203−205] High crystallinity index and crystallite size affect positively the levoglucosan production, whereas amorphous cellulose contributes more to the formation of char, gas, furfural, and HMF.[206] The selectivity toward levoglucosan with increasing crystallinity was found to be dependent on the allomorph too, at least for celluloses I and II.[207] Finally, higher DP favors levoglucosan production and depresses furans formation.[202]

Numerous studies were conducted to elucidate the effect of AAEMs on the cellulose decomposition mechanism under both slow and fast pyrolysis conditions. Many of them used microcrystalline cellulose from Sigma-Aldrich and reducing-end carbohydrates as reference compounds, whereas limited work has been performed using anhydrosugars, which actually prevail as intermediates during cellulose pyrolysis. The effect of the different types of cations was assessed as well as the role of the counterion, whereas the effect of the doping procedure received only limited attention. Among the three most used methods, ion exchange is the only one that enables the study of the catalytic effect of metal ions free of possible influences due to the concomitant presence of the counterion. Indeed, ion exchange allows for direct binding between the cellulose and the metal ions, while dry mixing does not produce any bonds, and wet impregnation is primarily a physical adsorption. In any case, all these treatments to produce cellulose-doped samples can induce some alterations in the properties of the biopolymer. Collard et al.[208] revealed that part of the cellulose crystalline phase was transformed into an amorphous phase due to the weakening of hydrogen bonds responsible for the cellulose structure.[208] Table 6 reports a list of the main studies conducted on this topic in the last 10 years and the most relevant results. Figure 6 summarizes the effects of AAEMs on primary and secondary reactions during cellulose pyrolysis.

Both AAEMs were found to shift the onset of cellulose decomposition toward lower temperatures[68,185,215] even though the effect of the doping procedure on the reduction of cellulose crystallinity cannot be neglected.[208] Gargiulo et al.[185] found that at a low heating rate, among the alkali metals, Na^+ was more effective than K^+ in lowering the onset of cellulose pyrolysis. A similar result was observed under fast pyrolysis conditions,[212] where the cellulose conversion, immediately after its heating up 325 °C, is higher for Na^+ than for K^+ loaded samples. In the same conditions, Mg^{2+} and Ca^{2+} were found to be more effective than alkali ions,[212] and this was confirmed also by Yu et al.[211] According to the cellulose decomposition mechanism discussed above, AAEMs, behaving as Lewis acids, weaken the hydrogen bonds between carbohydrates chains in the cellulose fibril and the glycosidic bonds inside the chain thus promoting the dehydration reactions at low temperature.[212] Compared to alkali metal ions, alkaline earth metal ions are stronger Lewis acids. At lower temperatures, AAEMs catalyze the dehydration reactions producing a more cross-linked structure, promote the formation of char and gaseous products (pathway 1, Figure 6) and, in the meantime, reduce the amount of unreacted cellulose undergoing depolymerization through the cleavage of the glycosidic bonds (pathway 2, Figure 6) and ring opening reactions (pathway 4, Figure 6).[68,209] This effect is evident even under fast pyrolysis conditions when charring reactions are depressed with respect to the devolatilization process.[9] As a general rule, char yield is contributed to by both primary and secondary reactions; however, it has been observed that AAEMs produce an increase of char yield even under conditions where the extent of secondary reactions is minimized, such as fast pyrolysis under vacuum and rapid quenching after reaching the maximum temperature.[9,214] Similarly to the relative ability of anticipating the onset of cellulose pyrolysis, the effectiveness of the catalytic activity of AAEMs on dehydration reactions has been also demonstrated.

By adding 0.1 mmol/$g_{cellulose}$ of Na^+ and K^+, Gargiulo at al.[185] observed an increase of char yield with respect to pure cellulose; such a result was more pronounced in the case of Na^+-doped samples at low heating rates (19 and 14 wt % for Na^+- and K^+-doped samples, respectively, instead of 5 wt % of pure cellulose, at 700 °C). A similar trend was observed by Zhao et al.[209] during TG experiments at 10 °C/min up to 700 °C. Conversely, Na^+ and K^+ were found to be almost equivalent in increasing the char yield in other studies conducted under fast pyrolysis conditions.[210] It can be speculated that under conditions where the dehydration reactions are less favored, the difference between the two cations is attenuated. However, it is not easy drawing a conclusive trend since the doping procedures and the way to express the content of the doping agent are not standardized. Indeed, some authors compare the effect of different types of cations added to the sample using the same weight percentage of the ion or of the corresponding salts, overlooking the difference in terms of molar contents, possibly achieving misleading conclusions in apparent contrast with other literature results. For example, Zhao et al.[209] concluded that Na^+ is more effective than K^+ in increasing char yield. Even though this agrees with the trend observed by doping the cellulose with the same amount of ions on a molar basis,[185] it is likely that the higher activity of Na^+ in increasing char yield is due to its high concentration in the doped sample[209] (0.019 and 0.014 mmol/$g_{cellulose}$ for Na^+ and K^+ doped samples, respectively). Conversely, Patwardhanet al.[150] observed the opposite effect between two alkali ions and, even more, a higher activity of K^+ with respect to Ca^{2+} and Mg^{2+}, probably because of the highest molar concentration of this cation in the doped sample.

Despite the stronger Lewis acidity of Mg^{2+}, Patwardhan et al.[150] found comparable char yields for the Ca^{2+}- and Mg^{2+}-doped samples (12.7 and 13.7 wt %, respectively), even if the former was present in higher molar concentration (0.16 and 0.11 mmol/$g_{cellulose}$ for Ca^{2+} and Mg^{2+}, respectively), and Zhu et al.[213] confirmed this trend. This result confirms that both primary and secondary reactions should be considered for the determination of the char yield. According to Liu et al.,[212] Mg^{2+}, a cation with a higher Lewis acidity, can affect dehydration reactions of cellulose more than Ca^{2+}, producing more primary char and less sugar structures. Given the lower amount of sugars, the production of secondary chars from sugar decomposition could be reduced. The relative weight of these two char fractions could be affected not only by the type of cation but also by the loading level, and both aspects will determine the final char yields. High cation loading greatly decreases sugar production, thus reducing the weight of the secondary char on the final char yield. Conversely, lower loading levels produce more sugars, thus increasing the probability of forming more secondary char.

https://doi.org/10.1021/acs.energyfuels.0c04046
Energy Fuels 2021, 35, 5407−5478

Table 6. Selected Scientific Papers Investigating the Effect of AAEMs on Cellulose Pyrolysis Since 2010

Feedstock	Experimental apparatus	T (°C)	HR (°C/min)	Doping method	Metallic ion	Counterion	Metallic ion content (mmol/$g_{cellulose}$)	Main results	ref
cellulose fibers (Sigma-Aldrich)	TG, thin bed reactor	700	4	wet impregnation	Na^+, K^+	Cl^-	0.1	Na^+ reduced condensable fraction yield. K^+ does not affect condensable fraction yield. Levoglucosan, HMF, and furfural yield decrease by 40%, 42%, and 81% respectively, and furfuryl alcohol increases by 126%.	185
cellulose fibers (Sigma-Aldrich)	TG, thin bed reactor	700	5	wet impregnation	K^+	Cl^-	0.07 0.15 0.27 0.41	K^+ shifts the main pyrolysis stage toward lower temperatures, decreases maximum devolatilization rate, and increases char yield. At low temperature, K^+ catalyzes char and gas formation. At high temperatures, K^+ promotes light oxygenates and char production, inhibiting levoglucosan formation. High K^+ concentration increases char and gas yields and decrease bio-oil yield.	68
microcrystalline cellulose (Sigma-Aldrich)	TG	700	10	physical mixng	Na^+ K^+	CO_3^{2-} Ac^- CO_3^{2-} Ac^-	0.019 0.012 0.014 0.010	Both alkali ions promote char formation. Na^+ and K^+ have higher catalytic activity in form of carbonates[b].	209
cellulose fibers (Sigma-Aldrich)	single shot micro-furnace	500	fast pyrolysis	wet impregnation	Na^+ K^+ Mg^{2+} Ca^{2+}	Cl^- Cl^- OH^- NO_3^- CO_3^{2-} HPO_4^{2-}	0–0.5 (ca.)	Condensable fraction from control sample at 400 °C is rich in anhydro sugars. At 600 °C, levoglucosan (48 wt %) and formic acid (28 wt %) are mostly produced. Cation activity on char yield is in the order of $K^+ > Mg^{2+} > Ca^{2+} > Na^+$[b]. Inorganic salts/ash doping decreases levoglucosan yield and increases glycolaldehyde yield. Ca^{2+} anticipates pyrolysis onset temperature. Mg^{2+} and Na^+ increases char yield in the order of $Mg^{2+} > Na^+$ (7- vs 5-fold).	150
cellulose fibers (Sigma-Aldrich)	micro-pyrolyzer	500	fast pyrolysis	wet impregnation	Na^+ K^+ Mg^{2+} Ca^{2+}	Ac^-	0.05 0.05 0.05 0.05–0.3	AAEMs reduce hydrocarbon yields in the order of $K^+ > Na^+ > Ca^{2+} > Mg^{2+}$. AAEMs increase the formation of thermally derived CO_x (about 2-fold in case of K^+ for both CO_2 and CO) and char (about 3-fold in case of both K^+ and Na^+) while decrease the condensable fraction.	210
cellulose fibers (Sigma-Aldrich)	drop tube, fixed bed	150–400	fast pyrolysis	wet impregnation	Na^+	Cl^-	0.025[a]	At 150 °C, Mg^{2+} is more effective in promoting formation of water-soluble intermediates (i.e., sugar and anhydro-sugar oligomers.)	211

https://doi.org/10.1021/acs.energyfuels.0c04046
Energy Fuels 2021, 35, 5407–5478

Table 6. continued

Feedstock	Experimental apparatus	T (°C)	HR (°C/min)	Doping method	Metallic ion	Counterion	Metallic ion content (mmol/$g_{cellulose}$)	Main results	ref
					Mg^{2+}	Cl^-		At 250 °C, both Na^+ and Mg^{2+} promote destruction of sugar ring structures, inhibit conversion of water-insoluble portion into water-soluble portion, and increase char yield during cellulose pyrolysis.	
								Yield of water-soluble intermediates from Na^+-doped cellulose yield is similar to the one from raw cellulose up to 250 °C but increases continuously up to 325 °C.	
								For Mg^{2+}-doped cellulose, the yield of water-soluble intermediates has a maximum at 250 °C.	
								Mg^{2+} increases formation of both anhydro-sugar and sugar oligomers at low temperature. Na^+ and Mg^{2+} promote formation of non-sugar products in both water-soluble and water-insoluble portions of solid residues from cellulose pyrolysis.	
cellulose fibers (Sigma-Aldrich)	pyroprobe	500	fast pyrolysis	wet impregnation	K^+	Cl^-	0−0.1[a]	In cellulose pyrolysis, K^+ and Ca^{2+} increase yields of volatile products and increase char yield.	9
					Ca^{2+}			K^+ has a higher inhibitory effect on formation of levoglucosan and favors light oxygenates (CO_2, HAA, acetic acid and acetol) except methyl glyoxal, while Ca^{2+} favors HMF, and levoglucosenone and has a stronger catalytic effect on secondary reactions of reaction intermediates.	
								Effect of Ca^{2+} on levoglucosan is enhanced during pyrolysis of cyclodextrin compared to cellulose.	
maltosan (Sigma-Aldrich)								Effects of K^+ on levoglucosan formation from different feedstocks follow the order of cellulose > cyclodextrin > maltosan.	
								In cyclodextrine and maltosan pyrolysis, K^+ and Ca^{2+} suppress HAA, acetol, and methyl glyoxal formation and promote char and CO_2 production.	
cyclodextrine (Sigma-Aldrich)									
microcrystalline cellulose (Sigma-Aldrich)	drop tube, fixed bed	325 at different holding times	fast pyrolysis	wet impregnation	Na^+	Cl^-	0.025[a]	Mg^{2+} and Ca^{2+} are more effective than Na^+ and K^+ to catalyze dehydration reactions of sugar structures.	212
					K^+			Depolymerization reactions are less influenced by AAEMs.	
					Mg^{2+}				
					Ca^{2+}				
microcrystalline cellulose (Alfa Aesar)	micro-pyrolyzer	500	fast pyrolysis	wet impregnation	Ca^{2+}	NO_3^-	0.025−0.5	Metal oxides have a negligible impact on distribution of cellulose pyrolysis products.	213
					Mg^{2+}		0.025−0.6	AAEMs affect primarily secondary reactions of volatile species within molten cellulose.	
				dry mixing	Ca^{2+}	O^{2-}	0.025−0.5	Ca^{2+} is more active than Mg^{2+} in promoting primary char formation, conversion of levoglucosan to light oxygenates and furans, and consumption of furans to secondary char and permanent gases.	
					Mg^{2+}		0.025−0.6	Ca^{2+} and Mg^{2+} increase the yield and C/O ratio of the condensable fraction and increase the yield of low molecular weight species.	
microcrystalline cellulose (Sigma-Aldrich)	screen heater	530	fast pyrolysis	wet impregnation	K^+	CO_3^{2-}	0.000014−0.14	K^+ decreases the yield of the condensable fraction from 0.96 to 0.52 g/g).	214

https://doi.org/10.1021/acs.energyfuels.0c04046
Energy Fuels 2021, 35, 5407−5478

Table 6. continued

Feedstock	Experimental apparatus	T (°C)	HR (°C/min)	Doping method	Metallic ion	Counterion	Metallic ion content (mmol/$g_{cellulose}$)	Main results	ref
						Cl^-	0.013	Anions depress levoglucosan formation in the order of Cl^- > OH^- > CO_3^{2-}.[b]	
						OH^-	0.018	the comparison is valid even if molar concentrations of salts are different because the salt exhibiting the highest activity is the one at the lowest concentration.	

[a]Expressed as mol of ion per mol of glucose unit. [b]The comparison made at the same weight concentrations of the ion/salt.

Overall, it can be concluded that the catalytic activity on dehydration reactions is higher for alkaline earth metals than for alkalis metals.[211,212]

AAEMs also affect the two competing pathways 2 and 4 (Figure 6). Pathway 2 occurs through the above-mentioned concerted mechanism and leads to oligomers forming levoglucosan and anhydrosugars through the levoglucosan-end mechanism[198] and levoglucosenone after dehydration reactions (pathway 7, Figure 6). Pathway 4 proceeds through ring opening reactions producing light oxygenates and permanent gases. However, other mechanisms (pathways 5 and 6, Figure 6) concur to the formation of light oxygenates, and they consist in the secondary decomposition of reaction intermediates (e.g., reducing-end sugars, anhydrosugars).

AAEMs catalyze the ring opening reactions directly from the cellulose structure leading to the formation of light oxygenates (especially formic acid, glycolaldehyde, and acetol) likely because of the interactions of the cations with the ring oxygen. As a result of competition among the pathways, lower levoglucosan yields were observed when metal-loaded samples are considered.[150,185] Light oxygenates were found to increase at low Ca^{2+} and K^+ loadings and to decrease at high loadings during cellulose pyrolysis.[9] As observed for char, also light oxygenates yield result from the relative weight of primary and secondary formation mechanisms. Leng et al.[9] compared the effect of increasing metal ions loading on cyclodextrin and cellulose, and they observed that during cycoldextrine pyrolysis light oxygenates production is depressed by the presence of metal ions. Since in the case of ciclodextrine they cannot be produced directly through ring opening reactions, but only through secondary decomposition of reaction intermediates, it can be concluded that Ca^{2+} and K^+ favor secondary char- and gas-forming reactions instead of light oxygenates production. Conversely, in the case of cellulose, where light oxygenates can be produced also from direct decomposition of the cellulose sugar rings, Ca^{2+} and K^+ favor this mechanism competing with levoglucosan formation. However, at high ions loading, especially for Ca^{2+}, as observed for cyclodextrin, Ca^{2+} and K^+ catalyze secondary char and gas formation producing lower amounts of light oxygenates. As for the reduction of levoglucosan yield, the following trend has been observed under fast pyrolysis: K^+ > Na^+ > Ca^{2+} > Mg^{2+}.[9,150]

The catalytic activity of K^+ is strongly correlated with the DP as demonstrated by Leng et al.,[9] who showed an enhanced effect of K^+ in reducing levoglucosan yield from cellulose with respect to cyclodextrin and maltosan. However, since Ca^{2+} acted as a catalyst in levoglucosenone production,[9] it could be inferred that the reduction of levoglucosan yield was due also to the increased dehydration to levoglucosenone.

Furans from cellulose pyrolysis consist basically in HMF, furfural, and furfurhyl alcohol, with the former prevailing on the other species. Their formation pathway (pathway 3, Figure 6) is initiated by the homolytic cleavage of the glycosidic bond leading also to light oxygenates[188] (pathway 2, Figure 6).The production of furfural and HMF through levoglucosan secondary reactions was also postulated; however, recent literature results supported their direct formation through ring opening and rearrangements reactions,[202] and such a pathway was found to be catalyzed by Ca^{2+}.[9]

Some studies investigated the effect of the counterion on the catalytic activity of alkali and alkaline earth ions. It was quite hard to compare the effect of the different anions since, as for the cations, the comparison was made at similar concentrations of

https://doi.org/10.1021/acs.energyfuels.0c04046
Energy Fuels 2021, 35, 5407−5478

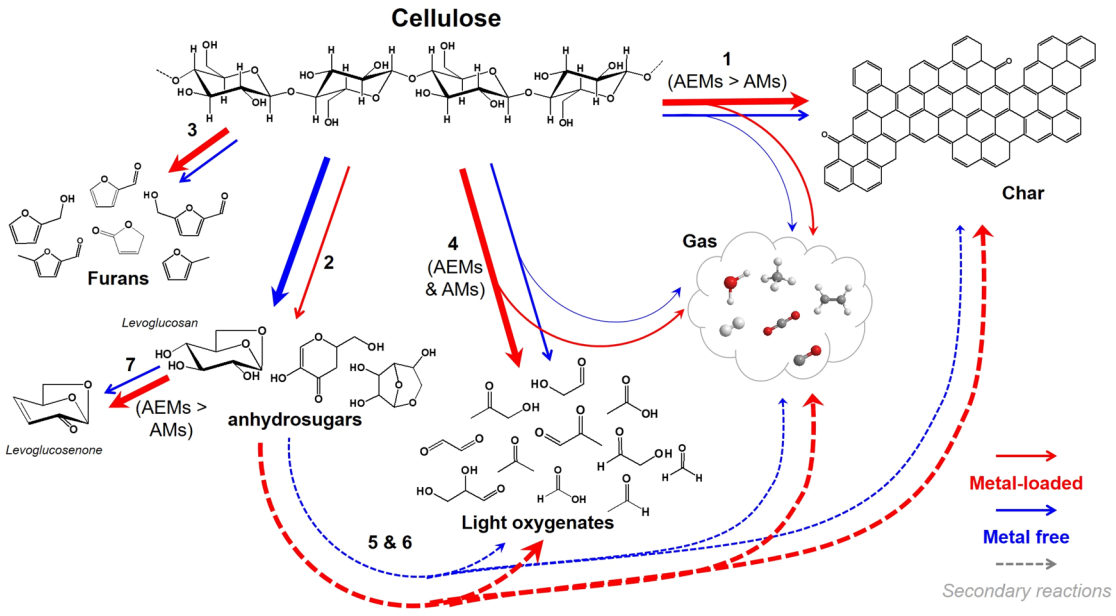

Figure 6. Effects of alkali metals (AMs) and alkali earth metals (AEMs) on primary and secondary reactions during cellulose pyrolysis. The size of the arrow reflects how favorable the pathway is with (red color) or without (blue color) metal ions; the larger the arrow is, the more favored the pathway is.

the salts on a weight percentage, thus corresponding to a different concentration on a molar basis. However, despite this difficulty, some speculations can be drawn. Patwardhan et al.[150] compared cellulose samples doped with different calcium salts and found that the effect of anions in decreasing thelevoglucosan yield follows the order of Cl^- > NO_3^- ≈ OH^- ≈ CO_3^{2-} > HPO_3^{2-}. Conversely, Fu et al.[215] established a different order for different potassium salts, namely, HCO_3^- > OH^- > Cl^- > CO_3^{2-}. Finally, Marathe et al.[214] found that in the case of levoglucosan the anions were active in the following order: Cl^- > OH^- > CO_3^{2-}. Considering the anions concentration on a molar basis, it is possible to conclude that among the different anions, the highest activity expressed by HCO_3^- is still valid since this anion has the lowest concentration in the doped sample.[215] The higher activity of Cl^- with respect to CO_3^{2-} observed by both Patwardhan et al.[150] and Marathe[214] is also confirmed since in both the cases Cl^- has a lower concentration in the doped samples. Finally, the lowest activity of HPO_3^{2-} among Cl^-, NO_3^-, and OH^- is confirmed since its molar concentration is the highest.[150] Nothing can be said about the relative effect of acetate and carbonate anions on charring reactions because the observed higher activity of carbonate[209] corresponds to a higher concentration of the salt on a molar basis.

Zhu et al.[213] observed that metal oxides have a negligible impact on the distribution of cellulose pyrolysis products; however, in this case, also the doping method could contribute to the observed lower activity. Metal ions in impregnated biomass were found to be uniformly dispersed[216] also because the wet impregnation allows for an ion exchange with the cations naturally present in biomass,[217] whereas dry mixing is not able to penetrate the compact crystalline structure of cellulose fibers.

5.2. Effect of AAEMs on Hemicellulose Decomposition.

As mentioned in Subsection 3.1, the hemicelluloses family includes many types of polysaccharides, such as xylans, mannans, xyloglucans, and mixed-linkage β-glucans. The thermal decomposition of the different monosaccharides in hemicellulose structures revealed that, overall, the products were similar from a qualitative point of view, but their relative abundances are different. Furans, ketones (mainly 1-hydroxy-2-propanone and furanone), and anhydrosugars (furanose and pyranose ring anhydrosugars for pentoses and hexoses, respectively) were the major products, with furfural being the most abundant among furans.[218,219] Differently from xylose and arabinose (pentose sugars), mannose and galactose (hexose sugars) also produced HMF.[220] The presence of uronic acids and acetyl groups mainly contribute to the formation of CO_2, formic acid, and acetic acid.[164,221]

In each hemicellulose type, the monosaccharides are organized in a complex polysaccharide structure, opening a wider spectrum of possibilities during biopolymer thermal decomposition. The hemicellulose pyrolytic behavior, indeed, depends not only on the mono/polysaccharide type but also on the thermal stability of the structure of the specific hemicellulose[156] (branching, glycosidic bond types, side groups). For example, hexose sugars are more thermally stable than pentose sugars. The more variegated and branched their organization is within the hemicellulose, the higher the probability of producing multiple types of macromolecular radicals (through the cleavage of glycosidic bonds) undergoing polymerization reactions to form char.[222] Thus, the investigation of pyrolysis chemistry of the various hemicelluloses can provide insights into the comprehension of the different decomposition mechanisms. In this regard, as described in detail in Subsection 4.2, also the extraction procedures should be considered as a factor affecting the chemical and structural variations of hemicelluloses. However, the main decomposition mechanisms were identified and supported also by recent studies adopting molecular simulations for pyrolysis of simple model molecules.[8]

At low temperature, O-acetyl groups at the C2 and C3 positions of the monosaccharides in the hemicellulose structure dissociate via cleavage of the C−O oxygen-bridged bond to yield acetic acid[222] or acetaldehyde,[223] with the former being the most favored. On the contrary, the formation of hydroxyacetaldehyde is prevented by the presence of an unsaturated C═C bond formed after scission of the O-acetyl group.[223] In the case of xylans, the main oligosaccharide backbone decomposes[222,224] to

https://doi.org/10.1021/acs.energyfuels.0c04046
Energy Fuels 2021, 35, 5407−5478

Table 7. Selected Scientific Papers Investigating the Effect of AAEMs on Hemicellulose Pyrolysis

Feedstock	Experimental apparatus	T (°C)	HR (°C/min)	Doping method	Metallic ion	Counterion	Metallic ion content ($mmol/g_{feedstock}$)	Main results	ref
xylan from beechwood (Sigma Aldrich)	TG	700	10	physical mixng	Na^+	CO_3^{2-}	1.9	The onset of xylan decomposition moves toward lower temperatures in presence of metallic salts.	209
					Na^+	Ac^-	1.2		
					K^+	CO_3^{2-}	1.4		
					K^+	Ac^-	1.0		
								All salts promote dehydration reactions and condensation reactions, are responsible for chars formation, and increase reactivity of branched chains.	
								Two peaks of the weight loss rate curve (dehydration and decomposition) were overlapped in presence of salts.	
switchgrass hemicellulose	single shot micro-pyro-lyzer	500	fast	wet impregnation	Na^+	Cl^-	0.86	AAEMs promote formation of noncondensable gases (mainly CO_2), light oxygenates, furfural, and char at the expense of anhydro xylose, xylose, and dianhydro xyloses. Na^+ and K^+ led to a decrease in xylose yield from 5 wt % to 2.2 and 1.6 wt %, respectively, while no sugars were detectable upon addition of alkaline earth metals.	164
					K^+		0.67		
					Mg^{2+}		0.53		
					Ca^{2+}		0.45		
								Alkali ions increase formation of CO_2 to a greater extent than the alkaline earth ions.	
								Results could be affected by higher molar concentration of alkali ions.	
								Char yield increases from 10.7 wt % for purified hemicellulose to 17.5 wt % in presence of alkali ions and 28−29 wt % in presence of alkaline earth ions.	
								Acetaldehyde yield increases in presence of alkali ions but decreases in presence of alkaline earth ions.	
								Formic acid and acetol yields decrease for all treatments.	
								Acetic acid yield increases with alkali ions and is not affected by alkali earth ions.	
								Furfural yield increases 70% in presence of alkali ions and 5-fold in presence of alkaline earth ions.	
								Switchgrass-derived ash suppresses the formation of furfural, dianhydro xylopyranose, and anhydroxylo-pyranose.	
xylan from birchwood (Carl Roth)	quartz reactor	450	5	dry mixing	K^+	CO_3^{2-}	0.72	The yield of the condensable fraction decreases in presence of K_2CO_3 and is enriched in aliphatic hydrocarbons.	233
xylan from oat spelt (Sigma-Aldrich)	TG	600, 900	25	wet impregnation	K^+	Ac^-	0.10	Pyrolysis products yields and characteristic temperatures are unchanged upon addition of K^+.	230
	micro-pyro-lyzer		fast						
xylan from beechwood (TCI chemicals)	entrained flow reactor	500	fast	dry mixing	Ca^{2+}	O^{2-}	10.75	Untreated xylan oil consist of catechols, which disappear with Ca^{2+} based-compounds pretreatments.	234
					Ca^{2+}	CHO^{2-}		Salt addition promotes the formation of alkylated cyclopentenones.	

https://doi.org/10.1021/acs.energyfuels.0c04046
Energy Fuels 2021, 35, 5407−5478

Table 7. continued

Feedstock	Experimental apparatus	T (°C)	HR (°C/min)	Doping method	Metallic ion	Counterion	Metallic ion content (mmol/$g_{feedstock}$)	Main results	ref
xylan from beechwood (Sigma-Aldrich)	TG, slow pyrolysis reactor	600, 700	5	demineralization through cation exchange resin	ash (mainly Na^+, Ca^{2+}, K^+)		Control: Na^+ 0.93, Ca^{2+} 0.12, K^+ 0.004.	The onset decomposition temperature of raw xylan is anticipated with respect to demineralized xylan.	154
							Demineralized sample: Na^+ 0.039, Ca^{2+} 0.026, K^+ n.d.	The two main peaks of the weight loss rate curve of raw xylan merge into one peak in the corresponding curve of demineralized xylan.	
								Raw xylan produces higher yield of char at the expense of the condensable fraction compared to demineralized xylan.	
								Demineralized xylan produces a higher yield of furfural and a lower yield of furfuryl alcohol compared to raw xylan.	
								The yield of dehydrate xylose sugars increases after demineralization.	
								Furfural yield is lower (about 0.07 wt % feedstock) than the one obtained in presence of steam (18 wt %), thus implying a relevant role of steam in the mechanism of furfural production.	
xylan from beechwood (Sigma-Aldrich)	slow pyrolysis reactor	700	7	demineralization through cation exchange resin	ash (mainly Na^+, Ca^{2+}, K^+)		Control: Na^+ 0.93, Ca^{2+} 0.12, K^+ 0.004.	K^+ promotes char and gas production (mainly CO_2) at the expense of the condensable fraction.	154
							Demineralized sample: Na^+ 0.039, Ca^{2+} 0.026, K^+ n.d		
				doping through cation exchange resin	K^+	Cl^-	0−0.031	At low doping levels, K^+ affects the yields of all pyrolysis products, while at high doping levels it affects only gas and liquid yields.	
								K^+ enhances CO release rate at low temperatures, where CO is released by carbonyls left from dehydration reactions of side-chain groups, while it depresses CO release at higher temperatures.	
								These two opposite effects do not produce changes in the final CO yield at low doping levels, while the CO yield increases at high doping levels. At high temperature, K^+ enhanced CH_4 and H_2 release.	
								At low doping levels, K^+ increases the CO_2 release rate in the lower temperature region, whereas the peak in the upper temperature region remains unchanged.	
								At higher doping levels, CO_2 is only slightly affected by further addition of K^+.	
								Both the first and the second peaks in the CO_2 release rate curve increase.	
xylan from beechwood (Megazyme)	TG quartz tube micro-pyrolyzer	400 220−340 255−590	10 10 fast	demineralization through acid washing (HCl in methanol)	ash (mainly Na^+ and Ca^{2+})			Raw xylan, containing Na^+ uronate groups, degrades over two different temperature ranges (identified as cleavage of xylan in xylose units and decomposition of xylose) differently from demineralized xylan, with free uronic acid groups, which degrades producing only one peak in the weight loss rate curve.	167
								Free uronic acid groups promote of furfural and 4-hydroxy-5 and 6-dihydro-2H-pyrtheformationan-2-	

https://doi.org/10.1021/acs.energyfuels.0c04046
Energy Fuels 2021, 35, 5407−5478

Table 7. continued

Feedstock	Experimental apparatus	T (°C)	HR (°C/min)	Doping method	Metallic ion	Counterion	Metallic ion content ($mmol/g_{feedstock}$)	Main results	ref
								one, while Na^+ uronate groups enhance fragmentation and deoxygenation reactions.	
xylan from beechwood (Sigma-Aldrich)	TG, pyrolyzer	700	5	demineralization through cation exchange resin	ash (mainly Na^+, Ca^{2+}, K^+)		Control: Na^+ 0.93, Ca^{2+} 0.12, K^+ 0.004.	CO and CO_2 follow a similar trend as the one observed in presence of K^+ in Giudicianni et al.[154]	235
							Demineralized sample: Na^+ 0.039, Ca^{2+} 0.026, K^+ n.d		
				doping through cation exchange resin	Na^+	Cl^-	0.046−0.49	Na^+ favors the production of propionic acid.	
								With increasing Na^+ cotent, the yield of formic and acetic acids, furfural, and other furans have a nonmonotonous trend.	
								Na^+ increases formation of low molecular weight compounds (hydroxy-ketones).	
xylan from beechwood (Sigma-Aldrich)	TG, slow pyrolysis reactor	700	7	wet impregnation, cation exchange	Na^+, K^+	Cl^-	Control: Na^+ 0.039, Ca^{2+} 0.026, K^+ n.d.	Metal ions in the form of chloride salts have a negligible effect on xylan pyrolysis when added through wet impregnation instead of cation exchange.	232
							K-doped sample (wet impregnation): K^+ 0.0077−0.38, Na^+ 0.039, Ca^{2+} 0.026.		
							K^+-doped sample (cation exchange): K^+ 0.307, Na^+ 0.039, Ca^{2+} 0.026.		
							Na^+-doped sample (wet impregnation): Na^+ 0.48, Ca^{2+} 0.026, K^+ n.d.		

https://doi.org/10.1021/acs.energyfuels.0c04046
Energy Fuels 2021, 35, 5407−5478

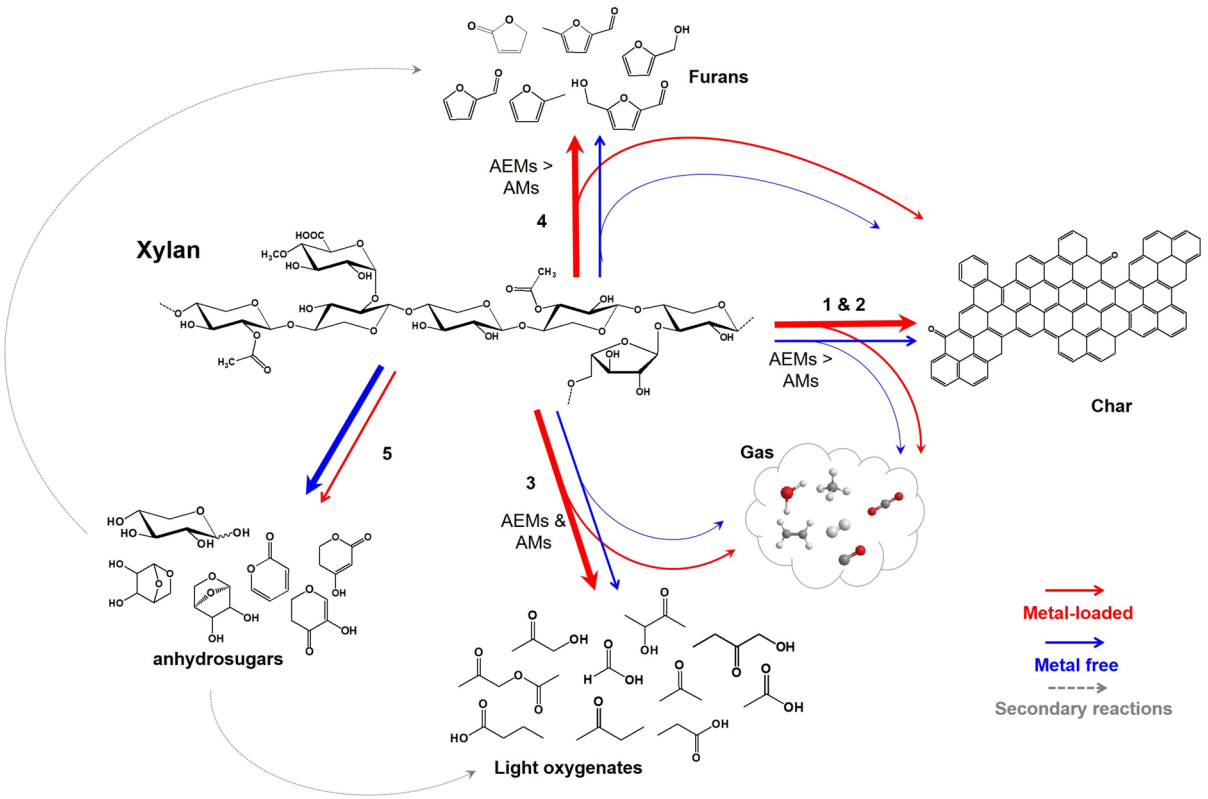

Figure 7. Effects of AMsAEMs on primary and secondary reactions during hemicellulose pyrolysis. The size of the arrow reflects how favorable the pathway is with (red color) or without (blue color) metal ions; the larger the arrow is, the more favored the pathway is.

form xylose and anhydrosugars.[155,164,225] Two competing reaction pathways are proposed for xylose decomposition, namely, dehydration to form anhydrosugars and ring opening reactions,[155,164,225] which convert xylose rings in the corresponding acyclic form undergoing a series of reactions leading to furfural (cyclization and dehydration) or, alternatively, light aldehydes and ketones[223,225,226] (through dehydration, enol-keto tautomerization, and retro aldol reactions). In the presence of 4-O-methylglucuronic acid units, Shen et al.[155] also proposed a second route for the formation of 2-furaldehyde from this unit; after cleavage of the glycosidic bond, ring opening and rearrangements occur through the elimination of CO_2 and methanol. 4-O-Methylglucuronic acid units were also supposed to contribute to the production of acetic acid through the cleavage of the carboxylic group.[155]

Two competitive pathways for anhydrosugars decomposition were postulated: dehydration to form dianhydrosugars or ring opening reactions to form lighter species, such as acetol and light aldehydes (methyl glyoxal and glycolaldehyde) as well as CO_2 and formic acid.[155,164]

Compared to cellulose, there are fewer studies focused on the effect of inherent metals on hemicellulose pyrolysis. However, this effect can be relevant since literature studies on wood chemistry revealed that most of the metal cations naturally present in biomass are impregnated in hemicelluloses.[227−229] To the best of our knowledge, only xylan was used as a hemicellulose proxy compound to study the effect of metal ions during pyrolysis. Xylan samples are mainly commercial materials and are extracted from hardwoods (beechwood and birchwood), switchgrass,[164] and oat spelt.[230] The xylan samples have been doped mainly with AAEMs. Both organic (acetate, formate) and inorganic salts (chlorides, nitrate, carbonates, oxides) have been used,[164,209,230−234] and the techniques used for doping were the same proposed for the cellulose: wet impregnation, dry mixing, and cation exchange.[164,209,231−236] However, the water solubility exhibited by xylan hampers a correct execution of the water impregnation procedure. Indeed, as underlined by Collard et al.[231] the impregnation solution cannot be removed by filtration but only by evaporation, leaving also precipitated salts in the sample.[231] Differently, the doping approach based on cationic exchange[232,235] takes advantage of the xylan water solubility ensuring a tight interaction between the metal ions and the polysaccharide,[232] and it avoids the presence of counterions that can hinder the catalytic effect of the added cations.

It is worth noting that commercial xylan samples can contain up to 6 wt % of ashes,[154,209] and if they are not removed before the doped sample preparation, their presence could attenuate the effect of further addition of metal ions by doping.[230] Giudicianni and colleagues demonstrated that beechwood xylan can be completely demineralized, and the glucuronic acid units present in its structure convert in the neutral form by using a cationic Dowex resin in the H-form.[154] The same authors showed that the demineralized beechwood xylan can be further doped with growing amounts of K^+ or Na^+ by using the same cationic Dowex resin in a K-form or Na-form, respectively,[235,236] and that such a procedure was more effective than wet impregnation for the investigation of the catalytic role of alkali ions in xylan pyrolysis.[232]

Table 7 summarizes the main studies conducted on this topic and the most relevant results. Figure 7 is a schematic representation of the effects of AAEMs on the primary and secondary reactions during hemicellulose pyrolysis.

https://doi.org/10.1021/acs.energyfuels.0c04046
Energy Fuels 2021, 35, 5407−5478

Xylan was often selected as a reference compound. It is worth noting that commercial xylan contains a relevant amount of metal ions contaminants[154] (mostly Na and Ca). Many studies neglected the effect of these metal ions providing misleading interpretation of the decomposition rate of this material obtained in thermogravimetric experiments, and sometimes, the metal doping produced only marginal effects probably because the alkali metal content of the raw xylan was already significant.[230] To gain insight on this aspect, some authors compared raw and demineralized xylan samples,[154,167] and they observed that raw xylan, containing mainly Na^+ ions bonded to the carboxylic group of the uronic acid, degrades over two different temperature ranges, producing two peaks in the weight loss rate curve. The two peaks come closer and merge in a single peak when demineralized xylan with free uronic acids degrades. It has been postulated that in the case of raw xylan, xylose units in the main chains allow the metal uronate group to decompose at lower temperatures (first peak in the weight loss rate curve), whereas the remaining xylose units decompose at higher temperature, producing a second peak.[167] The two weight loss peaks overlapped, and it was greatly anticipated when xylan was doped with high levels of Na^+ and K^+.[209]

Additionally, the doping procedure was found to affect the extent of the effect of metal ions on xylan pyrolysis. The results of Gargiulo et al.[232] revealed that the introduction of Na^+ and K^+ in the form of chloride salts through wet impregnation had only slight effects compared to doping through a cation exchange resin. It is likely that the cationic exchange approach ensures a more intimate contact and a tighter interaction between the polysaccharidic chain and the metal ions through ionic bonding. Moreover, a mitigation effect of the counterion (Cl^-) cannot be excluded when doping is performed through wet impregnation.[232]

As found for cellulose, also in the case of xylan-doped samples, many authors detected an increase of char and gas yields and a decrease of the condensable fraction yield.[154,164,209,232−236] The presence of metal salts promoted the formation of char, water, furfural, light oxygenated species, and gas at the expense of xylose, anhydro xylose, and dianhydro xylose.[154,164,167,209,235]

Among light oxygenates, alkali metals were found to rise acetaldehyde,[164] propionic acid, and hydroxy-ketones yields.[235] As for furfural production, opposing results were obtained by Giudicianni et al.[235] and Patwardhan et al.[164] by doping purified xylan and switchgrass hemicellulose, respectively. Patwardhan et al.[164] observed an increase of furfural in the Na^+-doped sample. On the contrary, Giudicianni et al.[235] showed that furfural yield had a nonmonotonous trend with Na^+ loading. However, the apparent disagreement could be explained by observing that the unique loading level of Na^+ doping studied in the case of switchgrass hemicellulose was higher than the loading range investigated in the case of purified xylan. Consequently, the observations of Giudicianni et al.[235] were related to doping conditions preceding the doping point investigated by Patwardhan et al.[164] Overall, this suggests that different competing mechanisms lead to the formation of furfural.[235] A similar conclusion can be achieved for carboxylic acids formation. In fact, Giudicianni et al.[235] observed a nonmonotonous trend of the yields of both formic and acetic acids at increasing Na^+ doping concentration, differently from Patwardhan et al.[164] that found a higher acetic acid yield and a lower formic acid yield for Na^+-doped hemicellulose.

As for the permanent gases, many authors[154,164,235,236] observed that the yield of CO_2 was significantly enhanced by the presence of Na^+ and K^+ or ash, whereas no significant change in the yield of CO was observed. The temperature profiles of CO_2 and CO release during slow pyrolysis experiments[154,235,236] revealed that the introduction of K^+ and Na^+ into the demineralized xylan sample affected differently the release rates of CO and CO_2. More specifically, by increasing the alkali ion content, the two peaks of the CO_2 release rate curve observed for the demineralized xylan behaved differently; the low temperature peak increases, whereas the peak in the upper temperature region remains unchanged. Overall, the CO_2 yield increases. As for CO, the presence of alkali ions clearly enhanced its release rate at low temperature, where CO is mainly released by the carbonyls left from dehydration reactions of side-chain groups. On the contrary, the presence of increasing amounts of alkali ions depresses the production of CO at higher temperature and promote CH_4 and H_2 formation.[154,235,236] Overall, the promotion of CO release in the lower temperature region was counterbalanced by the reduced CO release at higher temperatures.

In the end, it is possible to state that at low temperature alkali ions promote dehydration reactions and decomposition of side groups (pathways 1 and 2, Figure 7) forming char, water, CO_2, and CO, carboxylic acids), whereas at high temperature, they catalyze the ring scission (pathway 3, Figure 7) forming CO_2 and light oxygenates and dehydration reactions (pathway 4, Figure 7) forming furfural and char in competition with depolymerization, water addition, and sugar dehydration (pathway 5, Figure 7) forming anhydro xylose, xylose, and dianhydro xyloses.

The increased proportions of aliphatic hydrocarbons in the condensable fraction and the reduced proportion of oxygen containing groups may be attributed to the enhanced dehydration reaction in the presence of alkali ions.[233]

A different activity of AAEMs was observed.[164] Alkaline earth metals favor char and furfural production more than alkali metals, even though their molar concentration in the hemicellulose-doped sample was lower compared to that of alkali metals. The opposite trend was observed for CO_2, whereas acetic acid yield was not affected by alkali earth metals. However, it should be pointed out that alkaline earth metals were present in lower molar concentration than alkali metals and that the observations refer to one loading level. Different trends could be revealed if a range of doping levels would be investigated.[235]

5.3. Effect of AAEMs on Lignin Decomposition. Many authors investigated the decomposition pathways of lignin during pyrolysis. They pointed out that the complex structure of this macromolecule varies greatly depending on the plant species. Consequently, due to this variety as well as the difficulty of extracting native lignin without altering its original chemical structure, the study and the comprehension of the detailed reaction mechanisms have always been very challenging. A detailed description of the lignin macromolecule and its decomposition pathways can be found in ref 7. Overall, its conversion is mainly due to depolymerization of the polyaromatic structure and to the fragmentation of the propyl chains. These reactions produce a relevant amount of aromatic condensable species and gas, whereas the repolymerization reactions between aromatic rings represent the main pathway for char formation. Given the presence of three types of monomers and many substituted functional and oxygenated groups (phenolic hydroxyl, methoxyl, hydroxyl, carboxyl, and carbonyl groups), the types of bonds between the individual units are also very different, and they determine a distinct thermal stability of the macromolecule during pyrolysis. The cleavage of the ether

https://doi.org/10.1021/acs.energyfuels.0c04046
Energy Fuels 2021, 35, 5407−5478

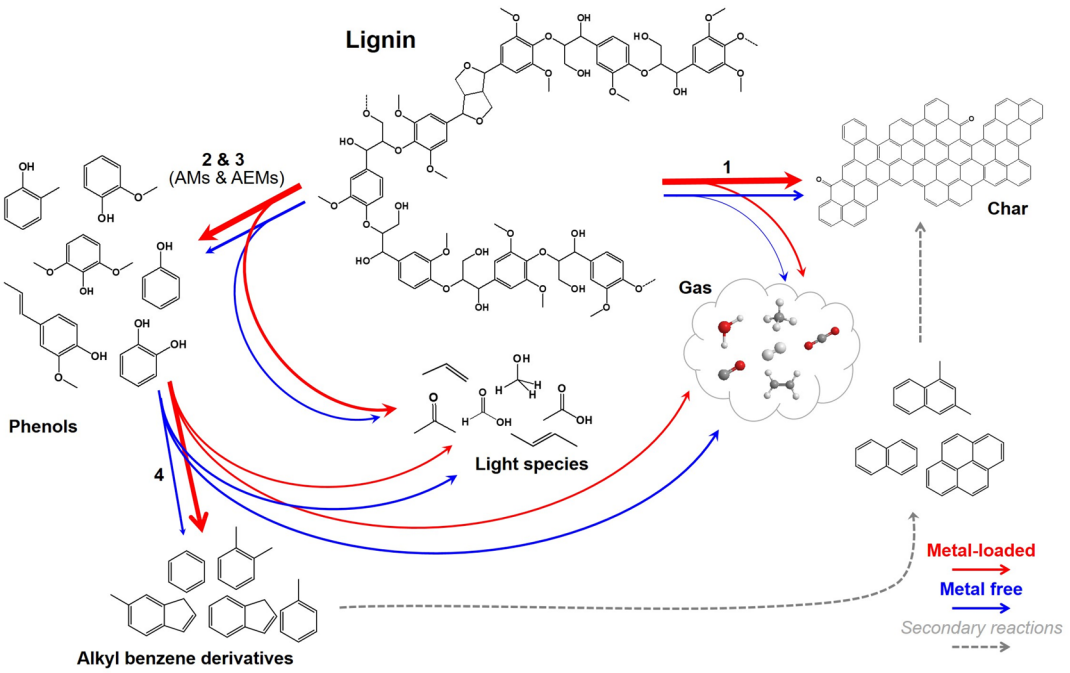

Figure 8. Effects of AMs and AEMs on the thermal decomposition of lignin. The size of the arrow reflects how favorable the pathway is with (red color) or without (blue color) metal ions; the larger the arrow is, the more favored the pathway is.

bond in its different forms, β−O−4 (the most frequent ether bond) and α−O−4, was investigated using different dimers as model compounds. It was found that for β−O−4 cleavage the most favored decomposition mechanism depends on the temperature[237−239] and on the methoxy substituents group in proximity of the ether bond.[240−242] However, many authors agree that α−O−4 cleavage was initiated by hemolytic reactions,[243−245] and this bond is less stable than β−O−4. Carbon−carbon bonds have a lower reactivity than ether bonds as the cleavage of linkages between carbon atoms in different aromatic rings is required. Their reactivity is affected also by the presence of alkyl, methyl, and hydroxyl groups in proximity of the bond, and among the different types of C−C bonds, Cα−Cβ bond in the β−1 linkage is characterized by the lowest stability.[224,238,246,247] Figure 8 is a schematic representation of the main decomposition pathways and of the effects of AAEMs on the primary and secondary reactions during lignin pyrolysis.

The phenyl compounds formed after the cleavage of aryl linkages (pathway 2, Figure 8) can evolve through secondary reactions. The propyl side chains on phenyl compounds are removed to form syringil units and guaiacyl units, and at high temperature, syringyl units release methoxy groups to form phenol and cathecol (pathway 3, Figure 8). The decomposition of methoxy groups can form methanol or methane (pathway 3, Figure 8). The hydroxyl groups are released at low temperature to form syringil and guaiacyl units with unsaturated side chains, whereas the decomposition of carboxyl and carbonyl groups produce CO_2, CO, and formaldehyde (pathway 3, Figure 8). In the end, two other important pyrolysis pathways leading to the formation of primary and secondary chars should be mentioned; primary char can be produced by the direct carbonization of lignin (pathway 1, Figure 8), while secondary char can be formed by the repolymerization of phenols derivatives[248] (Figure 8).

Lignin doping with specific ions (Li^+, Na^+, K^+, Cs^+, Mg^{2+}, Ca^{2+}, Ba^{2+}, Cu^{2+}[171,174,175,249]) has been widely performed. Wet impregnation with salts using distilled water[171,173,175,249] or ammonia solutions[231] followed by filtering and washing to remove any unbound metal ions has been widely adopted. This approach ensures homogeneous infusion of the salts into the lignin. The excessive impregnation method is also used[250] (KCl, $CaCl_2$, $FeCl_3$). Lignin is impregnated with metal salts solutions by ultrasonic immersion (0.5 h) and subsequent static immersion (12 h) followed by water evaporation. In the case of alkali ions (Na^+, K^+), both NaOH and Na_2CO_3 salts have been used,[171] but nitrate salts ($Fe(NO_3)_3{\cdot}9H_2O$, $Ni(NO_3)_2{\cdot}6H_2O$, KNO_3) have been preferred[231,249] because nitrates volatilize during heating, leaving negligible residue and do not add carbon to the samples, which would modify the carbon balance. AAEMs as acetate salts[175] have been also used because they decompose upon heating to pyrolysis temperatures, thus releasing AAEMs in a catalytically active form. Calcium oxide and calcium formate (CaO and $Ca(HCOO)_2$) were chosen in some specific studies[234] because calcium formate showed a particular action as a hydrogen donor and calcium oxide showed a significant deoxygenation activity. In some cases, alkaline ions in the forms of NaOH, KOH, Na_2CO_3, K_2CO_3,[172,173,209] CaO, and $Ca(HCOO)_2$[234] and HMs ($ZnCl_2$,[233] $FeSO_4$[251]) were introduced into the lignin by direct dry mixing.

Table 8 lists the relevant studies reporting the effect of alkali and alkaline earth ions on lignin pyrolysis, and the main results of these studies are summarized.

Demineralization of commercial lignin samples produced a different behavior during the thermal treatment when compared to the untreated samples. However, the obtained results seem to be influenced by the demineralization procedure. Sharma et al.[253] revealed that alkali lignin washed with hydrochloric and nitric acids produced more char and less condensable fraction than the raw sample. Conversely, alkali lignin samples washed with hydrofluoric acid produced a slightly lower char yield despite the reduction of the ash content.[176] However, the apparent contrast could be explained by the different strengths

https://doi.org/10.1021/acs.energyfuels.0c04046
Energy Fuels 2021, 35, 5407−5478

Table 8. Selected Scientific Papers Investigating the Effect of AAEMs on Lignin Pyrolysis

Feedstock	Experimental apparatus	T (°C)	HR (°C/min)	Doping method	Metallic ion	Counterion	Metallic ion content mmol/$g_{cellulose}$	Main results	ref
lignin alkali (Sigma-Aldrich)	TG	700	10	dry mixing	Na^+	CO_3^{2-}	1.9	Metal ions depress char yield.	209
					Na^+	Ac^-	1.2		
					K^+	CO_3^{2-}	1.4		
					K^+	Ac^-	1.0		
different types of pulp	foil pulse pyrolyzer	620	fast	ion exchange	Na^+	Cl^-	0.049	Na^+ affects the pyrolysis pattern. The yields of guaiacol, vinyl guaiacol, phenol, and catechol increase.	252
					Ca^{2+}	Cl^-	0.054	Methylguayacol yield decreases.	
				wet impregnation	Na^+	HCO_3^-	0.361		
					Na^+	SO_4^{2-}	0.487		
alkali lignin (Fisher Scientific)	quartz tube reactor with different heated zones	250−920	n.a.	demineralization through acid washing	ash (mainly Na^+ and K^+)		Control: 5.7[a]. Demineralized sample: 1[a].	At low temperature, the removal of ash increases char yield at the expense of volatiles.	253
								At high temperature, the washed sample produces less PAH.	
lignin organosol (Sigma-Aldrich)	vertical Pyrex reactor	450	5	dry mixing	K^+	CO_3^{2-}	0.72	K^+ does not affect the yields of gas, char, and condensable fraction.	233
								In the condensable fraction, H/C of the doped samples increases, while O/C decreases.	
induline AT (Mead-Westvaco)	entrained flow reactor	500	fast	wet impregnation	Ca^{2+}	OH^-	3.4	Formate-doped samples produce less char and gas and more condensable fraction.	254
						$COOH^-$	3.8, 7.7	In the condensable fraction, H/C of formate-doped samples increases, while O/C decreases.	
								Formate-doped samples produce more aromatics with less methoxy/hydroxy functionalities.	
induline AT (Mead-Westvaco)	entrained flow reactor	500	fast	wet impregnation	Ca^{2+}	O, $COOH_2^-$	10.8	In both $Ca(HCOO)_2$- and CaO-doped samples, the concentrations of catechols decrease and the one of alkylated phenols increase.	234
								CaO is more effective in depressing catechols production.	
								CaO promotes PAH formation. m-Cresol was selectively formed with both Ca-based pretreatments.	
								Ca containing compounds pretreatments (CaO more than $Ca(HCOO)_2$)shifted the molecular weight distribution of the whole oil toward lower molecular weights.	
alkali lignin (TCI)	TG	800	10	excessive impregnation method	K^+, Ca^{2+}	Cl^-	1.3	Char yield decreases with Ca^{2+} doping, while increases with K^+ doping. At low temperature, Ca^{2+} promotes the production of carboxylic acids by depolymerization and recombination.	250
	pyrolyzer	600	fast					The maximum weight loss rate at intermediate temperature is reduced in K^+-doped samples. At high temperature, K^+ promotes the production of CO and CO_2.	
								The activation energy of the thermal decomposition in the intermediate temperature range is lower in Ca^{2+}-doped sample. In the high temperature range it increases in metal-doped samples.	

https://doi.org/10.1021/acs.energyfuels.0c04046
Energy Fuels 2021, 35, 5407−5478

Table 8. continued

Feedstock	Experimental apparatus	T (°C)	HR (°C/min)	Doping method	Metallic ion	Counterion	Metallic ion content mmol/$g_{cellulose}$	Main results	ref
								In the low temperature region, Ca^{2+}-doped samples produce more water. In the intermediate temperature region, both metal ions (especially K^+) produce more CO_2. At high temperature, they promote CH_4 and CO production. The condensable fractions of the doped samples are enriched in phenols.	

[a]Expressed as wt %.

of the acid used for the demineralization step. It is not clear if the observed results for the sample washed with hydrochloric and nitric acids are due to the reduction of ash content or to changes that may have occurred in the structure of lignin due to the acid treatment.[131] On the contrary, it has been demonstrated that demineralization of alkali lignin with hydrofluoric acid does not produce a great alteration of the original lignin;[131,176] consequently, the results obtained with alkali lignin demineralized by washing the sample with hydrofluoric acid solution can be considered more representative of the real effect of ash during pyrolysis. Moreover, the results were consistent with the ones obtained by doping organosolv lignin, even though in this case the mild effects of K^+ on the yields of char, gas, and condensable fraction could be due to the doping procedure (dry mixing) which established a less intimate contact between the metal and lignin sample.[233] The increase in char production was attributed to a catalytic effect that promoted repolymerization reactions.[230]

Results of Wang et al.[250] seem to disagree with these observations showing that K^+- and Ca^{2+}-doped alkali lignin produced, respectively, more and less solid residue than the untreated sample during thermogravimetric analysis. However, if it is considered that a significant weight loss of the Ca^{2+}-doped sample was observed at low temperature and related to the release of adsorbed water, the amount of solid residue recalculated on a dry basis is higher than the one of the untreated sample, similarly to what was observed for the K^+-doped sample. The same explanation can be provided for the similar results obtained by Zhao et al.[209] with KAc-, Na_2CO_3-, and NaAc-doped alkali lignin.

Many authors agree that alkali and alkaline earth ions affect greatly the decomposition patterns of lignin despite its origin, producing a different distribution of the species in both gas and the condensable fraction. The presence of AAEMs was proven to catalyze the rupture of ether bonds and side-chain units promoting the production of LMW species at the expense of condensed aromatic molecules.[252,255] Both AAEMs were found to depress weight loss between 200 and 500 °C.[209,250] This is in agreement with Ca^{2+} indulin-doped samples that were found to produce a condensable fraction in which the molecular weight distribution is shifted toward lower molecular weights, indicating the enhancement of fragmentation reactions induced by Ca^{2+}.

DFT calculations of a β−O−4 type lignin dimer model compound (1-methoxy-2-(4-methoxyphenethoxy)benzene) supported this experimental evidence revealing that in the presence of alkali ions the dissociation energy of the Cβ−O bond decreases promoting homolytic and concerted decomposition reactions.[256]

Decarboxylation, decarbonylation and dihydroxylation reactions are promoted by metal ions which also affect the decomposition mechanism of methoxy groups bound to the aromatic structures. The release of small molecular weight species, such as CO_2 and CH_4, was enhanced by the presence of AAEMs.[209,250] In some cases,[176] only a slight increase of CO_2 yield was observed.

Na^+ enhances the removal of methoxy and hydroxyl groups from different types of pulp lignin determining an increase of the yield of guaiacol, vinyl guaiacol, phenol, and catechol and a decrease of the yield of methyl guaiacol.[252] Experimental data related to biomass pyrolysis confirmed the results obtained using lignin as feedstock. Fast pyrolysis of KCl-impregnated biomass favored the yields of guaiacol and phenols with unsaturated groups such as 4-vinylguaiacol and 4-vinylsyringol.[117,257] As

https://doi.org/10.1021/acs.energyfuels.0c04046
Energy Fuels 2021, 35, 5407−5478

observed also for hemicellulose, the ion exchange doping procedure was more effective than impregnation with salts since it produces comparable results even though the loading level is 1 order of magnitude lower.[252]

K^+ decreased the O/C ratio of the condensable fractions confirming an enhanced activity of the deoxygenation reactions.[233]

The production of catechols was significantly depressed in favor of alkylated phenols with the addition of Ca^{2+}, confirming that calcium compounds catalyze deoxygenation in the form of dihydroxylation.[234] m-cresol was selectively produced among the three cresol isomers. It was postulated that the complexation between metal and hydrogen on the hydroxyl functionality in the ortho position, with respect to the other hydroxyl group, hinders the abstraction of the hydrogen radical from the hydroxyl group allowing for the hydrogen abstraction from the benzene ring in meta position and the following methylation reaction on the same position.[234] CaO also promoted PAH formation.[234]

The type of counterion has a relevant effect on lignin pyrolysis. It was observed that the bicarbonate counterion is more effective than the sulfate in boosting the catalytic effect of the alkali metal ion on the removal of hydroxyl and methoxy groups.[252] Additionally, when the counterion decomposes during pyrolysis providing an in situ source of reactive hydrogen, such as in the case of $Ca(HCOO)_2$[254] the catalytic effect of hydrogen on the deoxygenation reaction prevails, producing reduced amounts of char and gas in favor of a condensable fraction with a reduced O/C content. The removal of hydroxyl and methoxy groups was enhanced producing more aromatic species and alkylated phenols from guaiacols.[254,258]

5.4. Effects of Inherent Inorganic Elements on Biomass Pyrolysis. The inorganic elements present in biomass, more specifically AAEMs, have a remarkable influence on biomass pyrolytic behavior, since they affect the initial temperature of decomposition, the maximum devolatilization rate and the temperature at which it occurs, and the products distributions (yields of char, gas, and condensable fraction) and their composition and characteristics. During biomass pyrolysis, these inorganic elements affect the decomposition of the organic matrix at a molecular level as discussed in detail in Subsections 5.1−5.3. In Table 9, a collection of literature data referring to the last 10 years on the effect of AAEMs on different types of lignocellulosic biomass is reported. Among the AAEMs, K, Na, Ca, and Mg are the most studied due to their high concentration in lignocellulosic biomass.

5.4.1. Effects on Characteristic Temperatures and Product Yields. As a general trend, according to the AAEMs effect on the single organic components of biomass, AAEMs (i) anticipate the onset of the decomposition reactions and of the maximum devolatilization rate temperature, (ii) favor the decomposition pathways leading to the production of low molecular condensable species and permanent gases, and (iii) determine the increase of the char yield due to the enhancement of dehydration reactions involving the holocellulosic components and the repolymerization reactions of unstable reaction intermediates. As pointed out in Subsections 5.1−5.3, similarly to the organic components, in the case of a real biomass, the doped samples are frequently compared using the same concentration on a weight basis of the metal ion detected on the sample and, sometimes, even of the salt used for the sample doping, which can lead to misleading results.

It was found that the electropositivity of the metal tends to be correlated with the extent of catalytic activity.[177] However, this cannot be considered a general rule since, as discussed for cellulose, alkaline earth metals are stronger Lewis acids than alkali metals, and they are more effective in weakening the hydrogen bonds between carbohydrates chains in the cellulose fibril and the glycosidic bonds inside the chain, promoting primary dehydration reactions.[212] Conversely, some authors found that Ca^{2+}[263] or alternatively Mg^{2+}[261] did not have any catalytic effect on the yields of the pyrolysis products.

Some unexpected results were obtained as shown in Table 9.[117,188,194,219,230,260] Eom et al.[117] found that the demineralization treatment performed by washing the poplar xylem tissue with HCl did not affect products yields despite the reduction of ash content. Demineralization procedures performed with strong inorganic acids could affect the relative content of the organic constituents by dissolving extractives and amorphous cellulose and hemicellulose and alter crystallinity and DP of cellulose (Figure 3). This could promote the production of char (since lignin content increases), thus going in the opposite direction of demineralization. The authors also conclude that high loadings of Ca^{2+} determine an increase of the maximum devolatilization temperature, whereas different heating rates in the range of 5−20 °C/min produced opposing effects on the char yield in the K^+-doped samples. Additionally, the doping treatment can alter the metal ions effect on the pyrolysis products yields as was observed by Nowakowski and Jones[230] and Safar et al.[194] The authors observed the presence of two resolved peaks in the weight loss rate curves of both cellulose and rubberwood-doped with K^+. It is inferred that the peak at low temperature and the significant increase of char yield were due to a partial modification of cellulose after impregnation.

Saddawi et al.,[188] in the case of willow, showed that the trend of the char yield with the Na^+ concentration is apparently not consistent with the literature as the samples with the highest Na^+ concentration produce comparable char yields. However, it should be considered that high loading levels increase the ash retention in char, and the char yield should be recalculated on a dry ash-free basis to assess the real effect of Na^+ on the pyrolysis mechanism. These effects should be considered when the doping element concentration is high enough to alter significantly the ash content in the final solid residue.[15] Some results that are also in disagreement with the literature were obtained for the gas yield. Lu et al.[260] found a decreased yield of gas for K^+-doped poplar samples. Shen et al.[265] found that the char yields of K^+-doped biomass occasionally decrease, and it was postulated that different K^+ salts could react at a different extent with carbon in char to favor the production of gas at high temperatures while consuming char.

Among the inherent inorganics, Si and also trace metals should be considered in some specific cases. As reported in Table 2, some agricultural residues, such as corn stalks, bagasse, rice straw and husks, wheat straw, and millet husks,[12] are characterized by high Si content.

The effect of Si was investigated at both low and high heating rates. Under slow pyrolysis conditions, the higher char yield of rice husk[12] and of reed and Douglas fir[271] with respect to other biomasses with lower Si content pyrolyzed under the same conditions was ascribed to the presence of Si. However, at a high temperature and heating rate, Trubetskaya and co-workers[92,272] did not report any relevant catalytic effect of Si during pyrolysis of rice husks.

https://doi.org/10.1021/acs.energyfuels.0c04046
Energy Fuels 2021, 35, 5407−5478

Table 9. Effect of AAEMs on Biomass Pyrolysis Products ([a])

Feedstock	Experimental apparatus	T (°C)	HR (°C/min)	Pretreatment	Method	Metallic ion	Counterion	Concentration	Main results	ref
xylem tissue of poplar wood	TG	550	5−20	demineralization	H_2O, HCl, HF washing				Data referred to HR = 10°C/min **Control**: T_{max} 357.3 °C, volatiles 88 wt %, char 12 wt % ***H_2O washing***: T_{max} 368.5 °C, volatiles 90.8 wt %, char 9.2 wt % ***HCl washing***: T_{max} 366.9 °C, volatiles 88.6 wt %, char 11.4 wt % ***HF washing***: T_{max} 368.4 °C, volatiles 90.5 wt %, char 9.5 wt %	117
xylem tissue of poplar wood	TG	550	5−20	demineralization and further doping	H_2O, HCl, HF washing followed by wet impregnation	K^+, Mg^{2+}, Ca^{2+}	Cl^-	salt solution: 0.05, 0.5 wt %	Data referred to HR = 10°C/min ***Control***: T_{max} 365.4 °C, volatiles 90.1 wt %, char 9.1 wt % ***KCl doping (0.05)***: T_{max} 360.2 °C, volatiles 88.6 wt %, char 11.4 wt % ***KCl doping (0.5)***: T_{max} 331.8 °C, volatiles 87.1 wt %, char 12.9 wt % ***$MgCl_2$ doping (0.05)***: T_{max} 365.4 °C, volatiles 91.2 wt %, char 8.8 wt % ***$MgCl_2$ doping (0.5)***: T_{max} 360.5 °C, volatiles 89.4 wt %, char 10.6 wt % ***$CaCl_2$ doping (0.05)***: T_{max} 374.2 °C, volatiles 90.8 wt %, char 9.2 wt % ***$CaCl_2$ doping (0.5)***: T_{max} 368.8 °C, volatiles 87.9 wt %, char 12.1 wt %	117
poplar wood	TG	416	5	doping	wet impregnation under pressure	K^+	Cl^-, CO_3^{2-}	salt solution: 0.5, 0.75 (KCl) and 0.8 (K_2CO_3) wt %	***Control***: T_{max} 275 and 349 °C, char 14.3 wt % ***KCl doping (low load)***: T_{max} 260 and 312 °C, char 24.0 wt % ***KCl doping (high load)***: T_{max} 260 and 309 °C, char 25.3 wt % ***K_2CO_3 doping***: T_{max} 220 and 297 °C, char 27.2 wt %	259
poplar wood	fixed bed reactor	550	fast pyrolysis	doping	wet impregnation	K^+	PO_4^{2-}	salt in the feedstock 8 wt %	***Control***: char 27.4 wt %, CF 50.0 wt %, gas 22.6 wt %	260

https://doi.org/10.1021/acs.energyfuels.0c04046
Energy Fuels 2021, 35, 5407−5478

Table 9. continued

Feedstock	Experimental apparatus	T (°C)	HR (°C/min)	Pretreatment	Method	Metallic ion	Counterion	Concentration	Main results	ref
									K doping: char 33.7 wt %, CF 46.8 wt %, gas 19.5 wt %	
yellow poplar wood	TG	800	10	demineralization and further doping	HF washing followed by wet impregnation	K^+	Cl^-	salt solution: 0.5, 1, 2 wt %	***Control***: T_{max} 356.6 °C, volatiles 93.2 wt %, char 6.8 wt % ***HF washing***: T_{max} 373.9 °C, volatiles 95.6 wt %, char 4.4 wt % ***K doping (0.5)***: T_{max} 373.1 °C, volatiles 93.7 wt %, char 6.3 wt % ***K doping (1)***: T_{max} 368.4 °C, volatiles 93.4 wt %, char 6.6 wt % ***K doping (2)***: T_{max} 359.0 °C, volatiles 90.9 wt %, char 9.1 wt %	257
yellow poplar wood	fluidized bed reactor	400, 500, 550	fast pyrolysis	demineralization and further doping	HF washing followed by wet impregnation	K^+	Cl^-	salt solution: 0.5, 1, 2 wt %	Data referred to T = 550 °C ***Control***: CF 46.8 wt %, char 5.8 wt %, gas 47.5 wt % ***HF washing doping***: CF 46.7 wt %, char 3.3 wt %, gas 50.0 wt % ***K doping (0.5)***: CF 45.7 wt %, char 5.3 wt %, gas 48.9 wt % ***K doping (1)***: CF 44.6 wt %, char 6.8 wt %, gas 48.6 wt % ***K doping (2)***: CF 48.1 wt %, char 7.3 wt %, gas 44.6 wt %	257
birch wood	TG	500	10	doping	wet impregnation	Mg^{2+}	Cl^-	cation in the feedstock: 1 wt %	***Control***: T_{max} 314 and 380 °C, char at 400 °C, 41 wt % ***Mg doping***: T_{max} 243 and 349 °C, char at 400 °C, 31 wt %	189
rubber wood	TG	800	20	doping	wet impregnation	K^+	CO_3^{2-}	salt solution: 0.004−0.36M	***Control***: T_{max} 319 and 366 °C, char at 800 °C, 13.4 wt % ***K doping (0.022M)***: T_{max} 194 and 268 °C, char at 800 °C, 38.1 wt %	194
pine wood chips	tandem microreactor system (Frontier Laboratories, Rx-3050 TR)	500	fast pyrolysis	doping	wet impregnation	Na^+, K^+, Mg^{2+}, Ca^{2+}	OH^-	cation in the feedstock: 0.1, 0.5, 1, 2 wt %	***Control***: char 12.3 wt % ***Na doping (2 wt %)***: char 24.5 wt % ***K doping (2 wt %)***: char ∼20 wt % ***Mg doping (2 wt %)***: char ∼12.5 wt %	261

https://doi.org/10.1021/acs.energyfuels.0c04046
Energy Fuels 2021, 35, 5407−5478

Table 9. continued

Feedstock	Experimental apparatus	T (°C)	HR (°C/min)	Pretreatment	Method	Metallic ion	Counterion	Concentration	Main results	ref
									Ca doping (2 wt %): char ∼18 wt %	
pine wood	TG	500	10	doping	wet impregnation	K^+	Cl^-	salt in the feedstock: 2 wt %	***Control***: char ∼28 wt % ***K doping***: char ∼32 wt %	262
pine wood	TG	850	500	doping	wet impregnation	K^+	Cl^-	salt in the feedstock: 2 wt %	***Control***: char ∼14 wt % ***K doping***: char ∼20 wt %	262
pine wood	TG	800	20, 30, 40, 50	doping	wet impregnation	K^+	NO_3^-	salt in the feedstock: 0.1, 0.3, and 0.5 mol/kg	Data referred to HR = 20 °C/min ***Control***: T_{max} 367.4 °C, char 24.3 wt % ***K doping (0.1)***: T_{max} 350.8 °C, char 25.2 wt % ***K doping (0.3)***: T_{max} 344.3 °C, char 29.3 wt % ***K doping (0.5)***: T_{max} 337.8 °C, char 29.5 wt %	37
pine wood	fixed bed reactor	500, 600, 700, 800	intermediate pyrolysis	doping	wet impregnation	K^+	NO_3^-	salt in feedstock: 0.1, 0.3, and 0.5 mol/kg	Data referred to T = 800 °C ***Control***: tar ∼3.6 wt %, char ∼16 wt % ***K doping (0.1)***: tar ∼3 wt %, char ∼20 wt % ***K doping (0.3)***: tar ∼2 wt %, char ∼22 wt % ***K doping (0.5)***: tar ∼3 wt %, char ∼24 wt %	37
pine wood	fluidized bed reactor	400	fast pyrolysis	demineralization	HNO_3, HCl, H_2SO_4, $H_2C_2O_4$ washing				***Control***: char 21.7 wt %, CF 57.5 wt %, gas 10.7 wt % ***HNO_3 (60 °C) washing***: char 22.1 wt %, CF 64.4 wt %, gas 4.8 wt % ***HNO_3 washing***: char 19.9 wt %, CF 65.9 wt %, gas 4.4 wt % ***HCl washing***: char 19.7 wt %, CF 61.7 wt %, gas 5.3 wt % ***H_2SO_4 washing***: char 20.7 wt %, CF 61.5 wt %, gas 4.2 wt % ***$H_2C_2O_4$ washing***:char 19.3 wt %, CF 66.9 wt %, gas 5.0 wt %	263
pine wood	fluidized bed reactor	400	fast pyrolysis	doping	wet impregnation	Na^+, K^+, Ca^{2+}	NO_3^-	cation in the feedstock: 87 (Na), 79.3 (K), 52.4 (Ca) μmol/g	***Control***: char 21.7 wt %, CF 57.5 wt %, gas 10.7 wt %	263

https://doi.org/10.1021/acs.energyfuels.0c04046
Energy Fuels 2021, 35, 5407−5478

Table 9. continued

Feedstock	Experimental apparatus	T (°C)	HR (°C/min)	Pretreatment	Method	Metallic ion	Counterion	Concentration	Main results	ref
									Na doping: char 25.8 wt %, CF 49.3 wt %, gas 11.8 wt % ***K doping***: char 25.2 wt %, CF 50.2 wt %, gas 12.4 wt % ***Ca doping***: char 22.0 wt %, CF 61.2 wt %, gas 6.3 wt %	
bamboo waste	fixed bed reactor	600	intermediate pyrolysis	doping	dry mixing	Na^+,K^+, Ca^{2+}, Mg^{2+}	OH^-, Ac^-, CO_3^{2-}, HCO_3^-	biomass to salt mass ratio 2:1	***Control***: char 18 wt %, CF 60 wt %, gas 18 wt % ***KOH doping***: char 19 wt %, CF 44 wt %, gas 34 wt % ***K_2CO_3 doping***: char 21 wt %, CF 41 wt %, gas 41 wt % ***$KHCO_3$ doping***: char 20 wt %, CF 43 wt %, gas 37 wt % ***KAc doping***: char 20 wt %, CF 40 wt %, gas 42 wt % ***NaOH doping***: char 19 wt %, CF 46 wt %, gas 25 wt % ***$Ca(OH)_2$ doping***: char 21 wt %, CF 41 wt %, gas 41 wt % ***$Mg(OH)_2$ doping***: char 21%, CF 45 wt %, gas 35 wt %	264
willow	TG	900	25	doping	wet impregnation	Na^+, K^+	CH_3COO^-	cations in the feedstock: K^+: 0, 0.05, 0.1, 0.25, 0.3 0.5, 0.75, 1.0, 1.5, and 2 wt %. Na^+: 0, 0.1, 0.25, 0.5, 1, and 2 wt %	***Control_1***: T_{max} ~392 °C, char 15% ***K doping (2 wt %)***: T_{max} ~335 °C, char ~22.5 wt % ***Control_2***: T_{max} ~373 °C, ~char 14% ***Na doping (2 wt %)***: T_{max} ~320 °C, char ~15 wt %	188
rice husk	TG	900	20	doping	dry mixing	K^+	OH^-, CO_3^{2-}, $C_2O_4^{2-}$	biomass to salt mass ratio 1:1	***Control***: T_{max} 366 °C, char (700 °C) 29.872 wt % ***KOH doping***: T_{max} 214 °C, char (700 °C) 59.629 wt % K_2CO_3 doping: T_{max} 359 °C, char (700 °C) 62.194 wt % ***$K_2C_2O_4$ doping***: T_{max} 368 °C, char (700 °C) 47.87 wt %	265
rice husk	tubular furnace	700	20	doping	dry mixing	K^+	OH^-, CO_3^{2-}, $C_2O_4^{2-}$	biomass to salt mass ratio 1:1	***Control***: CF ~29 wt %, char ~32 wt %, gas ~39 wt % ***KOH doping***: CF ~21 wt %, char ~20 wt %, gas ~59 wt %	265

https://doi.org/10.1021/acs.energyfuels.0c04046
Energy Fuels 2021, 35, 5407−5478

Table 9. continued

Feedstock	Experimental apparatus	*T* (°C)	HR (°C/min)	Pretreatment	Method	Metallic ion	Counterion	Concentration	Main results	ref
									K2CO3 doping: CF ∼23 wt %, char ∼22 wt %, gas ∼55 wt % ***$K_2C_2O_4$ doping***: CF ∼23 wt %, char ∼18 wt %, gas ∼59 wt %	
rice husk	one-stage fluidized bed/fixed bed reaction system	500, 600, 700, 800, 900	fast pyrolysis	doping	ionic exchange	K^+, Ca^{2+}	CO_3^{2-} (K), Ac^- (Ca)	salt solution: 0.2 M	Data referred to *T* = 700 °C ***Control***: CF 5.10 wt %, char 26.61 wt %, gas 68.29 wt % ***K_2CO_3 doping***: CF 4.23 wt %, char 32.75 wt %, gas 63.01 wt % ***CaAc doping***: CF 4.97 wt %, char 22.71 wt %, gas 72.32 wt %	190
rice husk	fluidized bed reactor	500, 700, 900	fast pyrolysis	demineralization	H_2O, HCl washing				Data referred to *T* = 700 °C ***Control***: CF 19.4 wt %, char 29.0 wt %, gas 51.6 wt % ***H_2O washing***: CF 20.8 wt %, char 25.4 wt %, gas 53.8 wt % ***HCl washing***: CF 21.2 wt %, char 23.2 wt %, gas 55.6 wt %	141
rice husk	TG	800	30	demineralization and further doping	CH_3COOH washing followed by wet impregnation	Na^+, K^+, Mg^{2+}, Ca^{2+}	CH_3COO^-	salt solution: 0.5 M	***Control***: char 26.6 wt % ***K doping***: char 38.0 wt % ***Na doping***: char 36.4 wt % ***Mg doping***: char 30.1 wt % ***Ca doping***: char 30.4 wt %	15
soybean hulls	TG	900	5, 10, 15, 20, 25	doping	wet impregnation	Na^+, Mg^{2+}	Cl^-	salt solution: 10, 20, and 30 wt %	Data referred to HR = 15 °C/min and 10 wt % of salt ***Control***: T_{max} 341 °C, volatiles 79.5 wt %, char 18.6 wt % ***Na doping***: T_{max} 342 °C, volatiles 73.4 wt %, char 26.6 wt % ***Mg doping***: T_{max} 248 °C, volatiles 69.5 wt %, char 30.5 wt %	186
pine bark	TG	600	10, 20, 50	demineralization and further doping	HNO_3 washing followed by wet impregnation	Ca^{2+}, Mg^{2+}, Na^+, K^+	NO_3^-	cation in the feedstock: 0.7-1 wt %	Data referred to HR = 10°C/min ***Control***: char ∼25.5 wt % ***K doping***: char ∼31.5 wt %	187

https://doi.org/10.1021/acs.energyfuels.0c04046
Energy Fuels 2021, 35, 5407−5478

Table 9. continued

Feedstock	Experimental apparatus	T (°C)	HR (°C/min)	Pretreatment	Method	Metallic ion	Counterion	Concentration	Main results	ref
									Na doping: char ∼32 wt % ***Mg doping***: char ∼29 wt % ***Ca doping***: char ∼28.5 wt %	
pubescens	fixed bed reactor	400	10	doping	wet impregnation	Mg^{2+}	Cl^-	salt solution: 5, 10, 15, 20 wt %	***Control***: CF 52.3 wt %, char 32.7 wt %, gas 15.0 wt % ***H_2O washing***: CF 56.2 wt %, char 30.9 wt %, gas 13.8 wt % ***HCl washing***: CF 54.7 wt %, char 29.1 wt %, gas 16.2 wt % ***Mg doping (5)***: CF 43.8 wt %, char 40.7 wt %, gas 15.4 wt % ***Mg doping (10)***: CF 39.3 wt %, char 44.0 wt %, gas 15.8 wt % ***Mg doping (15)***: CF 42.7 wt %, char 43.2 wt %, gas 14.9 wt % ***Mg doping (20)***: CF 43.4 wt %, char 43.8 wt %, gas 13.8 wt %	15
cotton stalks	fixed bed reactor	220–280	fast	doping	wet impregnation	Mg^{2+}	Cl^-	salt in the feedstock: 4.89, 9.02, 13.95, 18.54 wt %	Data referred to T = 260 °C Control: CF 5.98 wt %, char 82.87 wt %, gas 11.15 wt % ***Mg doping (4.89)***: CF 8.38 wt %, char 80.05 wt %, gas 11.57 wt % ***Mg doping (9.02)***: CF 10.32 wt %, char 78.35 wt %, gas 11.33 wt % ***Mg doping (13.95)***: CF 14.39 wt %, char 74.35 wt %, gas 11.26 wt % ***Mg doping (18.54)***: CF 16.26 wt %, char 69.35 wt %, gas 14.39 wt %	266
sweet sorghum bagasse	TG	900	10	doping	wet impregnation	Mg^{2+}	Cl^-	salt in the feedstock: 5, 10 and 20%	Data referred to T = 550 °C ***Control***: T_{max} 216.8 and 319.1 °C, volatiles 74.7 wt %, char 25.3 wt % ***Mg doping (5)***: T_{max} 151.8 and 232.7 °C, volatiles 67.1 wt %, char 32.9 wt %	267

https://doi.org/10.1021/acs.energyfuels.0c04046
Energy Fuels 2021, 35, 5407−5478

Table 9. continued

Feedstock	Experimental apparatus	T (°C)	HR (°C/min)	Pretreatment	Method	Metallic ion	Counterion	Concentration	Main results	ref
									Mg doping (10): T_{max} 175.2 and 300.3 °C, volatiles 61.6 wt %, char 38.4 wt % ***Mg doping (20)***: T_{max} 157.6 and 241.6 °C, volatiles 59.9 wt %, char 40.1 wt %	
rice straw	fixed bed microreactor	350, 420, 500	fast	demineralization	HF washing				Data referred to T = 500 °C ***Control***: CF ∼ 30 wt %, char ∼20 wt %, gas ∼50 wt % ***HF washing***: CF ∼34 wt %, char ∼9 wt %, gas ∼57 wt %	139
rice straw	fixed bed microreactor	700	10	demineralization	HCl washing				***Control***: CF ∼44 wt %, char ∼38 wt %, gas ∼18 wt % ***HCl washing***: CF ∼45 wt %, char ∼35 wt %, gas ∼12 wt %	268
wheat straw	fixed-bed reactor	n.a.	fast	demineralization	HNO_3 washing				***Control***: CF ∼ 56 wt %, char ∼24 wt %, gas ∼20 wt % ***HNO_3*** washing: CF ∼ 64 wt %, char ∼18 wt %, gas ∼12 wt %	115
barley straw	fixed-bed reactor	n.a.	fast	demineralization	HNO_3 washing				***Control***: CF ∼52 wt %, char ∼26 wt %, gas ∼21 wt % ***HNO_3 washing***: CF ∼63 wt %, char ∼19 wt %, gas ∼12 wt %	115
pine sawdust	entrained flow reactor	500	fast pyrolysis	doping	wet impregnation	Ca^{2+}	SO_4^{2-}, HCO_2^-, CO_3^{2-}, OH^-, O^{2-}	cation in the feedstock 0.43 g/g	***Control***: char 12 wt %, gas 58 wt % ***$CaSO_4$ doping***: char 11 wt %, gas 48 wt % ***$Ca(COOH)_2$ doping***: char 36 wt %, gas 61 wt % ***CaCO***3 doping: char 17 wt %, gas 51 wt % ***$Ca(OH)_2$ doping***: char 21 wt %, gas 33 wt % ***CaO doping***: char 13 wt %, gas 24 wt %	269
cypress wood sawdust	TG	800	5	doping	wet impregnation	Na^+, K^+, Ca^{2+}, Mg^{2+}	Cl^-	cation in the feedstock: 0.08−0.15 mol/kg	***Control***: T_{max} 343 °C, char 20.3 wt % ***K doping* (0.11)**: T_{max} 337 °C, char 21.54 wt %	270

https://doi.org/10.1021/acs.energyfuels.0c04046
Energy Fuels 2021, 35, 5407−5478

Table 9. continued

Feedstock	Experimental apparatus	T (°C)	HR (°C/min)	Pretreatment	Method	Metallic ion	Counterion	Concentration	Main results	ref
									Na doping (0.10): T_{max} 337 °C, char 20.77 wt %	
									Mg doping (0.10): T_{max} 355 °C, char 17.39 wt %	
									Ca doping (0.11): T_{max} 359 °C, char 16.72 wt %	
cypress wood sawdust	TG	800	5	demineralization	H_2O washing				***Control***: T_{max} 343 °C, char 20.3 wt %	270
									H_2O washing: T_{max} 358 °C, char 16.56 wt %	

[a]CF: condensable fraction.

On the contrary, trace metals may have some catalytic effects on biomass pyrolysis. Specifically, transition metals were investigated as catalysts in CFP where they are added on purpose in concentrations greatly higher than the ones typically found in natural biomass. A summary of the effect of these metals in CFP is out of the scope of this review, and the interested reader can refer to the pertinent literature.[2] Their effect on the pyrolysis of the natural biomass is often neglected because their concentration is typically in the order of ppm; a different approach should be used for hyperaccumulator plants grown on metal-contaminated soils. In these cases, some typical metal contaminants, especially HMs such as Pb, Cu, Zn and Cd, can be accumulated in the plants thus achieving non-negligible concentrations.[111]

Only a few studies on the pyrolysis of HMs-contaminated plants investigate also the possible catalytic effects induced by these metals. Table 10 shows the comparison between products yields obtained from pyrolysis of contaminated and control biomass samples.

The comparison is complicated if one considers that the presence of HMs induces modifications of the plant chemistry, both in the inorganic and the organic fractions. Consequently, it is challenging to understand if the observed effects are due to the presence of HMs or to the changes in the biomass, induced by their presence during plant growth. For example, the results of the study conducted by Al Chami et al.[274] seem to be affected by the higher AAEMs content of the contaminated biomass with respect to the control sample and not by the presence of Ni and Zn in the contaminated sample. In this case, the high content of AAEMs promotes dehydration reactions that lead to a higher char yield and a higher water content in the condensable fraction. To overcome this problem, some authors used doped samples to simulate the metal contamination.[273,275] However, the final ion concentration in the doped sample was often too high with respect to the typical values due to natural contamination, so the catalytic effect was overestimated.

The presence of Cu^{2+} during fast pyrolysis was found to increase the yields of the char and the condensable fraction at the expense of the gas yield. The catalytic effect of Cu^{2+} resulted in lower oxygen content in the condensable fractions, thus increasing its high heating value.[273] According to the results observed in the literature related to the use of Cu as a catalyst in CFP, this result can be explained with the ability of Cu^{2+} in promoting deoxygenation reactions and reactions between gaseous species (e.g., H_2) or light hydrocarbons and condensable species or char.[277,278] A different catalytic activity was observed for Pb^{2+} during pyrolysis of contaminated water hyacinth[275] and *Avicennia marina*.[276] Jiu et al.[275] detected an increase of the yield of the condensable fraction derived from the pyrolysis of contaminated water hyacinth at the expense of char and gas yields. This result seems to be related to the alteration of the decomposition mechanisms of carboxylic groups and the depolymerization reactions of hemicellulose and neutral detergent solutes (protein, fat, sugar), which produce more carboxylic acids and less aromatics and, accordingly, less CO_2 and more H_2. Conversely, He et al.[276] observed for the contaminated biomass an increase of char and gas yields and a reduction of the yield of the condensable fraction which resulted in enriched hydrocarbons.

As suggested by the results discussed so far, many deviations from the most common trends obtained in the literature exist, thus revealing that several factors affect the behavior of metals during the pyrolysis of biomass, especially in a real plant. The

https://doi.org/10.1021/acs.energyfuels.0c04046
Energy Fuels 2021, 35, 5407−5478

Table 10. Yields of Pyrolysis Products from Contaminated (a) and Control (b) Biomass Samples

		Metal (mg/kg)								Yield (wt %)			
Pyrolysis	Feedstock	Cd	Cu	Zn	Pb	As	Ni	T (°C)	Sample	Gas	Condensable fraction	Char	ref
fast	fir sawdast		5000−30,000 (a)					450	(a)	10	50	40	273
			0 (b)					450	(b)	25	42	33	
								500	(a)	17	55	30	
								500	(b)	27	47	27	
								550	(a)	28	52	27	
								550	(b)	30	44	25	
								600	(a)	22	50	25	
								600	(b)	35	42	20	
slow	*Sorghum bicolor*			180 (a)			80 (a)	450	(a)	12	30	50	274
				60 (b)			10 (b)	450	(b)	5	33	55	
fast								450	(a)	45	16	31	
								450	(b)	48	21	22	
fast	water hyacinth				60,000 (a)			375	(a)	2.5	57	47.5	275
					0 (b)			375	(b)	32	22.5	47	
								450	(a)	7.5	60	35	
								450	(b)	22	37.5	42	
								550	(a)	10	55	32	
								550	(b)	25	38	37	
slow	*Avicennia marina*	0.4 (a)	19.6 (a)	108.7 (a)	38.57 (a)	3.2 (a),	1.29 (a)	300	(a)	5.5	33	61.6	276
		0.014 (b)	7.96 (b)	12.63 (b)	0.748 (b)	0.352 (b)	0.515 (b)	300	(b)	4.4	35.3	60.2	
								400	(a)	16	43.6	40.4	
								400	(b)	14.4	46.8	38.8	
								500	(a)	20.9	46.9	32.1	
								500	(b)	18	51.2	30.9	
								600	(a)	23	46.8	30.2	
								600	(b)	20.1	51.2	28.3	
								700	(a)	25.1	46.2	28.8	
								700	(b)	21.9	51.3	26.8	
								800	(a)	26.7	45.4	27.9	
								800	(b)	23.2	50.8	25.9	

https://doi.org/10.1021/acs.energyfuels.0c04046
Energy Fuels 2021, 35, 5407−5478

Table 11. Variation Ranges of Bio-Oils Properties and Effect of Ash Content on Bio-Oil Properties from Switchgrass and *Festuca arundinacea*, (adapted from Kumar et al.,[42] Lehto et al.,[1] and Fahmi et al.[285])

		Switchgrass		*Festuca arundinacea*	
	Variation ranges	raw	washed	raw	washed
feedstock ash content, wt %	–	4.3	3.4	7.3	4.4
C, wt %	54–58 (w.f.)	38.3 (50.9 w.f.)	39.4 (47.6 w.f.)	32.1 (48.7 w.f.)	44.9 (63.4 w.f.)
H, wt %	5.5–7.0 (w.f.)	7.4 (6.2 w.f.)	6.7 (5.8 w.f.)	9.8 (9.1 w.f.)	9.2 (8.4 w.f.)
N, wt %	0–0.2 (w.f.)	0.1 (0.1 w.f.)	0.1 (0.1 w.f.)	1.4 (2.1 w.f.)	1.0 (1.4 w.f.)
O, wt %	35–55 (w.f.)	54.1 (42.7 w.f.)	53.6 (46.3 w.f.)	56.7 (40.0 w.f.)	44.9 (26.8 w.f.)
Water content, wt %	15–30[(a)]	24.7	17.2	34.1	29.2
Solids, wt %	0.2–1.0[(a)]	0.8	0.3	0.1	0.1
Ash, wt %	0–0.2[(a)]	–	–	–	–
Viscosity @ 40 °C, cSt	15–35[(b)]	34.2	33.3	10.9	13.5
Density @ 15 °C, kg/dm^3	1.1–1.3[(b)]	–	–	–	–
LHV, MJ/kg	13–18[(b)]	14.8	14.5	14.5	19.7
pH	2–3[(b)]	2.9	2.8	3.2	3

catalytic effects of metals can be enhanced or attenuated by different factors acting at a multiscale level and, often, interacting between them:

- At molecular scale: Chemical interactions between metal ions and the inorganic fraction as well as between metal ions and the organic components could induce metal devolatilization[14] and/or passivation.[279] Both alkali and alkaline earth metals, especially Na and K if present in free ion form, could react with the organic volatile species released during pyrolysis and easily be transferred to the vapor phase.[280] The extent of these reactions is affected by the concentration of the organic species in the gas phase (and consequently by the devolatilization rate and the carrier gas type and dilution) and by the mass transfer limitations inside the particle.[14] In addition, some inorganic species (e.g., $Ca(OH)_2$) were found to react with the inherent inorganic elements in the biomass altering their properties and making them inactive.[279]
- At particle scale: Particle size and evolution of the char porous structure affect the mass and heat transfer inside the biomass particle; variations of the residence time of the volatiles inside the particle and the intraparticle thermal gradient induce a different extent of the metals catalytic activity. Moreover, the selectivity toward some decomposition mechanisms induced by the metal ions modifies the endothermicity/exothermicity of the thermal decomposition steps that affect the temperature at particle and even at reactor levels. In this regime, pyrolysis products are determined by the interplay between heat transfer and chemistry according to the values of the Py number.[259]
- At reactor scale: Reactor fluid dynamics affect the residence time of the volatiles evolving from the biomass particles/bed, whereas reactor configuration can induce thermal gradients inside the particle/bed and inside the gas phase modulating accordingly the occurrence and the extent of the catalytic activity of the metal ions.

5.4.2. Effects on Composition and Properties of Condensable Fraction. The analysis of the effect of AAEMs on the single biomass organic components revealed that these elements: (i) promote dehydration reactions of the holocellulosic matrix, (ii) favor the ring opening reactions of the carbohydrates-based oligomers, (iii) catalyze the secondary decomposition of the anhydrosugars and their repolymerization to form secondary char, (iv) catalyze the rupture of ether bonds and side-chain units inside the lignin macromolecule, and (v) promote the deoxygenation of the aromatic structures through decarboxylation, decarbonylation, and dihydroxylation and demethylation reactions.

According to the above-mentioned effects, many authors in presence of AAEMs detected higher yields of water and LMW species. Among the typical products of the holocellulosic fraction decomposition, lower yields of levoglucosan and anhydrosugars were detected in favor of aldehydes, ketones, and ethers. No obvious trends were observed for acetic acid and furans, especially HMF and furfural. Some authors[15,264,267] observed an increase of the acetic acid yield and of acids in general with the addition of alkali metals and Mg^{2+}, even though opposite results were obtained by Liu et al.[266] The authors found that by doping the biomass with Mg^{2+}, K^+, and Na^+ the formation of HMF was suppressed and that Ca^{2+} doping had the same effect on furfural.[269] In contrast, some authors[15,266,267] observed that Mg^{2+} increased furfural yield, and Mahadevan et al.[261] confirmed that the alkaline earth metals enhanced the formation of furans. Inconsistent results among different studies were found for furans yields after biomass demineralization through acid washing.[15,115,268]

However, as discussed in Subsections 5.1 and 5.2, Giudicianni et al.[235] observed a nonmonotonous trend of the yields of furfural, formic, and acetic acids at increasing Na^+ doping concentration, suggesting that different competing mechanisms could lead to the formation of these compounds.

Among the lignin-derived species, alkali metals promote the production of phenols and, in particular, they determine an increase of the guaiacols yield, whereas alkaline earth metals seem to inhibit their production.[281] Case et al.[269] observed that there was a shift from catechols to phenols and an increase of alkylated phenols when pyrolyzing Ca^{2+}-doped pine wood.

The condensable fraction contains a relevant percentage of heavy components[282] responsible for the high bio-oil viscosity[283] and formation of coke upon heating.[219] Heavy components consist mostly in O-containing species.[284] AAEMs were found to depress the formation of these components through two main mechanisms: (i) the breakage of active O-containing functional groups in heavy phenolics (catalytic effect) and (ii) the inhibition of radical recombination to form heavy phenolics and carbohydrates[284] (inhibitory effect). AAEMs can promote the secondary reactions of the volatile compounds, especially at higher temperatures, leading to the

https://doi.org/10.1021/acs.energyfuels.0c04046
Energy Fuels 2021, 35, 5407−5478

Table 12. Effect of Inorganic Macroelements Contents on Char Characteristics

Yield	It increases with AAEMs content and decrease in presence of high contents of aluminosilicates
Ultimate composition	AAEMs decrease C and increase O content (on daf basis). Aluminosilicates increase C content and reduce O content.
Ash content	It increases with inorganic elements content
HHV	It decreases with inorganic elements content
BET	It decreases with AAEMs and Si content
CEC	It increases with both total metals and AAEMs content
AEC (anion exchange capacity)	It increases with soluble anions content
pH	It increases with AAEMs content
Reactivity in oxidizing atmosphere	As AAEMs content increases it increases at low temperature and d, whereas it decreases at high conversion/temperature

formation of lighter species. Xiong et al.[284] found that the presence of AAEMs promoted the decomposition of heavy components in the bio-oil obtained from sawdust under different temperatures and heating rates to form additional compounds with a molecular weight of 200−300 Da, and this effect was enhanced as temperature increased. The reason for this result was ascribed to the favored breakage of the O-containing functional groups in heavy phenolics and, at higher temperatures, also to the release of AAEMs which recombined with radicals generated from biomass decomposition. High heating rates promoted the inhibitory effect on the heavy components formation but, on the other side, depressed the release of AAEMs,[285] thus weakening the inhibitory effects. K^+ has a stronger effect then Ca^{2+} on the total content of heavy components; more specifically, K^+ increased the content of single ring aromatic components while Ca^{2+} decreased the content of the 2−3 ring aromatic components.[284]

The changes in the chemical composition correspond to changes in the viscosity and the heating value as shown in Table 11.

5.4.3. Effects on Char Properties. The initial concentrations of inorganic elements are associated with their contents in the final solid residues since even if some inorganics are devolatilized during char production,[286] they are mostly retained in its structure. However, the chemical forms in which they are in the parent feedstock evolve during the pyrolysis process because of the interactions with both organic and inorganic matters, which affect their release and their intrinsic characteristics.[14] Many studies demonstrated that Cl is mostly released at temperatures below 500 °C,[287,288] even though a residual release was observed during straw pyrolysis between 700 and 900 °C.[289] It was speculated that the release of Cl at low temperature is caused by a reaction between KCl and some organic functional groups, probably carboxylic groups to form HCl.[290] However, this point is still debated since other authors proposed the reaction between KCl and organics groups to form CH_3Cl.[291−293]

Since S is present in a variety of compounds in biomass, both organic and inorganic, its devolatilization occurs mainly in two temperature ranges. Organic S is released during protein decomposition at temperatures lower than 500 °C,[294−296] while only a residual release is observed at higher temperatures since inorganic S in soluble form (mainly sulfate) is transformed in insoluble S (CaS, K_2S), and it is retained in the char.[296] Also Fe, Mn, and P are retained during pyrolysis, but P turns into more stable forms as temperature increases. The alkali metals are typically present in the biomass in the form of carbonates, whereas only a very low fraction is associated with the organic matrix, and it is released below 400 °C. On the contrary, the decomposition and the release of alkali metal carbonates occur at very high temperatures,[297] or they could be retained in a stable form if incorporated in silicates. Ca and Si, located in the cell wall, and Mg, bound with ionic and covalent bonds to organic molecules, are released at high temperatures. Different pyrolysis conditions promote the formation of crystalline silicates[298,299] or amorphous silicon oxides.[92]

The retained inorganic elements contribute to the properties of char both directly, through their intrinsic characteristics, and some of them (mainly AAEMs) also indirectly acting as a catalyst during the transformation of organic matter. Table 12 summarizes the effect of the most abundant inorganic elements on the chemical composition and textural characteristics of char. Two examples of chars produced under slow pyrolysis from raw and demineralized biomass are also given in Table 3 to highlight the effect of AAEMs content.

A reduced content of AAEMs promotes the production of organic volatiles which are compounds rich in O, thus affecting positively the C content of the remaining char (despite the lower yield) at the expense of the O content.[302] Consistently, raw rice straw-derived char (Table 13) has a lower C content and higher O content than char obtained from washed samples. However, also the presence of other inorganic elements could affect the biomass devolatilization. Rodriguez Correa et al.[302] observed that aluminosilicates such as kaolinite contained in macauba enhanced the release of O-containing groups, which lead to char with a higher C content in the raw sample than in the washed sample, thus explaining also the results obtained by Tomczyk et al.[301] on raw and washed cotton stalks (Table 13). The N content in the char is only slightly affected by the presence of AAEMs, since Ca^{2+} and K^+ can catalyze the cleavage of N-containing species such as NH_3 and HCN.[302,303] The inorganic

Table 13. Chars from Slow Pyrolysis of Raw and Washed Rice Straw at 550 °C[300] and Cotton Stalks at 500°C[301]

	Rice straw		Cotton stalk	
feedstock	raw	washed	raw	washed
ash, wt %	13.3	12.8	5.54	3.92
K, mg/kg	19,300	3250	9500	1700
Ca, mg/kg	3500	3100	8800	6500
Mg, mg/kg	2500	1800	2750	1500
Na, mg/kg	1500	380	800	150
C, wt %	53.2	58.7	70.32	72.78
H, wt %	2.6	2.5	2.26	2.32
N, wt %	0.9	0.8	1.32	1.35
O, wt %	8	7.8	7.58	9.17
volatiles, wt %	16.3	16.6	26.79	25.27
fixed carbon, wt %	48.4	53.2	54.69	60.35
ash, wt %	35.3	30.2	18.52	14.38
HHV, MJ/kg	18.3	19.3	26.59	27.07
BET, m^2/g	67.5	79.7	134.63	189.27
pH	–	–	9.02	8.37

https://doi.org/10.1021/acs.energyfuels.0c04046
Energy Fuels 2021, 35, 5407−5478

elements content is positively correlated to the char ash content, thus affecting negatively its HHV.

As described in Section 2.3, the morphological characteristics of char evolve as the pyrolysis temperature increases. The presence of inorganic elements in the form of heteroatoms in the organic matter prevents an excessive closing of the graphene-like layers during the graphitization of the char at high temperature, determining the formation of micropores. However, AAEMs were found to depress the formation of larger molecules at low temperature and favor the formation of secondary char at high temperature, reducing the total void volume of the char and its specific surface area. Moreover, if high amounts of alkaline metals and silicates are present, sintering phenomena can occur due to the formation of low melting point salts. For example, rice husk char obtained under high temperature and heating rate and quickly cooled showed a glassy structure composed of an amorphous silica phase.[92] Consistently, higher values of the specific surface area were observed for woody chars characterized by low ash content compared to herbaceous plant-derived chars.[304]

It is known that AAEMs in the form of salts are mostly responsible for the alkaline pH together with the removal of acidic groups as pyrolysis temperature increases.[305] The CEC for lignocellulosic biomasses was found to have a strong positive relationship with both the total metals and soluble cations contents. However, it is worth noting that char CEC cannot be predicted based only on the metals content but also on the concentration of the acidic functional groups. On the contrary, soluble anions contribute mostly to the AEC. Zhao et al.,[306] for example, found that the high AEC values in grass- and straw-derived chars were probably due to the high Cl^- concentration.

Inorganic elements retained in the char after the pyrolytic stage can play a catalytic role in subsequent oxidation reactions under both gasification and combustion conditions. A recent review of Dahou et al.[307] discussed the results of the most relevant studies on the effect of inorganic elements on char reactivity under gasification conditions, pointing out that some aspects do not yet have a clear consensus in the literature. Alkali metals were found to increase char reactivity in the order of K > Na,[308] whereas other elements such as Al, P, and Si showed an inhibitory effect.[309] Due to their high amount in the biomass, K and Si were mostly studied. Several mechanisms for K action were speculated, all of them based on the formation of active K intermediates, even though the type of intermediates is still debated.[307] A mechanical effect due to char swelling in the presence of K was also postulated, but this speculation was not supported by any experimental evidence.[310] Opposing results were obtained at high char conversion. Some biomasses showed an increase of the gasification rate probably due to the enhanced effect of alkali metal concentration at high temperature[311] and to the release of active K intercalated between graphitic layers in the char structure. Other biomasses showed a decreased reactivity probably due to the reduction of the available char surface due to pore collapse[312] or to the formation of an inert physical barrier on the char surface by the melted potassium silicates.[313] In general, Si, P, and Al can exert an inhibitory action on char reactivity by forming silicates, aluminates, and phosphates with AAEMs thus making them inactive.[307] However, Trubetskaya[272] observed that the reactivities of rice husk and pine wood chars generated in a drop tube reactor at 1400 °C were similar despite the high Si content of rice husk char, indicating a slight influence of the amorphous Si oxides detected in the char structure on the char reactivity.

The effect of AAEMs on char reactivity under combustion conditions was found to be positive for char prepared at low temperatures[314,315] due to the formation of K active intermediates as observed under gasification conditions. However, Zolin et al.[314] showed that chars prepared at T > 1200 °C from straw, raw and demineralized, had a lower reactivity in the presence of higher AAEMs concentrations. Several mechanisms were considered responsible of these results: (a) the formation of some discrete crystalline regions promoted by inorganic elements and (b) the reduction of the available char surface due to the volatile condensation inside the char pores or to the formation of inert ash layers.[316] In any case, at high temperature, it should be considered that the effect of thermal annealing on char reactivity could be predominant with respect to the catalytic action of AAEMs.

5.4.4. Effects on Gas Composition. Given the predominant interest in the condensable and solid products of pyrolysis, the effect of inherent inorganic elements on the release of the gaseous species and on the composition of the gaseous product was under investigated. Some authors studied the evolution of the gaseous species from slow pyrolysis of the main biomass components, demineralized and doped with different alkali elements.[9,68,164,176,215,225,235]

Slow pyrolysis of cellulose impregnated with increasing concentration of K salts resulted in an increase of both CO and CO_2 production from primary decomposition reactions as well as of CH_4 and H_2 from secondary decomposition of volatiles.[68,215] The increased production of CO_2 was detected also for fast pyrolysis of KCl- and $CaCl_2$-impregnated cellulose.[9] Ferreiro et al.[68] observed that, overall, the composition of the gas obtained at 700 °C under slow pyrolysis conditions was only slightly affected by the presence of KCl, and a small increase of the CO content was observed at the expense of the CO_2 content.[68]

The effects of AAEMs on the gas released from hemicellulose pyrolysis was studied using xylan from beechwood with different AAEMs contents as the reference compound.[235] By increasing the alkali metals content, the release of CO_2 and CO at low temperature was enhanced, whereas the release of CO at higher temperature was reduced. Overall, this corresponded to a slightly higher content of CO_2 at the expense of CO in the gas produced under slow pyrolysis conditions at 700 °C.[235] A similar effect on CO_2 and CO yields was observed also for fast pyrolysis of o-acetyl-4-O-methylglucurono-xylan extracted from beechwood[225] and for purified switchgrass-extracted hemicellulose.[164] However, at high Na^+ concentrations (>2 wt %), a strong reduction of CO_2 content and a corresponding increase of the CO content was observed due to the significant promotion of CO release at low temperature.[235] The yields of H_2 and CH_4 increased with alkali content, but only slight effects on their content in the gas were noticed.[235]

Concerning the effect of inorganic elements on pyrolysis gas from lignin, it was observed that the qualitative trends of the release rate of the main gaseous species were not altered by the presence of inorganic elements.[176] However, they promoted an increase of CO_2 and H_2 contents in the gas at the expense of CO content, whereas CH_4 and C_2 contents were only negligibly affected. Demineralized lignin doped with K^+ confirmed these trends.[176]

Among the studies discussed in Subsection 5.4 (Table 10), only few of them reported the composition of the pyrolysis gas for real biomasses.[141,264,265] Moreover, Chen et al.[264] and Shen et al.[265] used high ratios of biomass to salt to promote a chemical

https://doi.org/10.1021/acs.energyfuels.0c04046
Energy Fuels 2021, 35, 5407−5478

Table 14. Effect of Inorganic Elements on Composition and LHV of Pyrolysis Gas[141]

Feedstock	Pyrolysis conditions	T (°C)	Concentration	Pretreatment	CH_4 (wt %)	CO_2 (wt %)	CO (wt %)	H_2 (wt %)	LHV (MJ/kg)
rice husk	fast	500		raw	8.0	45.2	46.6	0.2	8.9
				H_2O washing	8.6	38.7	52.5	0.2	9.8
				HCl washing	9.6	30.1	60.1	0.2	11.1
		700		raw	11.5	25.6	61.4	1.5	13.8
				H_2O washing	11.2	19.1	68.4	1.3	14.0
				HCl washing	10.8	9.3	78.6	1.2	14.8
		900		raw	13.6	11.5	72.8	2.1	16.6
				H_2O washing	11.4	8.5	78.3	1.8	15.7
				HCl washing	10.0	6.2	82.3	1.5	15.1

activation during the pyrolysis process, so that their results cannot be considered representative of the extent of the effect of inherent inorganic elements that, typically, are present in greatly lower concentrations. Data on gas yields obtained from fast pyrolysis of raw and demineralized rice husks at 500, 700, and 900 °C[141] were used to calculate the gas composition as wt % considering only the main gaseous species, namely, CO, CO_2, CH_4, and H_2. These data are reported in Table 14 together with the calculated low heating value. At all the investigated temperatures, the pyrolysis of raw biomass, characterized by a higher content of inorganic elements, produced a gas richer in CO_2 at the expense of CO, in agreement with the data reported by Demirbaş.[317] At 500 and 700 °C, the contents of CH_4 and H_2 change negligibly in the different samples, whereas at the highest temperature, both CH_4 and H_2 contents increased in the raw sample due to the enhanced effects of the secondary reactions.

6. TECHNICAL AND SAFETY ISSUES RELATED TO PRESENCE OF INHERENT INORGANIC ELEMENTS IN BIOMASS PYROLYSIS

The presence of specific inherent metals in biomass is known to adversely affect the pyrolysis process under several points of view: Biomass decomposition pathways, reactor performance, bio-oil storage and utilization, bio-oil upgrade, and release/accumulation of toxic species.

6.1. Biomass Decomposition Pathways. As extensively discussed in Section 5, the yield and the quality of the condensable fraction decreased at increasing AAEMs concentration due the thermal degradation of the desired products into light gases. This effect is particularly noticeable in fast pyrolysis conditions, when the aim of the process is precisely to maximize the yield of bio-oil while preserving its quality and was already discussed in Section 5.2.

6.2. Reactor Performance. The inorganic compounds present in biomass which are concentrated in the ashes during its thermochemical conversion can be the cause of technical problems at high process temperatures typical of gasification and combustion.[318,319] Slagging and fouling phenomena may create deposits on the reactor walls, thus being detrimental for the heat transfer. Moreover, inorganic compounds can also be corrosive for the plant materials, thus increasing the maintenance costs and reducing the plant lifetime. Finally, they may be responsible for bed agglomeration due to the occurrence of melting phenomena, which are particularly noticeable in the presence of some inorganic elements forming low melting point eutectics. Vassilev et al.[6] extensively reviewed ash fusion and ash formation mechanisms of different biomass types during combustion and concluded that certain associations of inorganic elements based on their content, speciation, and origin can be used for predicting the ash fusion, slagging, deposit formation, fouling, agglomeration, sintering, or corrosion problems. Trubetskaya[272] compared woody and herbaceous biomass under high temperature fast pyrolysis conditions pointing out the pivotal role of Si and K in determining the formation of low melting point ash. A positive aspect is that K was found to have an active role in reducing soot formation. However, at the typical temperature of slow and fast pyrolysis for char and bio-oil production, all these phenomena are less relevant, and some of them, such as bed agglomeration, cannot be ascribed to the presence of inorganic elements.[320]

6.3. Bio-Oil Storage and Utilization. A secondary effect of the presence of alkali metals in the biomass during pyrolysis is due to their transfer in the condensable fraction, causing an increase of the phase separation in the bio-oil with time. This is an additional effect to the normal aging typical of the bio-oil, and it can be attributed to the reduction of surfactant species produced during the pyrolysis process.[321] However, the aging of the bio-oil is also affected by the alkali metals presence in the feedstock, and it has been demonstrated that a simple washing treatment of the feedstock led to a significant improvement of the bio-oil stability. This is particularly evident for feedstocks with a high ash content.[285,322]

The presence of char particles increases the aging of the bio-oil due to the catalytic effect of metal elements in the char, like calcium, magnesium, aluminum, and zinc. Their presence favors the oxidative processes, and small char particulates themselves may act as condensation nuclei promoting the formation of residues and deposits.[323,324]

Possible effects of the presence of inorganic species presence in bio-oil during its combustion are corrosion, erosion, and deposition, and their relevance depends on how they are present in the bio-oil, either if they are present as solid particulates (a typical example is the residual char particles that have not been removed by filtration) or as inorganic species that are dissolved in the bio-oil.

In the case of solid particulates, the main drawbacks, in addition to the deposition of sludges in the containers and the potential clogging of small passages, are the possible erosion effects that small particles have on the pumps, atomizers, and, in general, on all the metallic surfaces when high velocity flows occur, since solid particulates in the bio-oil have a very small size (below 10 μm) and may act as inception nuclei promoting the formation of higher quantities of particulate during combustion.[1] For all these reasons, the particulate content in bio-oil should be as low as possible and at least below 0.1 wt %.[325] These particles may be filtered out, but the reduction of the number of

https://doi.org/10.1021/acs.energyfuels.0c04046
Energy Fuels 2021, 35, 5407−5478

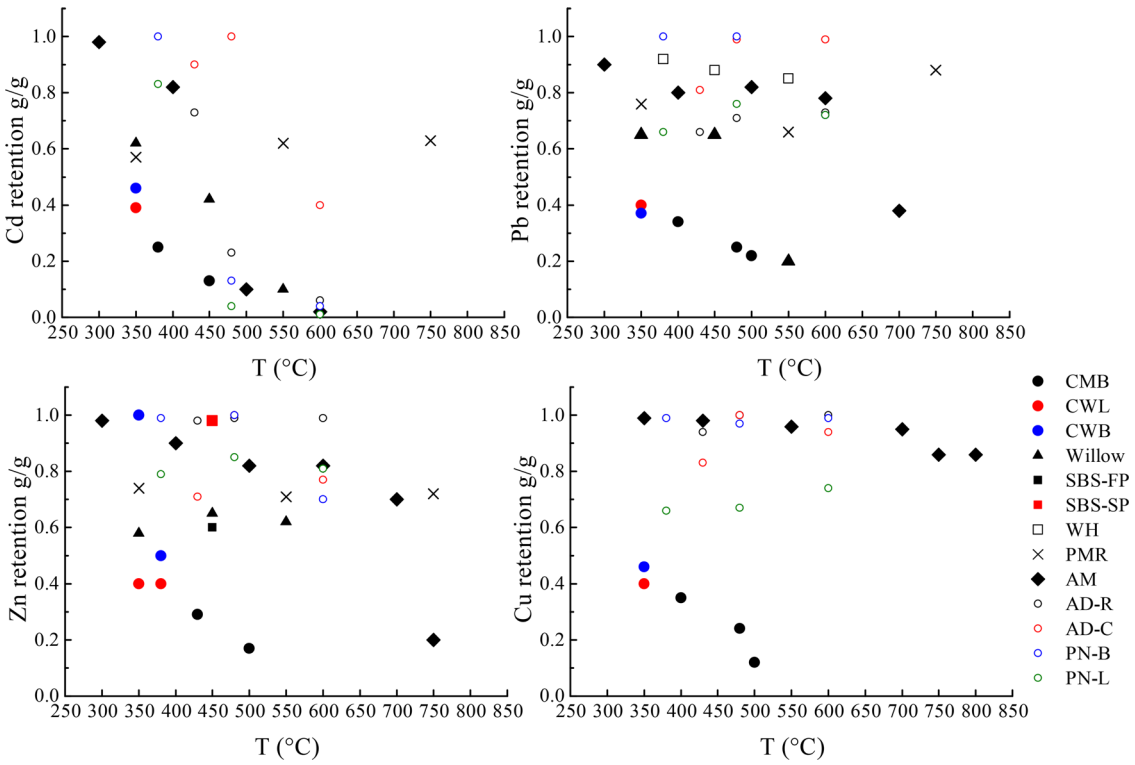

Figure 9. HMs retention in the char obtained under different pyrolysis temperatures from CMB and CS[337] (maatheide birch and sunflower), CWL and CWB[338] (willow leaves and branches), willow,[339] SBS-FP and SBS-SP[274] (*Sorghum bicolor* L. from fast and slow pyrolysis, respectively), WH[275] (water hyacinth), PMR[340] (*Brassica juncea*), AM[276] (*Avicennia marina*), AD-R and AD-C (*Arundo donax* rhizomes and culms), and PN-B and PN-L[111] (*Populus nigra* branches and leaves).

very small particles (below 1 μm) in the bio-oil is quite expensive. In addition, there is evidence that the use of hot gas filters to remove particulates and other contaminants reduces significantly the carbon yield of bio-oil.[14]

Also, the content of inorganic species in the bio-oil should be kept at the lowest possible amount. However, even if a clear indication of the maximum amount of inorganic content in the bio-oil cannot be given since the acceptable maximum content depends on the specific application,[14] there is a general indication to keep the chlorine content in the order of 0.1−0.2 wt %.[326] An analysis of the possible implication of inorganic contaminants in the fast pyrolysis bio-oil during combustion in gas turbine engines, leading to some general criteria to evaluate the quality of the pyrolysis oil, is given in ref 325.

It is important to stress that the inorganic presence effects not only depend on their concentrations but also on their interactions. For example, during bio-oil combustion in gas turbines and engines, the presence of significant amounts of alkali metals, when also sulfur is present, may be the cause of corrosion of metal parts in combustion devices. In this case, by removing either the sulfur or the alkali, the problem is removed, and the presence of a significant amount of only one of these species does not generate corrosion problems.[327] However, the standard water removal methods used to remove alkali metals can be hardly applied due to the solubility of a significant portion of bio-oil in water. In this case, it may be convenient to remove the sulfur or modify the bio-oil production process to reduce the alkali metals and/or sulfur concentration. On the other hand, there are some inorganic species, like chlorine, that are the cause of significant hot corrosion phenomena both by themselves or in the presence of alkali metals. In this latter case, the presence of alkali metals favors the deposition of chlorinated compounds on the metal surfaces producing favorable conditions for local corrosion phenomena. A comprehensive review of the possible deposition and corrosion phenomena caused by inorganic elements presence and in particular of chlorine during pyrolysis products combustion has been published by Niu et al.[326]

The removal of ashes and other contaminants by filtering bio-oil directly in the fast pyrolysis reactor has been proposed as a possible way of mitigating the typical drawbacks of post processing filtering, i.e., deposition in the filter (with relevant pressure losses) and carbon to oil yield reduction.[328]

Pyrolysis/combustion integrated solutions are available (e.g., Pyreg process[329]) where the vapor phase produced through fast pyrolysis (condensable and non-condensable gases) is directly oxidized under MILD conditions.[330]

6.4. Bio-Oil Upgrade. The selective production of platform chemicals through CFP is based on the catalyst efficiency and duration. Despite the promising results obtained with the available large catalysts pool such as zeolites and activated carbons,[2] CFP suffers from the high cost of the catalyst production and the technical problems due to the catalyst deactivation.[58] Catalyst deactivation can occur during both in situ and ex situ CFP and is greatly affected by the presence of inherent inorganic metals in biomass. The mechanisms of interaction between metals and catalysts are different depending on the CFP modality; during in situ CFP, the catalysts are in direct contact with the metals in the biomass, whereas in ex situ CFP, metals come in contact with the catalysts due to their partial devolatilization during pyrolysis (Subsection 5.4). Most of the studies dealing with the catalyst deactivation during in situ CFP revealed that over time the metal deposition on the catalyst surface is accompanied by the reduction of the deoxygenating activity of the catalyst[331−333] and by a gradual switch of the

https://doi.org/10.1021/acs.energyfuels.0c04046
Energy Fuels 2021, 35, 5407−5478

selectivity from aromatic hydrocarbons to alkylated phenols.[331] Besides AAEMs, also Cu and Fe were found to deposit with a deposition rate faster for K than for the other metals phenols.[331] Few papers exist which compared the effect of inherent biomass metals on the catalyst deactivation in the two CFP modalities. Iisa et al.[334] reported an increased accumulation of K and Ca in both the CFP configurations, whereas Mg and Fe where found to accumulate only during in situ CFP. A different result was obtained by Kalogiannis et al.,[11] who compared the results of their ex situ experiments with the ones obtained in the same reactor operated in in situ mode. The biomass inherent metals deposited on the catalyst only during in situ CFP experiments, whereas in ex situ runs, they accumulated only in the first reactor with the consequent extension of the catalyst lifetime.

6.5. Release/Accumulation of Toxic Species. Inherent inorganic species may cause safety problems both directly through the release of toxic inorganic elements and indirectly by catalyzing the production and the further release of harmful organic and inorganic compounds.

Concerning the toxic inorganic elements, the environmental effect may be noticeable when HMs-contaminated biomass is used as feedstock. In this case, it is mandatory to monitor the HMs behavior during the pyrolysis process and the influence of the process condition on them. The confinement of HMs in the char has the advantage of producing a condensable fraction suitable to be used as biofuel as it is or to be further upgraded to transport fuel. HMs are largely retained in char, and their concentration increased with an increasing severity of the pyrolysis conditions as more and more volatile matter is driven off.[111,335,336] Figure 9 shows the retention of some HMs in the char at different pyrolysis temperatures. Despite the large variations observed for all the metals, a general trend can be outlined which indicates Cd as the most volatile.[111,337,338,341] Also, some discrepancies exist on the HMs recovery determined by the pyrolytic regime. As depicted in Figure 9, except for Cd, the points in the higher recovery region (retention > 0.6) refer to low heating rate during pyrolysis[111,274−276] (5−30 °C/min). Conversely, the points located in the lower recovery region refer mostly to fast pyrolysis conditions.[337−339] For example, Al Chami et al.[274] reported that Zn and Ni recovery is higher when the process is carried out at 20 °C/min compared to flash conditions.

Many of these HMs were stabilized within the char structure since they undergo chemical transformations during pyrolysis especially due to the interactions with other inorganic elements[111,339−343] and were less prone to affect the environment where char is applied, at least in the short to medium terms.[344]

An indirect effect of the presence of AAEMs on the release of toxic organic compounds is related to the PAH formation. Most of the studies dealing with the PAH formation mechanisms in pyrolysis were conducted under high temperature conditions in order to simulate the pyrolytic stage preceding the biomass combustion. Wang et al.[345] found that as temperature increased from 900 to 1200 °C, the content of single ring aromatics in the tar produced from slow pyrolysis of wheat straw decreased from 69.52% to 37.96%, while PAH content increased from 8.35% to 38.55%. A reduced content of AAEMs obtained through a leaching pretreatment promoted the formation of higher average ring number PAH, and this effect was attributed to the reduced content of K capable of catalyzing the decomposition of tar and heavy PAH in the raw straw. Opposite results were obtained under low temperature conditions between 400 and 600 °C[346] where the mechanism for the formation of PAH is attributable to precursors formed in the solid char matrix,[347] and the temperature is too low for the PAH decomposition. The addition of alkali metals to cellulose resulted in a higher yield of PAH due to the high char yields, whereas the concentration of PAH into the char samples was not affected by the presence of alkali metals.[346]

The chemical transformations and release of N and S compounds during pyrolysis were studied with the ultimate purpose of predicting and further preventing the emission of NOx and SOx during pyrolysis products combustion. K, Ca, Fe, Al, and Si have different effects on the extent and on the type of transformation of N compounds in pyrolysis, also depending on the process temperature.[97] For example the presence of K was detrimental for NOx precursors at high temperature, whereas it promoted their formation at low temperature. The opposite effect was observed in the presence of Ca.[303] SOx precursors were released under pyrolysis as H_2S and COS at low temperature, and no evidence of the AAEMs effect on their release in the gas phase under pyrolysis conditions was reported.[294]

In the biomass pyrolysis process, the presence of Cl may cause problems in the further utilization of the products through corrosion and deposition phenomena. However, it may contribute to the formation of dioxins (PCDDs) and dibenzofurans (PCDFs). Recent studies reported the formation of these compounds, even though in lower amounts than in combustion conditions, also during pyrolysis of high Cl content biomass, especially in the presence of Cu that acted as a catalyst in the formation of these harmful compounds.[348] Most PCDD/Fs produced during the biomass pyrolysis process are found in the bio-oil or gas phase, even though traces were found also in biochars.[349]

6.6. Pretreatments for Reduction of Inherent Inorganic Elements Content. Regardless of the specific inorganic species, and the specific technological problems, it is advisable reduction of the total ash content prior biomass pyrolytic treatment fast pyrolysis. To this end, both physical and chemical pretreatments may be applied. A detailed review of possible pretreatments for reducing the content of inherent inorganic elements in the biomass can be found in Kumar et al.,[42] who discussed their effects on the bio-oil yield and quality and char characteristics.

Water extraction and acid washing are the most investigated pretreatments which could be applied in commercial-scale conversion plants. It is worth noting that their application produced modifications of both the inorganic elements contents and the organic matrix at different extents. Their removal efficiency was already presented in the Section 4.1.

Overall, water extraction is an efficient and cost-effective technique for biomass pretreatment, even though a certain additional cost should be considered for the need of drying the pretreated biomass before pyrolysis.[350]

Even though the acid pretreatments were more effective than the water extraction, it is worth noting that they affect also the organic matrix by dissolving the extractives and breaking the linkages between the biomass organic components, thus reducing the initial mass of the biomass. Moreover, this kind of pretreatment has a higher environmental impact due to the residual acid leachate that may contain also HMs.[350] The overall costs should take into account the additional energy input required for pretreated biomass drying, use of chemicals, use of expensive alloys resistant to acid corrosion for the reactor

https://doi.org/10.1021/acs.energyfuels.0c04046
Energy Fuels 2021, 35, 5407−5478

construction, and increased maintenance operations of the reactors deteriorated by the acid leaching solutions.[351]

An alternative to the removal of inorganic elements is to reduce their catalytic activity or their devolatilization by doping the biomass with proper compounds capable of reacting with them during the pyrolysis process to form noncatalytic mineral forms (passivation)[352] or less volatile minerals that are retained in the char in less mobile and safe forms. Dalluge et al.[353] and Kuzhiyil et al.[352] found that infused mineral acids are effective in passivating AAEMs also in high ash content biomasses such as switchgrass and corn stover. Moreover, the literature suggests that some metals form complexes with P, Ca, Fe, or Si during pyrolysis, and they are thermally stable even at high temperatures. This approach is particularly attractive when there is the risk of HMs removal through leaching pretreatment and was found to be very effective for many HMs except for Cd.[341] With respect to washing pretreatments, AAEMs passivation requires relatively little water and, consequently, lower energy input for the subsequent drying. For AAEMs passivation, the water to biomass ratio can be strongly reduced since it is only necessary to homogeneously distribute the acid throughout the biomass. For example, Dalluge et al.[353] used a water to biomass ratio of 1:1 to infuse red oak.

Air classification is another effective means to remove exogenous soil ash from biomass.[354] Ash content in the range of 36−50 wt % was found to be removed through air classification from loblolly pine logging residues[354] and from corn stover and switchgrass,[355] even though the AAEMs removal was not always efficient. Unfortunately, this removal is accompanied by the loss of biomass that, in some cases, was very high, thus causing additional cost to the process. Some recent papers evaluated the overall capital and operating costs for air classification and acid leaching per dry ton processed, revealing that costs for acid leaching were 20 times higher than for air classification.[356] This result suggested air classification as a first pretreatment stage to concentrate exogenous ash into a fraction of the biomass. Then, leaching of that fraction could be performed in a second stage to lower inherent inorganics content, and finally, the leached fraction should be recombined with the lower ash content fraction derived from air classification.[357]

Finally, in order to have a feedstock that meets specifications required for pyrolysis in terms of ash content, another effective strategy could be the blending of different types of biomass. It allows using also low quality biomass by avoiding expensive pretreatments, for example, mixing woody and herbaceous samples.[358] Many authors showed that the physical properties and the distribution of the vapor phase pyrolysis products and pyrolysis products yields are proportional to the ratio of the different feedstocks in the blended samples, thus confirming that blending can be considered a viable strategy for using low quality biomass for producing pyrolysis products meeting the required quality standards.[359−361] Moreover, preliminary defoliation and debarking is suggested for reducing problems during thermochemical conversion. Also, plant age should have be considered since late harvest cause an increase of ash content.[362] On the contrary, delaying harvest of perennial crops from autumn to late winter/early spring results in a decrease of ashes, likely for the leaf fall and retranslocation of nutrients (e.g., K, P, Cl and S) toward the underground reserve organs.[363,364]

7. PREDICTIVE APPROACHES FOR CATCHING EFFECTS OF INHERENT METALS ON PYROLYSIS KINETICS

Although experimental works are more reliable in terms phenomenological realism, their combination with computational science has been proved to be crucial for research since it enlightens physical and chemical phenomena that occur in a pyrolysis reactor. It is irrefutable that modeling involves a high effectiveness in optimizing the operating conditions of the pyrolysis process and accuracy in testing its limits. Another strong benefit of modeling relies on the low-cost exploration of the potential benefits, costs, and risks associated when selecting feedstock and operation conditions to be provided to the reactor in order to achieve the required products yields.[365]

Modeling the pyrolysis behavior involves a high level of complexity that has captured the focus of many researchers in addressing this matter using different modeling approaches.[8] The most common approaches are based on the chemical percolation devolatilization (CPD),[366,367] modified CPD,[368] distributed activation energy (DEAM),[369,370] and chemical kinetic models.[67,371−375] The selected approach often depends on many aspects, but regardless of that, chemical kinetic models are proven to give better results in comparison to other models.[376−378]

Some reviews have focused on a large number of studies centered on the kinetic modeling of biomass slow and fast pyrolysis processes.[7,20,379] There are various kinetic models with distinct levels of complexity. In the class of simpler models, there are, for example, the single first-order reaction model (SFOM), which considers only one biomass component and one stage of decomposition, the three-parallel model (3PM),[20] which describes the decomposition of the three major components of biomass (cellulose, hemicellulose, lignin), and the five-parallel model (5PM) with the inclusion of the pyrolysis of the extractives.[369] These models do not make use of the fundamental components since they are not easy to quantify and are also modified with the conversion level. Therefore, the practical approach employed is based on global descriptions that do not consider the interactions within and between the solid and gas phases.[20] Moreover, most of these models rely on linear regression methods such as the Kissinger−Akahira−Sunose (KAS)[311,380] or Flynn−Wall−Ozawa (FWO)[311,381] to estimate the kinetic parameters (activation energy and pre-exponential factor) of one or multiple conversion stages of one single biomass component. However, when multicomponent mechanisms that consider several parallel reactions come in place, the usage of these methods can become a challenge, and their results may be uncertain.[382] With the continuous increase of computing power, optimization methods have emerged as an alternative for the estimation of multiple kinetic parameters and of stoichiometric coefficients for mass balance calculations present in detailed mechanisms that consider product speciation.[67,382,383] These models include those proposed by Ranzi et al.,[372] Debiagi et al.,[64] and Dussan et al.,[375,384] which describe in detail the pyrolysis behavior of the major organic components of biomass, while considering product speciation and different components structures that depend on the biomass type and intrinsic organic composition. These models can represent a good basis where they can easily include the catalytic effects or even the release of different AAEMs. Due to the extensive biomass database presented in the work of Debiagi et al.,[64] it is believed that this kinetic mechanism considers at some extent

https://doi.org/10.1021/acs.energyfuels.0c04046
Energy Fuels 2021, 35, 5407−5478

the inherent interactions between the organic components and the catalytic effect of alkaline earth metal (AAEM) species during the pyrolysis process, however, in a very general way.[372] There are a few kinetic mechanisms that are able to describe in detail the secondary gas phase reactions, such as reforming, cracking, and polymerization of tars.[64,235,371] Nevertheless, the effect of AAEMs as catalysts in the promotion of char reactions, cracking of tars, and inhibition of PAH and soot during the pyrolysis process is still not accounted for, although it is especially important as a prestage of the gasification process where a clean gas is desirable.[365]

In this present review, focus is majorly given to the role of KCl in the pyrolysis of lignocellulosic biomass, since an overview of the chemical composition of this type of biomass shows that potassium and chloride are of special interest since they represent the major species in the ash composition[4,288,385] and are mostly present in biomass in the ion state and in the form of mineral particles.[386]

Only a few attempts were made to include the catalytic effect of AAEMs in the pyrolysis kinetic mechanisms.[9,68,287,387−391] Ranzi et al.[372] proposed a modification to a previous kinetic mechanism[392] to predict the ashes catalytic effect during biomass fast pyrolysis. The activation energies of the catalyzed dehydration, homolytic cleavage, and heterolytic fission reactions, also mentioned in the work of Leng et al.,[388] were adjusted using a global ash factor (AF = tanh(ash/2), where ash is the content of ash in wt %) in a nondimensional form, and it was applied to the decomposition reactions of cellulose and hemicellulose. Nevertheless, results showed that these slight modifications can improve the overall predictions, but there is still room for improvement, especially regarding heterogeneous reactions and secondary reactions involving char, i.e., dehydration and other decomposition reactions that represent ash catalytic effects should be included in the mechanism. A method similar to that in ref 372 was used by Trendewicz et al.,[389] but it was only applied to cellulose pyrolysis in a fluidized bed reactor. The results showed that the modified cellulose pyrolysis mechanism was able to capture with good accuracy the catalytic effect of potassium on the pyrolysis products yields. Moreover, the model predictions were able to capture the inhibition of levoglucosan formation and the enhancement of the formation of char, water, and gases. Ferreiro and co-workers[68,387] proposed a modification on both cellulose and hemicellulose submechanisms of Ranzi et al.[372] to include reactions that capture the catalytic KCl effects on the slow pyrolysis of the two components. Extensive experimental data sets obtained from thermogravimetric analyzer (TGA) and pyrolysis reactor measurements,[68,236] with different KCl concentrations, were used to estimate the global reaction kinetic parameters and molar coefficients, where the catalytic effects were observed in relation to the potassium concentration included in each sample. In the work of Ferreiro et al.,[68] the authors decided to maintain the characteristics of the cellulose submechanism of Ranzi et al.[372] and performed a deeper analysis of the major gaseous species $_{22}$, and CH_4). Regarding cellulose predictions, the modified mechanism was able to capture with good accuracy the catalytic effects of KCl, such as the general mass loss profiles, promotion in the formation of char and gases at the expense of the condensable fraction, early release of CO and CO_2, dehydration reactions that occur due the earlier depolymerization of large components, and inhibition of levoglucosan and aldehydes formation. However, the modified mechanism was not able to predict the release of H_2 and CH_4 since the original chrematistics of the bio-PoliMi model were kept, showing that a restructuration is required for capturing the release of these species. Furthermore, the modified mechanism was not able to predict the occurrence of secondary gas phase reactions observed in the experimental results at higher temperatures, as shown in Figure 10.

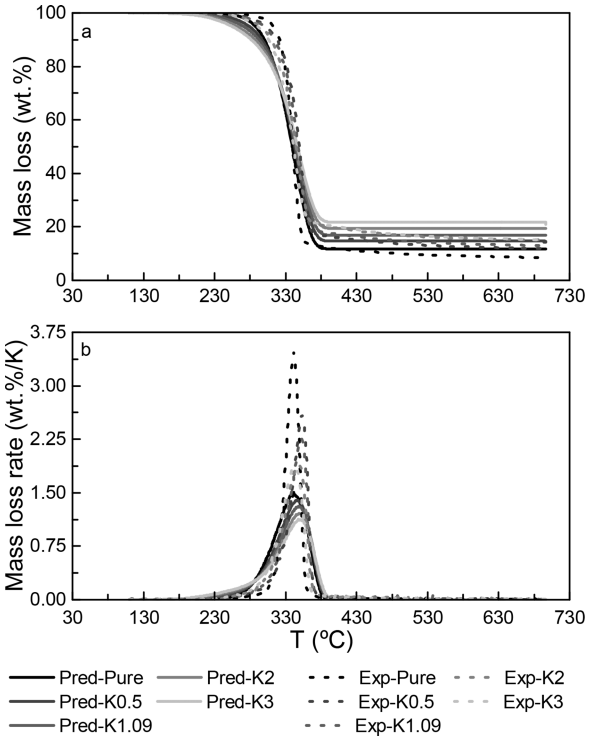

Figure 10. Influence of KCl concentration on the experimental and predicted TG (a) and differential TG (b) profiles.[68]

Trubetskaya et al.[390] modeled the influence of potassium during the fast pyrolysis of woody and herbaceous biomass using a combination of kinetic and particle models. The authors proposed a three-reaction mechanism to predict the pyrolysis behavior in an entrained flow reactor (EFR). The catalytic effect of potassium was accounted for through the char yield; i.e., adding potassium decreases the activation energy required for the reaction from metaplast to char to occur, promoting its formation. Recently, Trubetskaya et al.[391] modeled the influence of ash content on the fast pyrolysis products yields of three lignocellulosic synthetic components (cellulose, hemicellulose, and lignin). In this work, the authors proposed a set of correlations that can be applied to each component in order to predict the solids and major gas species yields (CO, CO_2, CH_4, and H_2). The inorganic content was considered to be inert, contributing in this way only to the final amount of char. The authors proposed five different models that considered different key variables. The obtained results led the authors to conclude that the first model proposed could be extended, and additional parameters were progressively included, but always balancing the addition of new parameters with the overfitting risks. All the proposed models neglect the presence of the extractives. The catalytic reactions considered in the models are reported in Table 5 and numbered from (1) to (5); models (1)−(3) were used for char yield predictions, while models (4) and (5) were used for char and total gas yields and individual major gas species yields. Models (1)−(3) were not able to predict the gas phase

https://doi.org/10.1021/acs.energyfuels.0c04046
Energy Fuels 2021, 35, 5407−5478

Table 15. Catalytic Reactions and Correlations That Can Capture AAEMs Effects in Pyrolysis of Biomass Components

Component	Catalytic reaction	ref
Cellulose	$E_{R_2} = 19{,}100 - 600(\mathrm{AF} - 0.5)\,(\mathrm{kcal/kmol})$	371
	R_2:CELL $\rightarrow 0.4C_2H_4O_2 + 0.05C_2H_2O_2 + 0.15CH_3CHO + 0.25C_6H_6O_3 + 0.35C_3H_6O + 0.15CH_3OH + 0.2CH_2O + 0.61CO + 0.35CO_2 + 0.05H_2 + 0.93H_2O + 0.02HCOOH + 0.05C_3H_6O_2 + 0.05GCH_4$	
	$E_{R_4} = 31{,}000 - 1000(\mathrm{AF} - 0.5)\,(\mathrm{kcal/kmol})$	
	R_4:CELL $\rightarrow 5H_2O + 6$Char	
Hemicellulose	$E_{R8} = 3000 - 1000 \times (\mathrm{AF} - 0.5)\,(\mathrm{kcal/kmol})$	
	R_8:HCE $\rightarrow 0.4H_2O + 0.79CO_2 + 0.05HCOOH + 0.69CO + 0.01GCO + 0.01GCO_2 + 0.35GH_2 + 0.3CH_2O + 0.9GCOH_2 + 0.625GCH_4 + 0.375C_2H_4 + 0.875$Char	
Cellulose	$k = 1.41 \times 10^7(s^{-1})\cdot T^{0.281}\cdot\exp(-22.1\,(\mathrm{kcal/kmol})/RT)$	68, 387
	CELL + KCl $\rightarrow 4.81$Char $+ 3.21H_2O + 0.59CO + 0.60CO_2 + 1.79GH_2$ + KCl	
Hemicellulose	HCE + AM $\rightarrow a_1$HCE1 $+ a_2$HCE2	
	HCE + AM $\rightarrow b_1$Char $+ b_2H_2O + b_3$GCO $+ b_4GCO_2 + b_5GH_2 + b_6GCH_4 + b_7GCOH_2$ + AM	
Cellulose	$Ea_{\text{homolytic cleavage}}(K) = 100.16\cdot K^{0.0168}$	389
	$Ea_{\text{heterolytic fission}}(K) = 118.99\cdot K^{0.056}$	
	$Ea_{\text{dehydration}}(K) = 124.52\cdot K^{-0.03}$	
	CELL $\rightarrow 3$Char $+ H_2O + 2CO + CO_2 + 4H_2$	
Biomass	$E_{a,\text{metaplast}\rightarrow\text{Char}} = \Omega_K(K)\cdot E_{a,\text{metaplast}\rightarrow\text{Char}}$	390
	$\Omega_K(K) = 1 - a_1\cdot(1 - \exp(K/a_2)^2)$	
Synthetic components	(1) $\gamma = a_1\gamma_{\text{cell}}y_{\text{cell}} + a_2\gamma_{\text{xyl}}y_{\text{xyl}} + a_3\gamma_{\text{lig}}y_{\text{lig}}$	391
	(2) $\gamma = b_1((\gamma_{\text{cell}}y_{\text{cell}})^{b_2} + (\gamma_{\text{xyl}}y_{\text{xyl}})^{b_3} + (\gamma_{\text{xyl}}y_{\text{xyl}})^{b_4})\gamma_{\text{ash}}^{b_5}$	
	(3) $\gamma = c_1(\gamma_{\text{cell}}y_{\text{cell}} + \gamma_{\text{xyl}}y_{\text{xyl}} + \gamma_{\text{lig}}y_{\text{lig}})^{c_2}\gamma_{\text{ash}}^{c_3}$	
	(4) $\gamma = d_1(\gamma_{\text{cell}}y_{\text{cell}} + \gamma_{\text{xyl}}y_{\text{xyl}} + \gamma_{\text{lig}}y_{\text{lig}})^{d_2}\gamma_{\text{ash}}^{d_3}T_{\text{reac}}^{d_4}$	
	(5) $\gamma = (e_1\gamma_{\text{cell}}y_{\text{cell}} + e_2\gamma_{\text{xyl}}y_{\text{xyl}} + e_3\gamma_{\text{lig}}y_{\text{lig}})\gamma_{\text{ash}}^{e_4}T_{\text{reac}}^{e_5}$	

data, while models (4) and (5), with the explicit inclusion of temperature as a fitting parameter, were able to predict with good accuracy the yields of char as gas individual yields, with temperature being the most sensitive variable. However, none of the models include the effects of heat and mass transfer which could further improve predictions. Jeong et al.[393] proposes a different approach to study the influence of AAEMs in the pyrolysis of lignin. This approach is based on a density functional theory (DFT). Due to the complexity of lignin's structure only three $\beta-O-4$ model dimers are commonly used as representatives, since they symbolize the majority of interunit linkages (p-hydroxyphenylglycerol-β-guaiacyl ether (HGE), guaiacylglycerol-β-guaiacyl ether (GGE), and syrin-gylglycerol-β-guaiacyl ether (SGE)). The authors studied, at a molecular level, the interactions between the GGE dimmer complexes with different AAEMs. In this sense, DFT calculations were

https://doi.org/10.1021/acs.energyfuels.0c04046
Energy Fuels 2021, 35, 5407−5478

Table 16. Possible Potassium Transformation Paths in Generality of Thermochemical Conversion Processes

Potassium possible transformation paths	ref
$2C + 2K_2CO_3 \rightarrow 2K + 3CO$	377
$2K(g) + \rightarrow K_2O+CO$	
$K_2O + CO_2 \rightarrow K_2CO_3$	
$2KCl + nSiO_2 + H_2O \rightarrow K_2O(SiO_2)_n + 2HCl$	287
$2HCl + 0.5O_2 \rightarrow Cl_2 + H_2O$	
Inorganic $K(K^+) \rightarrow \varphi_1KCl + \varphi_2K_2SO_4 + \varphi_3K_2CO_3$	395
Organic $K(R - COOK) \rightarrow Char - K$	
Organic $K(R - COOK) \rightarrow R - COOH(carboxylgroups) + CO_2 + K(g)$	
$R - COOH(carboxyl\ groups) + KCl \leftrightarrow R - COOK + \alpha_1HCl + \alpha_2CH_3Cl$	
$KCl(s) \rightarrow KCl(g)$	
$K_2SO_4(s) \rightarrow K_2SO_4(g)$	
$K_2SO_4(s) + H_2O \rightarrow 2KOH + SO_2 + 0.5O_2$	
$K_2CO_3(s) \rightarrow K_2CO_3(g)$	
$K_2CO_3(s) + H_2O \rightarrow 2KOH + CO_2$	
$S^{-2} \rightarrow Crystallized\ S - Compounds$	
$Crystallized\ S - Compounds \rightarrow SO_2$	
$K + H_2O \rightarrow K - O - C + H_2$	280
$K - O - C + C \rightarrow C - O + K$	
$C - O + K - O - C \rightarrow K + CO_2$	
$CM - K + H \rightarrow CM + H - K$	
$CM - CH_3 - COO - K + H \rightarrow CM - H + CH_3COOK$	
$CM - K + R \rightarrow CM + R - K$	
$R - COOH(s) + KCl(s) \leftrightarrow R - COOH(s) + HCl(g)$	397
$K + Cl + M \rightarrow KCl + M$	398, 399
$KCl + H \leftrightarrow HCl + K$	
$KOH + HCl \leftrightarrow KCl + H_2O$	
$KOH + H \leftrightarrow K + H_2O$	
$HCl + H \leftrightarrow Cl + H_2$	
$KOH+HCl \leftrightarrow KCl + H_2O$	400
$K_2CO_3 + 2\ HCl \leftrightarrow 2\ KCl + CO_2 + H_2O$	
$(Ca -)Potassium\ carbonate(s) + H_2O \rightarrow 2KOH(g) + CO_2(g)(+ CaO(s))$	297, 401
$Char - COOK + MCl \rightarrow Char - COOM + HCl$	
$Char - COOK \rightarrow Char + CO_2 + K$	
$Char - C_6H_5 - OH + K \rightarrow Char - C_6H_5 - OK + H$	
$K_2CO_3 \rightarrow 2K + CO_2 + 0.5O_2$	

performed in order to determine the low energy conformations of metal−GGE complexes and hence to find the optimal binding site of each AAEMs and clarify how it influences the depolymerization reactions of lignin. The authors concluded that the preferred binding sites for all AAEMs were O($C\beta$) and O(methoxy), since these resulted in the most stabilized complex energy. This study gives a strong contribution to the development of kinetic mechanisms since it enlightens about the preferred paths of lignin depolymerization reactions when the catalytic effects of AAEMs are present. Table 15 summarizes

https://doi.org/10.1021/acs.energyfuels.0c04046
Energy Fuels 2021, 35, 5407−5478

the above reviewed catalytic reactions and correlations that can capture AAEMs effects in the pyrolysis of biomass components.

Simple models like those presented in Table 15 are extremely valuable since they allow the recognition of important key variables, such as reaction temperature, AAEMs or ash concentration, and other empirical coefficients, that can enlighten future tryouts and the development of kinetic and mechanistic models.[391] It is clear that due to the accounted difficulty of this matter, more efforts should be redirected to this topic. Moreover, it is known that the presence of different AAEMs can lead to different reactive behaviors,[235] especially during the secondary gas phase reactions.[376,377] Chloride eases the mobility of AAEMs, especially potassium, and stabilizes high temperature gas phase alkali-containing species,[287] while potassium has a catalytic effect on its thermo-chemical conversion processes.[287,385] It is also worth noting that a few studies have revealed that silica, which does not catalyze the pyrolysis process of biomass, may prevent the release of potassium to the gas phase if the K/Si ratio is small.[288,376,377] Umeki et al.[394] studied the catalytic activity of ash during the gasification of different biomass char samples. The authors proposed a three-parallel model reaction to describe the different regimes observed during the overall conversion rate of biomass char, each related to the dynamic change of the catalytic activity. It was concluded that the model was sensitive to the amount of silicon in the ash-forming elements of the used samples. The model presented good results for the samples with low amounts of silicon. As for the samples with high contents of silicon, the model only showed accuracy for gasification operating conditions using mixtures of CO_2 and CO. The model was not applicable under steam gasification conditions since no change in the catalytic activity was observed in the predictions. Trubetskaya et al.[92] also observed that the presence of silica slightly decreases char reactivity and can affect its mechanical integrity. The influence of Si during biomass pyrolysis and gasification is a subject that should take more attention in future works.

Finally, it is still necessary to propose kinetic mechanisms that can capture the progress of the release of KCl from biomass during the pyrolysis process. One possible way of achieving this purpose is to integrate the possible KCl vaporization reaction paths in the existent kinetic mechanisms, as seen in the work of Fatehi et al.[395] The model developed in the work of Fatehi et al.[395] is able to study the interactions between organic and inorganic compounds (K/S/Cl) in the solid structure of biomass and to predict the temporal release of some K/S/Cl components from biomass pyrolysis. Although some limitations were noted, this work represents the first attempt to model the release of important trace element species during pyrolysis and has opened new possibilities in the development of kinetic mechanisms. Table 16 summarizes possible K transformation paths in the generality of thermochemical conversion processes.[280,287,297,395−401]

8. CONCLUSIONS AND PERSPECTIVES

The present review provides an extensive discussion on the role of the inherent inorganic elements, especially metals, in biomass pyrolysis. Some important general conclusions were identified, along with numerous challenges and obstacles that still need to be addressed:

- The studies dealing with the effects of AAEMs on pyrolysis of the biomass main organic components suffer from strict constraints that limit the possibility to explore the wide variety of organic components that characterize biomass (e.g., different types of hemicellulose and lignin). The challenge is to optimize the extraction procedures to obtain the components directly from the real biomasses with a 2-fold aim of limiting their alterations and reducing as much as possible the presence of residual inorganic elements. It is strongly recommended to adopt also advanced characterization techniques to take into account the variegated chemical composition of each biomass component. In any case, as a direction for future research on this topic, it is pivotal to extend the studies also to other under investigated biomass components such as pectin and extractives and to couple studies of the pyrolysis process to a detailed characterization of the organic and inorganic matrices in the starting material in order to provide detailed and quantitative insights.
- As a general trend, the inherent inorganic elements present in biomass, more specifically AAEMs, (i) anticipate the onset of the decomposition reactions and of the maximum devolatilization rate temperature, (ii) favor the decomposition pathways leading to the production of low molecular condensable species and permanent gases, and (iii) determine the increase of the char yield. However, in order to implement reliable kinetic models, it is important to evaluate the catalytic effects of inherent inorganic elements from a quantitative point of view. Given the considerable complexity of the numerical approach, it is important to evaluate the minimum threshold below which the catalytic effects are negligible, as well as the maximum threshold above which these effects level off. Moreover, such an approach would allow highlighting nonmonotonous effects on the yield of some species of interest (as for example has been observed for furfural and some carboxylic acids). The effect of the different chemical forms in which inorganic elements are present in the biomass should be assessed as it could affect the nature and extent of their catalytic action (attention should be payed to devolatilization and passivation phenomena and to the effect of counterions).
- Inherent inorganic elements produce undesired and unsafe phenomena during pyrolysis and the further utilization of the products. Some of them are still scarcely explored, and their comprehension could boost the exploitation of biomass from low quality soils (e.g., salty or contaminated soils). Among the different approaches adopted at laboratory scale for the removal of inorganic matter from biomass, organic acid leaching has to be preferred. This method could be attractive also at commercial scale if the aqueous acid fraction deriving from biomass pyrolysis is used since it is less attractive from an energetic point of view, and its use could avoid the use of external chemicals. However, a detailed cost analysis under different scenarios is needed for comparing all the others pretreatments to evaluate their feasibility at a commercial scale.

AUTHOR INFORMATION

Corresponding Author

Paola Giudicianni − *Istituto di Scienze e Tecnologie per l'Energia e la Mobilità Sostenibili, CNR, Naples, Italy;*

https://doi.org/10.1021/acs.energyfuels.0c04046
Energy Fuels 2021, 35, 5407−5478

orcid.org/0000-0002-6700-8205;
Email: paola.giudicianni@stems.cnr.it

Authors

Valentina Gargiulo − *Istituto di Scienze e Tecnologie per l'Energia e la Mobilità Sostenibili, CNR, Naples, Italy;* orcid.org/0000-0002-6517-2263

Corinna Maria Grottola − *Istituto di Scienze e Tecnologie per l'Energia e la Mobilità Sostenibili, CNR, Naples, Italy*

Michela Alfè − *Istituto di Scienze e Tecnologie per l'Energia e la Mobilità Sostenibili, CNR, Naples, Italy;* orcid.org/0000-0001-8930-1210

Ana Isabel Ferreiro − *IDMEC, Mechanical Engineering Department, Instituto Superior Te′cnico, Universidade de Lisboa, Lisboa, Portugal*

Miguel Abreu Almeida Mendes − *IDMEC, Mechanical Engineering Department, Instituto Superior Te′cnico, Universidade de Lisboa, Lisboa, Portugal*

Massimo Fagnano − *Department of Agricultural Science, University of Naples Federico II, Portici, NA, Italy*

Raffaele Ragucci − *Istituto di Scienze e Tecnologie per l'Energia e la Mobilità Sostenibili, CNR, Naples, Italy*

Complete contact information is available at: https://pubs.acs.org/10.1021/acs.energyfuels.0c04046

Author Contributions

‖P. Giudicianni and V. Gargiulo contributed equally.

Author Contributions

The manuscript was written through contributions of all authors. All authors have given approval to the final version of the manuscript.

Notes

The authors declare no competing financial interest.

Biographies

Paola Giudicianni is a researcher at STEMS-CNR (Science and Technology for Sustainable Energy and Mobility). She is chemical engineer with a Ph.D. in chemical, materials, and industrial product engineering (University Federico II, Naples, Italy). Her scientific expertise covers thermochemical conversion processes of lignocellulosic biomasses. Her research activities deal with the characterization of the slow pyrolysis process through both experimental and numerical approaches with a focus on valorization of the biochar.

Valentina Gargiulo holds a Master's degree (2005) and a Ph.D. (2009) in chemistry from the University Federico II, Naples, Italy. In July 2020, she obtained a position as a researcher at the Italian Research Council (CNR), and since October 2020, she has been a member of the STEMS-CNR permanent staff. Her research activities deal with the synthesis and characterization of advanced materials, the characterization and treatment of pyrolysis feedstocks and products, and the chemico-physical analysis of complex carbonaceous materials.

Corinna Maria Grottola is a scientist at STEMS-CNR. She is an environmental engineer with a Ph.D. in industrial product and process engineering (University Federico II, Naples, Italy). Her scientific expertise covers thermochemical conversion processes of lignocellulosic contaminated biomasses. Her research is focused on the characterization of the slow pyrolysis process through physical−chemical (porosity, gas chromatography) and optical analyses (infrared laser based) of the products, with peculiar attention to char valorization as a bioproduct.

Michela Alfè is a researcher at STEMS-CNR, previously IRC-CNR, located in Naples, Italy. She graduated in chemistry and obtained a Ph.D. in chemical engineering (University Federico II, Naples, Italy). Her highly inter- or multidisciplinary activities are focused in two strategic areas, energy and environment and material science, and include the synthesis of innovative materials for applications in energetic processes (solid sorbents for CCS, water treatment, sensoristic, photoactive materials).

Ana Isabel Ferreiro obtained two Masters' degrees, in physics and in mechanical engineering, from the Instituto Superior Técnico (IST) de Lisboa. Since 2015, she has been part of the research group of Combustion and Sustainable Development of the Energy and Fluid Mechanics Center of the Associated Energy, Transport, and Aeronautics Laboratory (LAETA-IDMEC), at IST. Currently, she is a Ph.D. student at the Instituto Superior Técnico. She has (co)authored eight papers in international peer-reviewed journals and 13 communications at international scientific meetings.

Miguel Abreu Almeida Mendes is an assistant professor in the Mechanical Engineering Department of the Instituto Superior Técnico. During his academic studies, he has received the Young Researchers UTL/Deloitte Award. As a postdoctoral researcher, he worked at the Freiberg University of Mining and Technology and the Engler-Bunte-Institute at the Karlsruhe Institute of Technology, Germany. During these periods, he participated in industrial and European projects taking leading and comanagement roles. He has coauthored 32 scientific articles in high quality scientific journals.

Massimo Fagnano graduated in agronomy from the University Federico II, Naples, Italy, and is a now a full professor of agronomy and agroecology there. He has authored 86 papers (HI = 19) about air pollution effects on crops, soil fertility management, organic farming, phytoremediation, soil erosion, salinity stress, cropping systems for climate change mitigation, energy crops, and biofuels. He is also the principal investigator of European (LIFE11/ENV/IT 275, ECOR-EMED) and Italian (MIUR-PRIN 2017 BHH84R, RIZOBIOREM) research projects.

Raffaele Ragucci is a senior researcher at STEMS-CNR. He graduated in electronic engineering from the University Federico II, Naples, Italy. His scientific expertise covers advanced combustion processes, high pressure combustion diluted (MILD) combustion, pyrolysis of biomasses and lignocellulosic wastes, optical diagnostics, spray atomization, evaporation and combustion, and design and control of lab-scale reactors.

■ ACKNOWLEDGMENTS

This work was supported by PRIN RIZOBIOREM: Progetti Di Ricerca Di Rilevante Interesse Nazionale − Bando 2017 Prot. 2017BHH84R and by the Fundação para a Ciência e a Tecnologia (FCT), through IDMEC, under LAETA, projects PTDC/EME-EME/30300/2017 and UIDB/50022/2020. A.I. Ferreiro acknowledges FCT for the provision of the scholarship SFRH/BD/129693/2017. The authors express their gratitude to the professor Mario Costa who had profoundly shaped and supported the scientific collaboration between STEMS-CNR and IST.

■ REFERENCES

(1) Lehto, J.; Oasmaa, A.; Solantausta, Y.; Kytö, M.; Chiaramonti, D. Review of fuel oil quality and combustion of fast pyrolysis bio-oils from lignocellulosic biomass. *Appl. Energy* **2014**, *116*, 178−190.

(2) Dai, L.; Wang, Y.; Liu, Y.; He, C.; Ruan, R.; Yu, Z.; Jiang, L.; Zeng, Z.; Wu, Q. A review on selective production of value-added chemicals via catalytic pyrolysis of lignocellulosic biomass. *Sci. Total Environ.* **2020**, *749*, 142386.

(3) Cha, J. S.; Park, S. H.; Jung, S. C.; Ryu, C.; Jeon, J. K.; Shin, M. C.; Park, Y. K. Production and utilization of biochar: A review. *J. Ind. Eng. Chem.* **2016**, *40*, 1−15.
(4) Vassilev, S. V.; Baxter, D.; Andersen, L. K.; Vassileva, C. G. An overview of the chemical composition of biomass. *Fuel* **2010**, *89* (5), 913−933.
(5) Vassilev, S. V.; Baxter, D.; Andersen, L. K.; Vassileva, C. G.; Morgan, T. J. An overview of the organic and inorganic phase composition of biomass. *Fuel* **2012**, *94*, 1−33.
(6) Vassilev, S. V.; Baxter, D.; Vassileva, C. G. An overview of the behaviour of biomass during combustion: Part II. Ash fusion and ash formation mechanisms of biomass types. *Fuel* **2014**, *117*, 152−183.
(7) Wang, S.; Dai, G.; Yang, H.; Luo, Z. Lignocellulosic biomass pyrolysis mechanism: A state-of-the-art review. *Prog. Energy Combust. Sci.* **2017**, *62*, 33−86.
(8) Kostetskyy, P.; Broadbelt, L. J. Progress in Modeling of Biomass Fast Pyrolysis: A Review. *Energy Fuels* **2020**, *34* (12), 15195−15216.
(9) Leng, E.; Costa, M.; Gong, X.; Zheng, A.; Liu, S.; Xu, M. Effects of KCl and CaCl2 on the evolution of anhydro sugars in reaction intermediates during cellulose fast pyrolysis. *Fuel* **2019**, *251*, 307−315.
(10) Weber, K.; Quicker, P. Properties of biochar. *Fuel* **2018**, *217*, 240−261.
(11) Kalogiannis, K. G.; Stefanidis, S. D.; Lappas, A. A. Catalyst deactivation, ash accumulation and bio-oil deoxygenation during ex situ catalytic fast pyrolysis of biomass in a cascade thermal-catalytic reactor system. *Fuel Process. Technol.* **2019**, *186*, 99−109.
(12) Raveendran, K.; Ganesh, A.; Khilar, K. C. Influence of mineral matter on biomass pyrolysis characteristics. *Fuel* **1995**, *74* (12), 1812−1822.
(13) Iliopoulou, E. F.; Triantafyllidis, K. S.; Lappas, A. A. Overview of catalytic upgrading of biomass pyrolysis vapors toward the production of fuels and high-value chemicals. *WIREs Energy Environ.* **2019**, *8* (1), e322.
(14) Leijenhorst, E. J.; Wolters, W.; van de Beld, L.; Prins, W. Inorganic element transfer from biomass to fast pyrolysis oil: review and experiments. *Fuel Process. Technol.* **2016**, *149*, 96−111.
(15) Liu, Z.; Wang, L. A.; Xiao, H.; Guo, X.; Urbanovich, O.; Nagorskaya, L.; Li, X. A review on control factors of pyrolysis technology for plants containing heavy metals. *Ecotoxicol. Environ. Saf.* **2020**, *191*, 110181.
(16) Zhang, Y.; Kajitani, S.; Ashizawa, M.; Miura, K. Peculiarities of rapid pyrolysis of biomass covering medium-and high-temperature ranges. *Energy Fuels* **2006**, *20* (6), 2705−2712.
(17) Fytili, D.; Zabaniotou, A. Utilization of sewage sludge in EU application of old and new methods—a review. *Renewable Sustainable Energy Rev.* **2008**, *12*, 116−140.
(18) Lee, X. J.; Ong, H. C.; Gan, Y. Y.; Chen, W. H.; Mahlia, T. M. I. State of art review on conventional and advanced pyrolysis of macroalgae and microalgae for biochar, bio-oil and bio-syngas production. *Energy Convers. Manage.* **2020**, *210*, 112707.
(19) Chisti, Y. Biodiesel from microalgae. *Biotechnol. Adv.* **2007**, *25*, 294−360.
(20) Di Blasi, C. Modeling chemical and physical processes of wood and biomass pyrolysis. *Prog. Energy Combust. Sci.* **2008**, *34*, 47−90.
(21) Di Blasi, C. Combustion and gasification rates of lignocellulosic chars. *Prog. Energy Combust. Sci.* **2009**, *35*, 121−140.
(22) Cetin, E.; Moghtaderi, B.; Gupta, R.; Wall, T. F. Influence of pyrolysis conditions on the structure and gasification reactivity of biomass chars. *Fuel* **2004**, *83*, 2139−2150.
(23) Roy, C.; Yang, J.; Blanchette, D.; Korving, L.; De Caumia, B. Development of a Novel Vacuum Pyrolysis Reactor with Improved Heat Transfer Potential. In *Developments in Thermochemical Biomass Conversion*; Bridgwater, A. V., Boocock, D. G. B., Eds.; Springer: Dordrecht, 1997; pp 351−367.
(24) Mok, W. S. L.; Antal, M. J. Effects of pressure on biomass pyrolysis. I. Cellulose pyrolysis products. *Thermochim. Acta* **1983**, *68*, 155−164.
(25) Antal, M. J.; Allen, S. G.; Dai, X.; Shimizu, B.; Tam, M. S.; Grønli, M. G. Attainment of the theoretical yield of carbon from biomass. *Ind. Eng. Chem. Res.* **2000**, *39*, 4024−4031.
(26) Antal, M. J.; Croiset, E.; Dai, X. F.; De Almeida, C.; Mok, W. S. L.; Norberg, N.; Richard, J.-R.; Al Majthoub, M. High yield biomass charcoal. *Energy Fuels* **1996**, *10*, 652−658.
(27) Blackadder, W.; Rensfelt, E. A Pressurized Thermo Balance for Pyrolysis and Gasification Studies of Biomass, Wood and Peat. In *Fundamentals of Thermochemical Biomass Conversion*; Overend, R. P., Milne, T. A., Mudge, L. K., Eds.; Springer Netherlands, 1985; pp 747−759.
(28) Mahinpey, N.; Murugan, P.; Mani, T.; Raina, R. Analysis of bio-oil, biogas, and biochar from pressurized pyrolysis of wheat straw using a tubular reactor. *Energy Fuels* **2009**, *23*, 2736−2742.
(29) Pindoria, P. V.; Megaritis, A.; Messenbock, R. C.; Dugwell, D. R.; Kandiyoti, R. Comparison of the pyrolysis and gasification of biomass: effect of reacting gas atmosphere and pressure on Eucalyptus wood. *Fuel* **1998**, *77*, 1247−1251.
(30) Hornung, A. Biomass Pyrolysis. In *Encyclopedia of Sustainability Science and Technology*; Meyers, R. A., Ed.; Springer, New York, 2012.
(31) Li, L.; Rowbotham, J. S.; Greenwell, C. H.; Dyer, P. W. *An Introduction to Pyrolysis and Catalytic Pyrolysis: Versatile Techniques for Biomass Conversion*; Elsevier, 2013.
(32) Wang, Z.; Cao, J.; Wang, J. Pyrolytic characteristics of pine wood in a slowly heating and gas sweeping fixed-bed reactor. *J. Anal. Appl. Pyrolysis* **2009**, *84* (2), 179−184.
(33) DeSisto, W. J.; Hill, N.; Beis, S. H.; Mukkamala, S.; Joseph, J.; Baker, C.; Ong, T.-H.; Stemmler, E. A.; Wheeler, M. C.; Frederick, B. G.; et al. Fast pyrolysis of pine sawdust in a fluidized-bed reactor. *Energy Fuels* **2010**, *24* (4), 2642−2651.
(34) Ben, H.; Ragauskas, A. J. Comparison for the compositions of fast and slow pyrolysis oils by NMR characterization. *Bioresour. Technol.* **2013**, *147*, 577−584.
(35) Zmiewski, A. M.; Hammer, N. L.; Garrido, R. A.; Misera, T. G.; Coe, C. G.; Satrio, J. A. Exploring the products from pinewood pyrolysis in three different reactor systems. *Energy Fuels* **2015**, *29* (9), 5857−5864.
(36) Hoekstra, E.; Van Swaaij, W. P.; Kersten, S. R.; Hogendoorn, K. J. Fast pyrolysis in a novel wire-mesh reactor: Decomposition of pine wood and model compounds. *Chem. Eng. J.* **2012**, *187*, 172−184.
(37) Guo, F.; Liu, Y.; Wang, Y.; Li, X.; Li, T.; Guo, C. Pyrolysis kinetics and behavior of potassium-impregnated pine wood in TGA and a fixed-bed reactor. *Energy Convers. Manage.* **2016**, *130*, 184−191.
(38) Ningbo, G.; Baoling, L.; Aimin, L.; Juanjuan, L. Continuous pyrolysis of pine sawdust at different pyrolysis temperatures and solid residence times. *J. Anal. Appl. Pyrolysis* **2015**, *114*, 155−162.
(39) Evans, R. J.; Milne, T. A. Molecular characterization of the pyrolysis of biomass. 1. Fundamentals. *Energy Fuels* **1987**, *1*, 123.
(40) Gargiulo, V.; Alfè, M.; Giudicianni, P.; Ragucci, R. A study on the structural features of the water-insoluble fraction(WIF) isolated from biomass slow steam pyrolysis liquids. *J. Anal. Appl. Pyrolysis* **2016**, *121*, 128−137.
(41) Scholze, B.; Meier, D. J. Characterization of the water-insoluble fraction from pyrolysis oil (pyrolytic lignin). Part I. PY-GC/MS, FTIR, and functional groups. *J. Anal. Appl. Pyrolysis* **2001**, *60*, 41−54.
(42) Kumar, R.; Strezov, V.; Weldekidan, H.; He, J.; Singh, S.; Kan, T.; Dastjerdi, B. Lignocellulose biomass pyrolysis for bio-oil production: A review of biomass pre-treatment methods for production of drop-in fuels. *Renewable Sustainable Energy Rev.* **2020**, *123*, 109763.
(43) Alsbou, E. M. Pyrolysis Bio-Oil as a Renewable Fuel and Source of Chemicals: Its Production, Characterization and Stability. Doctoral dissertation, Memorial University of Newfoundland, 2014.
(44) Yang, Z.; Kumar, A.; Huhnke, R. L. Review of recent developments to improve storage and transportation stability of bio-oil. *Renewable Sustainable Energy Rev.* **2015**, *50*, 859−870.
(45) Hwang, H.; Lee, J. H.; Moon, J.; Kim, U. J.; Choi, I. G.; Choi, J. W. Influence of K and Mg concentration on the storage stability of bio-oil. ACS Sustain. *ACS Sustainable Chem. Eng.* **2016**, *4*, 4346−4353.

https://doi.org/10.1021/acs.energyfuels.0c04046
Energy Fuels 2021, 35, 5407−5478

(46) IEA Bioenergy. https://www.ieabioenergy.com/installations/ (accessed September 01, 2020).
(47) Canadian Institute of Forestry/Institut forestier du Canada (CIF-IFC). https://www.cif-ifc.org/wp-content/uploads/2019/10/2019ConfPres_S08P3_An-Overview-of-the-Biomass-Thermochemical-Conversion-Research-at-CanmetENERGY-Ottawa-for-the-Utilization-of-Forestry-Residues_Dillon-Mazerolle.pdf (accessed September 2020).
(48) Perkins, G. Integration of biocrude production from fast pyrolysis of biomass with solar PV for dispatchable electricity production. *Clean Energy* **2018**, *2* (2), 85−101.
(49) Fraunhofer-Institut für Umwelt-, Sicherheits- und Energietechnik UMSICHT. https://www.umsicht-suro.fraunhofer.de/en/Our_Solution/tcr-technology.html (accessed September 2020).
(50) Bioeconomy Institute at Iowa State University. https://www.biorenew.iastate.edu/research/thermochemical/autothermal/ (accessed September 2020).
(51) Mikula, K.; Soja, G.; Segura, C.; Berg, A.; Pfeifer, C. Carbon Sequestration in Support of the "4 per 1000" Initiative Using Compost and Stable Biochar from Hazelnut Shells and Sunflower Husks. *Processes* **2020**, *8* (7), 764.
(52) Sotoudehniakarani, F.; Alayat, A.; McDonald, A. G. Characterization and comparison of pyrolysis products from fast pyrolysis of commercial Chlorella vulgaris and cultivated microalgae. *J. Anal. Appl. Pyrolysis* **2019**, *139*, 258−273.
(53) Thermal and Catalytic Process Development Unit (TCPDU), NREL. https://www.nrel.gov/bioenergy/tcpdu.html (accessed September 01, 2020).
(54) BTG Bioliquids. https://www.btg-btl.com/en/technology#BTL (accessed September 2020).
(55) Agricultural Research Service (ARS), U.S. Department of Agriculture (USDA). https://ir.library.msstate.edu/handle/11668/18874 (accessed September 2020).
(56) Research institute of Sweden; https://www.ri.se/en/test-demo/pyrolysis (accessed September 01, 2020).
(57) Twence. https://www.twence.nl/en/twence/news/2018/BTG-BTL-hands-over-Empyro-to-Twence.html#:~:text=Empyro%2C%20which%20specialises%20in%20the,Marc%20Kapteijn%2C%20Director%20of%20Twence (accessed September 1, 2020).
(58) Griffin, M. B.; Iisa, K.; Wang, H.; Dutta, A.; Orton, K. A.; French, R. J.; Santosa, D. M.; Wilson, N.; Christensen, E.; Nash, C.; et al. Driving towards cost-competitive biofuels through catalytic fast pyrolysis by rethinking catalyst selection and reactor configuration. *Energy Environ. Sci.* **2018**, *11*, 2904−2918.
(59) Schnitzer, M. I.; Monreal, C. M.; Jandl, G.; Leinweber, P.; Fransham, P. B. The conversion of chicken manure to biooil by fast pyrolysis II. Analysis of chicken manure, biooils, and char by curie-point pyrolysis-gas chromatogra- phy/mass spectrometry (Cp Py-GC/MS). *J. Environ. Sci. Health, Part B* **2007**, *42*, 79−95.
(60) Glaser, B.; Haumaier, L.; Guggenberger, G.; Zech, W. The 'Terra Preta' phenomenon: a model for sustainable agriculture in the humid tropics. *Naturwissenschaften* **2001**, *88*, 37−41.
(61) Harvey, O. R.; Herbert, B. E.; Rhue, R. D.; Kuo, L. J. Metal interactions at the biochar− water interface: energetics and structure−sorption relationships elucidated by flow adsorption microcalorimetry. *Environ. Sci. Technol.* **2011**, *45*, 5550−56.
(62) Lua, A. C.; Yang, T.; Guo, J. Effects of pyrolysis conditions on the properties of activated carbons prepared from pistachio-nut shells. *J. Anal. Appl. Pyrolysis* **2004**, *72*, 279−87.
(63) Gargiulo, V.; Gomis-Berenguer, A.; Giudicianni, P.; Ania, C. O.; Ragucci, R.; Alfè, M. Assessing the potential of biochars prepared by steam-assisted slow pyrolysis for CO2 adsorption and separation. *Energy Fuels* **2018**, *32*, 10218−10227.
(64) Debiagi, P.; Gentile, G.; Cuoci, A.; Frassoldati, A.; Ranzi, E.; Faravelli, T. A predictive model of biochar formation and characterization. *J. Anal. Appl. Pyrolysis* **2018**, *134*, 326−335.
(65) Neves, D.; Thunman, H.; Matos, A.; Tarelho, L.; Gómez-Barea, A. Characterization and prediction of biomass pyrolysis products. *Prog. Energy Combust. Sci.* **2011**, *37*, 611−630.
(66) *Phyllis2, Energy Research Centre of the Netherlands, Database for Biomass and Waste*. https://phyllis.nl/ (accessed October 01, 2020).
(67) Ferreiro, A. I.; Giudicianni, P.; Grottola, C. M.; Rabaçal, M.; Costa, M.; Ragucci, R. Unresolved Issues on the Kinetic Modeling of Pyrolysis of Woody and Nonwoody Biomass Fuels. *Energy Fuels* **2017**, *31*, 4035−4044.
(68) Ferreiro, A. I.; Rabaçal, M.; Costa, M.; Giudicianni, P.; Grottola, C. M.; Ragucci, R. Modeling the impact of the presence of KCl on the slow pyrolysis of cellulose. *Fuel* **2018**, *215*, 57−65.
(69) Rowell, R. M.; Pettersen, R.; Han, J. S.; Rowell, J. S.; Tshabalala, M. A. Cell Wall Chemistry. In *Handbook of Wood Chemistry and Wood Composites*; Rowell, R. M., Ed.; CRC Press, 2013; pp 33−72.
(70) Scheller, H. V.; Ulvskov, P. Hemicelluloses. *Annu. Rev. Plant Biol.* **2010**, *61* (1), 263−289.
(71) Naseem, A.; Tabasum, S.; Zia, K. M.; Zuber, M.; Ali, M.; Noreen, A. Lignin-derivatives based polymers, blends and composites: a review. *Int. J. Biol. Macromol.* **2016**, *93*, 296−313.
(72) Bajpai, P. Wood and Fiber Fundamentals. In *Biermann's Handbook of Pulp and Paper*; Vol. *1*: Raw Material and Pulp Making; Elsevier, 2018; pp 19−74.
(73) Debiagi, P. E. A.; Pecchi, C.; Gentile, G.; Frassoldati, A.; Cuoci, A.; Faravelli, T.; Ranzi, E. Extractives extend the applicability of multistep kinetic scheme of biomass pyrolysis. *Energy Fuels* **2015**, *29*, 6544−6555.
(74) Pattathil, S.; Hahn, M. G.; Dale, B. E.; Chundawat, S. P. Insights into plant cell wall structure, architecture, and integrity using glycome profiling of native and AFEXTM-pre-treated biomass. *J. Exp. Bot.* **2015**, *66* (14), 4279−4294.
(75) Kirkbey, E. Introduction, Definition and Classification of Nutrients. In *Marschner's Mineral Nutrition of Higher Plants*; Academic Press, 2012; pp 3−5.
(76) Arnon, D. I.; Stout, P. R. The essentiality of certain elements in minute quantity for plants with special reference to copper. *Plant Physiol.* **1939**, *14*, 371.
(77) Marschner, H. *Marschner's Mineral Nutrition of Higher Plants*; Academic Press, 2011.
(78) Rennenberg, H.; Brunold, C. H.; De Kok, L. J.; Stulen, I. *Sulfur Nutrition and Sulfur Assimilation in Higher Plants*; SPB Academic Publishing: The Hague, The Netherlands, 1990; pp 3−76.
(79) Pilon-Smits, E. A.; Quinn, C. F.; Tapken, W.; Malagoli, M.; Schiavon, M. Physiological functions of beneficial elements. *Curr. Opin. Plant Biol.* **2009**, *12*, 267−274.
(80) Zevenhoven, M.; Yrjas, P.; Skrifvars, B. J.; Hupa, M. Characterization of ash-forming matter in various solid fuels by selective leaching and its implications for fluidized-bed combustion. *Energy Fuels* **2012**, *26*, 6366−6386.
(81) Benson, S. A.; Holm, P. L. Comparison of inorganics in three low-rank coals. *Ind. Eng. Chem. Prod. Res. Dev.* **1985**, *24*, 145−9.
(82) Kleinhans, U.; Wieland, C.; Frandsen, F. J.; Spliethoff, H. Ash formation and deposition in coal and biomass fired combustion systems: Progress and challenges in the field of ash particle sticking and rebound behavior. *Prog. Energy Combust. Sci.* **2018**, *68*, 65−168.
(83) Dambrine, E.; Martin, F.; Carisey, N.; Granier, A.; Hällgren, J. E.; Bishop, K. Xylem sap composition: a tool for investigating mineral uptake and cycling in adult spruce. *Plant Soil* **1995**, *168*, 233−241.
(84) McKendry, P. Energy production from biomass (part 1): overview of biomass. *Bioresour. Technol.* **2002**, *83* (1), 37−46.
(85) Werkelin, J.; Skrifvars, B. J.; Hupa, M. Ash-forming elements in four Scandinavian wood species. Part 1: Summer harvest. *Biomass Bioenergy* **2005**, *29* (6), 451−466.
(86) Monti, A.; Di Virgilio, N.; Venturi, G. G. Mineral composition and ash content of six major energy crops. *Biomass Bioenergy* **2008**, *32* (3), 216−223.
(87) Giudicianni, P.; Pindozzi, S.; Grottola, C. M.; Stanzione, F.; Faugno, S.; Fagnano, M.; Fiorentino, N.; Ragucci, R. Pyrolysis for exploitation of biomasses selected for soil phytoremediation:

https://doi.org/10.1021/acs.energyfuels.0c04046
Energy Fuels 2021, 35, 5407−5478

Characterization of gaseous and solid products. *Waste Manage.* **2017**, *61*, 288−299.
(88) Giudicianni, P. Personal communication, 2020.
(89) Suárez-García, F.; Martínez-Alonso, A.; Fernández Llorente, M.; Tascón, J. M. D. Inorganic matter characterization in vegetable biomass feedstocks. *Fuel* **2002**, *81* (9), 1161−1169.
(90) Johansson, A. C.; Wiinikka, H.; Sandström, L.; Marklund, M.; Öhrman, O. G.; Narvesjö, J. Characterization of pyrolysis products produced from different Nordic biomass types in a cyclone pilot plant. *Fuel Process. Technol.* **2016**, *146*, 9−19.
(91) Almuina-Villar, H.; Lang, N.; Anca-Couce, A.; Röpcke, J.; Behrendt, F.; Dieguez-Alonso, A. Application of laser-based diagnostics for characterization of the influence of inorganics on the slow pyrolysis of woody biomass. *J. Anal. Appl. Pyrolysis* **2019**, *140*, 125−136.
(92) Trubetskaya, A.; Jensen, P. A.; Jensen, A. D.; Steibel, M.; Spliethoff, H.; Glarborg, P.; Larsen, F. H. Comparison of high temperature chars of wheat straw and rice husk with respect to chemistry, morphology and reactivity. *Biomass Bioenergy* **2016**, *86*, 76−87.
(93) Frandsen, F. Ash Formation, Deposition and Corrosion When Utilizing Straw for Heat and Power Production. Doctorial Thesis, DTU Chemical Engineering, 2010.
(94) Queirós, C. S. G. P.; Cardoso, S.; Lourenço, A.; Ferreira, J.; Miranda, I.; Lourenço, M. J. V.; Pereira, H. Characterization of walnut, almond, and pine nut shells regarding chemical composition and extract composition. *Biomass Convers. Biorefin.* **2020**, *10* (1), 175−188.
(95) Setter, C.; Silva, F. T. M.; Assis, M. R.; Ataíde, C. H.; Trugilho, P. F.; Oliveira, T. J. P. Slow pyrolysis of coffee husk briquettes: Characterization of the solid and liquid fractions. *Fuel* **2020**, *261*, 116420.
(96) Elbersen, W.; Lammens, T. M.; Alakangas, E. A.; Annevelink, B.; Harmsen, P.; Elbersen, B. Lignocellulosic Biomass Quality: Matching Characteristics with Biomass Conversion Requirements. In *Modeling and Optimization of Biomass Supply Chains*; Academic Press, 2017; pp 55−78.
(97) Kataki, R.; Konwer, D. Fuelwood characteristics of some indigenous woody species of north-east India. *Biomass Bioenergy* **2001**, *20* (1), 17−23.
(98) Liu, Q.; Chmely, S. C.; Abdoulmoumine, N. Biomass treatment strategies for thermochemical conversion. *Energy Fuels* **2017**, *31* (4), 3525−3536.
(99) Stavridou, E.; Hastings, A.; Webster, R. J.; Robson, P. R. The impact of soil salinity on the yield, composition and physiology of the bioenergy grass Miscanthus× giganteus. *GCB Bioenergy* **2017**, *9* (1), 92−104.
(100) Stavridou, E.; Webster, R. J.; Robson, P. R. Novel Miscanthus genotypes selected for different drought tolerance phenotypes show enhanced tolerance across combinations of salinity and drought treatments. *Ann. Bot.* **2019**, *124* (4), 653−674.
(101) Akinshina, N.; Azizov, A.; Karasyova, T.; Klose, E. On the issue of halophytes as energy plants in saline environment. *Biomass Bioenergy* **2016**, *91*, 306−311.
(102) Baxter, X. C.; Darvell, L. I.; Jones, J. M.; Barraclough, T.; Yates, N. E.; Shield, I. Study of Miscanthus x giganteus ash composition−Variation with agronomy and assessment method. *Fuel* **2012**, *95*, 50−62.
(103) Lindström, E.; Sandström, M.; Boström, D.; Öhman, M. Slagging characteristics during combustion of cereal grains rich in phosphorus. *Energy Fuels* **2007**, *21* (2), 710−717.
(104) Rocco, C.; Agrelli, D.; Tafuro, M.; Caporale, A. G.; Adamo, P. Assessing the bioavailability of potentially toxic elements in soil: a proposed approach. *Ital. J. Agron.* **2018**, *13* (Suppl. 1), 16−22.
(105) Visconti, D.; Fiorentino, N.; Caporale, A. G.; Stinca, A.; Adamo, P.; Motti, R.; Fagnano, M. Analysis of native vegetation for detailed characterization of a soil contaminated by tannery waste. *Environ. Pollut.* **2019**, *252*, 1599−1608.
(106) Agrelli, D.; Caporale, A. G.; Adamo, P. Assessment of the Bioavailability and Speciation of Heavy Metal (loid) s and Hydrocarbons for Risk-Based Soil Remediation. *Agronomy* **2020**, *10*, 1440.
(107) Fagnano, M.; Visconti, D.; Fiorentino, N. (2020). Agronomic Approaches for Characterization, Remediation, and Monitoring of Contaminated Sites. *Agronomy* **2020**, *10*, 1335.
(108) Demirbas, A. Potential applications of renewable energy sources, biomass combustion problems in boiler power systems and combustion related environmental issues. *Prog. Energy Combust. Sci.* **2005**, *31*, 171−192.
(109) Bolan, N. S.; Park, J. H.; Robinson, B.; Naidu, R.; Huh, K. Y. Phytostabilization: a green approach to contaminant containment. *Adv. Agron.* **2011**, *112*, 145−204.
(110) Jha, A. B.; Misra, A. N.; Sharma, P. Phytoremediation of Heavy Metal-Contaminated Soil Using Bioenergy Crops. In *Phytoremediation Potential of Bioenergy Plants*; Springer, Singapore, 2017; pp 63−96.
(111) Grottola, C. M.; Giudicianni, P.; Pindozzi, S.; Stanzione, F.; Faugno, S.; Fagnano, M.; Fiorentino, N.; Ragucci, R. Steam assisted slow pyrolysis of contaminated biomasses: Effect of plant parts and process temperature on heavy metals fate. *Waste Manage.* **2019**, *85*, 232−241.
(112) Tőzsér, D.; Magura, T.; Simon, E. Heavy metal uptake by plant parts of willow species: a meta-analysis. *J. Hazard. Mater.* **2017**, *336*, 101−109.
(113) Yu, C.; Thy, P.; Wang, L.; Anderson, S. N.; VanderGheynst, J. S.; Upadhyaya, S. K.; Jenkins, B. M. Influence of leaching pretreatment on fuel properties of biomass. *Fuel Process. Technol.* **2014**, *128*, 43−53.
(114) Said, N.; Bishara, T.; García-Maraver, A.; Zamorano, M. Effect of water washing on the thermal behavior of rice straw. *Waste Manage.* **2013**, *33*, 2250−2256.
(115) Stefanidis, S. D.; Heracleous, E.; Patiaka, D. T.; Kalogiannis, K. G.; Michailof, C. M.; Lappas, A. A. Optimization of bio-oil yields by demineralization of low quality biomass. *Biomass Bioenergy* **2015**, *83*, 105−115.
(116) Jiang, L.; Hu, S.; Sun, L.; Su, S.; Xu, K.; He, L.; Xiang, J. Influence of different demineralization treatments on physicochemical structure and thermal degradation of biomass. *Bioresour. Technol.* **2013**, *146*, 254−260.
(117) Eom, I.-Y.; Kim, J.-Y.; Lee, S.-M.; Cho, T.-S.; Choi, I.-G.; Choi, J.-W. Study on the thermal decomposition features and kinetics of demineralized and inorganic metal-impregnated lignocellulosic biomass. *J. Ind. Eng. Chem.* **2012**, *18*, 2069−2075.
(118) Lu, X.; Han, T.; Jiang, J.; Sun, K.; Sun, Y.; Yang, W. Comprehensive insights into the influences of acid-base properties of chemical pretreatment reagents on biomass pyrolysis behavior and wood vinegar properties. *J. Anal. Appl. Pyrolysis* **2020**, *151*, 104907.
(119) Javed, M. A. Acid treatment effecting the physiochemical structure and thermal degradation of biomass. *Renewable Energy* **2020**, *159*, 444−450.
(120) Asadieraghi, M.; Daud, W. M. A. W. Characterization of lignocellulosic biomass thermal degradation and physiochemical structure: Effects of demineralization by diverse acid solutions. *Energy Convers. Manage.* **2014**, *82*, 71−82.
(121) Das, P.; Ganesh, A.; Wangikar, P. Influence of pretreatment for deashing of sugarcane bagasse on pyrolysis products. *Biomass Bioenergy* **2004**, *27*, 445−457.
(122) Persson, H.; Kantarelis, E.; Evangelopoulos, P.; Yang, W. Wood-derived acid leaching of biomass for enhanced production of sugars and sugar derivatives during pyrolysis: Influence of acidity and treatment time. *J. Anal. Appl. Pyrolysis* **2017**, *127*, 329−334.
(123) Persson, H.; Yang, W. Catalytic pyrolysis of demineralized lignocellulosic biomass. *Fuel* **2019**, *252*, 200−209.
(124) Rodríguez-Machín, L.; Arteaga-Pérez, L. E.; Pérez-Bermúdez, R. A.; Casas-Ledón, Y.; Prins, W.; Ronsse, F. Effect of citric acid leaching on the demineralization and thermal degradation behavior of sugarcane trash and bagasse. *Biomass Bioenergy* **2018**, *108*, 371−380.
(125) Oudenhoven, S. R. G.; Westerhof, R. J. M.; Aldenkamp, N.; Brilman, D. W. F.; Kersten, S. R. A. Demineralization of wood using wood-derived acid: Towards a selective pyrolysis process for fuel and chemicals production. *J. Anal. Appl. Pyrolysis* **2013**, *103*, 112−118.
(126) Oudenhoven, S. R. G.; Westerhof, R. J. M.; Kersten, S. R. A. Fast pyrolysis of organic acid leached wood, straw, hay and bagasse:

https://doi.org/10.1021/acs.energyfuels.0c04046
Energy Fuels 2021, 35, 5407−5478

Improved oil and sugar yields. *J. Anal. Appl. Pyrolysis* **2015**, *116*, 253−262.
(127) Reza, M. T.; Emerson, R.; Uddin, M. H.; Gresham, G.; Coronella, C. J. Ash reduction of corn stover by mild hydrothermal preprocessing. *Biomass Convers. Bior.* **2015**, *5*, 21−31.
(128) Edmunds, C. W.; Hamilton, C.; Kim, K.; Chmely, S. C.; Labbé, N. Using a chelating agent to generate low ash bioenergy feedstock. *Biomass Bioenergy* **2017**, *96*, 12−18.
(129) Hörhammer, H.; Dou, C.; Gustafson, R.; Suko, A.; Bura, R. Removal of non-structural components from poplar whole-tree chips to enhance hydrolysis and fermentation performance. *Biotechnol. Biofuels* **2018**, *11* (1), 222.
(130) Das, O.; Sarmah, A. K. Mechanism of waste biomass pyrolysis: Effect of physical and chemical pre-treatments. *Sci. Total Environ.* **2015**, *537*, 323−334.
(131) Eom, I. Y.; Kim, K. H.; Kim, J. Y.; Lee, S. M.; Yeo, H. M.; Choi, I. G.; Choi, J. W. Characterization of primary thermal degradation features of lignocellulosic biomass after removal of inorganic metals by diverse solvents. *Bioresour. Technol.* **2011**, *102* (3), 3437−3444.
(132) Mayer, Z. A.; Apfelbacher, A.; Hornung, A. Effect of sample preparation on the thermal degradation of metal-added biomass. *J. Anal. Appl. Pyrolysis* **2012**, *94*, 170−176.
(133) Ratnasari, D. K.; Horn, A.; Brunner, T.; Yang, W.; Jönsson, P. G. The thermal degradation of lignocellulose biomass with an acid leaching pre-treatment using a H-ZSM-5/Al-MCM-41 catalyst mixture. *Fuel* **2019**, *257*, 116086.
(134) Dong, Q.; Zhang, S.; Zhang, L.; Ding, K.; Xiong, Y. Effects of four types of dilute acid washing on moso bamboo pyrolysis using Py−GC/MS. *Bioresour. Technol.* **2015**, *185*, 62−69.
(135) Deng, L.; Zhang, T.; Che, D. Effect of water washing on fuel properties, pyrolysis and combustion characteristics, and ash fusibility of biomass. *Fuel Process. Technol.* **2013**, *106*, 712−720.
(136) Liu, X.; Bi, X. T. Removal of inorganic constituents from pine barks and switchgrass. *Fuel Process. Technol.* **2011**, *92* (7), 1273−1279.
(137) Vamvuka, D.; Sfakiotakis, S. Effects of heating rate and water leaching of perennial energy crops on pyrolysis characteristics and kinetics. *Renewable Energy* **2011**, *36* (9), 2433−2439.
(138) Chen, D.; Gao, D.; Capareda, S. C.; Shuang, E.; Jia, F.; Wang, Y. Influences of hydrochloric acid washing on the thermal decomposition behavior and thermodynamic parameters of sweet sorghum stalk. *Renewable Energy* **2020**, *148*, 1244−1255.
(139) Eom, I.-Y.; Kim, J.-Y.; Lee, S.-M.; Cho, T.-S.; Yeo, H.; Choi, J.-W. Comparison of pyrolytic products produced from inorganic-rich and demineralized rice straw (Oryza sativa L.) by fluidized bed pyrolyzer for future biorefinery approach. *Bioresour. Technol.* **2013**, *128*, 664−672.
(140) Cen, K.; Zhang, J.; Ma, Z.; Chen, D.; Zhou, J.; Ma, H. Investigation of the relevance between biomass pyrolysis polygeneration and washing pretreatment under different severities: Water, dilute acid solution and aqueous phase bio-oil. *Bioresour. Technol.* **2019**, *278*, 26−33.
(141) Hu, S.; Jiang, L.; Wang, Y.; Su, S.; Sun, L.; Xu, B.; He, L.; Xiang, J. Effects of inherent alkali and alkaline earth metallic species on biomass pyrolysis at different temperatures. *Bioresour. Technol.* **2015**, *192*, 23−30.
(142) Ma, Y.; Zhang, H.; Yang, H.; Zhang, Y. The effect of acid washing pretreatment on bio-oil production in fast pyrolysis of rice husk. *Cellulose* **2019**, *26* (15), 8465−8474.
(143) Verma, R.; Verma, S. K.; Verma, S.; Wang, J.; Liu, J.; Jing, B.; Rakesh, K. P. Value-addition of wheat straw through acid treatment and pyrolysis of acid treated residues. *J. Cleaner Prod.* **2021**, *282*, 124488.
(144) Lateef, H. U.; Kazmi, M.; Tabish, A. N.; Cheema, I. I.; Rashid, M. I. Effect of demineralization on physiochemical and thermal characteristics of wheat straw. *Energy Sources Part A* **2020**, 1−10.
(145) Karnowo; Zahara, Z. F.; Kudo, S.; Norinaga, K.; Hayashi, J. I. Leaching of alkali and alkaline earth metallic species from rice husk with bio-oil from its pyrolysis. *Energy Fuels* **2014**, *28* (10), 6459−6466.
(146) Ragucci, R.; Giudicianni, P.; Cavaliere, A. Cellulose slow pyrolysis products in a pressurized steam flow reactor. *Fuel* **2013**, *107*, 122−130.
(147) Zhang, Z.; Zhu, M.; Zhang, D. A Thermogravimetric study of the characteristics of pyrolysis of cellulose isolated from selected biomass. *Appl. Energy* **2018**, *220*, 87−93.
(148) Sun, X.-F.; Sun, R.-C.; Su, Y.; Sun, J.-X. Comparative study of crude and purified cellulose from wheat straw. *J. Agric. Food Chem.* **2004**, *52*, 839−847.
(149) Kalpana, V. P.; Perarasu, V. T. Analysis on cellulose extraction from hybrid biomass for improved crystallinity. *J. Mol. Struct.* **2020**, *1217*, 128350.
(150) Patwardhan, P. R.; Satrio, J. A.; Brown, R. C.; Shanks, B. H. Influence of inorganic salts on the primary pyrolysis products of cellulose. *Bioresour. Technol.* **2010**, *101* (12), 4646−4655.
(151) Haldar, D.; Purkait, M. K. Micro and nanocrystalline cellulose derivatives of lignocellulosic biomass: A review on synthesis, applications and advancements. *Carbohydr. Polym.* **2020**, *250*, 116937.
(152) Ebringerová, A. Structural diversity and application potential of hemicelluloses. *Macromol. Symp.* **2005**, *232*, 1−12.
(153) Peng, F.; Bian, J.; Peng, P.; Xiao, H.; Ren, J.-L.; Xu, F.; Sun, R.-C. Separation and characterization of acetyl and non-acetyl hemicelluloses of Arundo donax by ammonium sulfate precipitation. *J. Agric. Food Chem.* **2012**, *60*, 4039−4047.
(154) Giudicianni, P.; Gargiulo, V.; Grottola, C. M.; Alfè, M.; Ragucci, R. Effect of alkali metal ions presence on the products of xylan steam assisted slow pyrolysis. *Fuel* **2018**, *216*, 36−43.
(155) Shen, D. K.; Gu, S.; Bridgwater, A. V. Study on the pyrolytic behaviour of xylan-based hemicellulose using TG−FTIR and Py−GC−FTIR. *J. Anal. Appl. Pyrolysis* **2010**, *87*, 199−206.
(156) Werner, K.; Pommer, L.; Broström, M. Thermal decomposition of hemicelluloses. *J. Anal. Appl. Pyrolysis* **2014**, *110*, 130−137.
(157) Branca, C.; Di Blasi, C.; Mango, C.; Hrablay, I. Products and kinetics of glucomannan pyrolysis. *Ind. Eng. Chem. Res.* **2013**, *52*, 5030−5039.
(158) Ghalibaf, M.; Doddapaneni, T. R. K. C.; Alén, R. Pyrolytic behavior of lignocellulosic-based polysaccharides. *J. Therm. Anal. Calorim.* **2019**, *137*, 121−131.
(159) Sporck, D.; Reinoso, F. A.; Rencoret, J.; Gutiérrez, A.; José, C.; Ferraz, A.; Milagres, A. M. Xylan extraction from pretreated sugarcane bagasse using alkaline and enzymatic approaches. *Biotechnol. Biofuels* **2017**, *10*, 296.
(160) Rowley, J.; Decker, S. R.; Michener, W.; Black, S. Efficient extraction of xylan from delignified corn stover using dimethyl sulfoxide. *3 Biotech* **2013**, *3*, 433−438.
(161) Jin, X.; Hu, Z.; Wu, S.; Song, T.; Yue, F.; Xiang, Z. Promoting the material properties of xylan-type hemicelluloses from the extraction step. *Carbohydr. Polym.* **2019**, *215*, 235−245.
(162) Hutterer, C.; Fackler, K.; Potthast, A. The fate of 4-O-Methyl glucuronic acid in hardwood xylan during alkaline extraction. *ACS Sustainable Chem. Eng.* **2017**, *5*, 1818−1823.
(163) Arai, T.; Biely, P.; Uhliariková, I.; Sato, N.; Makishima, S.; Mizuno, M.; Nozaki, K.; Kaneko, S.; Amano, Y. Structural characterization of hemicellulose released from corn cob in continuous flow type hydrothermal reactor. *J. Biosci. Bioeng.* **2019**, *127*, 222−230.
(164) Patwardhan, P. R.; Brown, R. C.; Shanks, B. H. Product distribution from the fast pyrolysis of hemicellulose. *ChemSusChem* **2011**, *4*, 636−643.
(165) Sharma, R. K.; Hajaligol, M. R. Effect of pyrolysis conditions on the formation of polycyclic aromatic hydrocarbons (PAHs) from polyphenolic compounds. *J. Anal. Appl. Pyrolysis* **2003**, *66* (1−2), 123−144.
(166) Peng, F.; Ren, J. L.; Xu, F.; Bian, J.; Peng, P.; Sun, R. C. Comparative study of hemicelluloses obtained by graded ethanol precipitation from sugarcane bagasse. *J. Agric. Food Chem.* **2009**, *57* (14), 6305−6317.
(167) Wang, J.; Asmadi, M.; Kawamoto, H. The effect of uronic acid moieties on xylan pyrolysis. *J. Anal. Appl. Pyrolysis* **2018**, *136*, 215−221.

https://doi.org/10.1021/acs.energyfuels.0c04046
Energy Fuels 2021, 35, 5407−5478

(168) Kai, D.; Tan, M. J.; Chee, P. L.; Chua, Y. K.; Yap, Y. L.; Loh, X. J. Towards lignin-based functional materials in a sustainable world. *Green Chem.* **2016**, *18* (5), 1175−1200.
(169) Castro-Díaz, M.; Vega, M. F.; Díaz-Faes, E.; Barriocanal, C.; Musa, U.; Snape, C. Evaluation of demineralized lignin and lignin-phenolic resin blends to produce biocoke suitable for blast furnace operation. *Fuel* **2019**, *258*, 116125.
(170) Fierro, V.; Torne-Fernandez, V.; Celzard, A.; Montane, D. Influence of the demineralisation on the chemical activationof Kraft lignin with orthophosphoric acid. *J. Hazard. Mater.* **2007**, *149*, 126−133.
(171) Guo, D.-L.; Wu, S-b.; Liu, B.; Yin, X-l.; Yang, Q. Catalytic effects of NaOH and Na2CO3 additives on alkali lignin pyrolysis and gasification. *Appl. Energy* **2012**, *95*, 22−30.
(172) Peng, C.; Zhang, G.; Yue, J.; Xu, G. Pyrolysis of lignin for phenols with alkaline additive. *Fuel Process. Technol.* **2014**, *124*, 212−221.
(173) Guo, D-l; Yuan, H-y; Yin, X-l; Wu, C-z; Wu, S-b; Zhou, Z-q. Effects of chemical form of sodium on the product characteristics of alkali lignin pyrolysis. *Bioresour. Technol.* **2014**, *152*, 147−153.
(174) Patwardhan, P. R.; Brown, R. C.; Shanks, B. H. Understanding the fast pyrolysis of lignin. *ChemSusChem* **2011**, *4*, 1629−1636.
(175) Dalluge, D. L.; Kim, K. H.; Brown, R. C. The influence of alkali and alkaline earth metals on char and volatile aromatics from fast pyrolysis of lignin. *J. Anal. Appl. Pyrolysis* **2017**, *127*, 385−393.
(176) Giudicianni, P.; Ferreiro, A. I.; Gargiulo, V.; Alfe, M.; Costa, M.; Rabacal, M.; Ragucci, R. Effect of KCl doping on the slow pyrolysis of lignin. *Chem. Eng. Trans.* **2020**, *80*, 109−114.
(177) Nzihou, A.; Stanmore, B.; Lyczko, N.; Minh, D. P. The catalytic effect of inherent and adsorbed metals on the fast/flash pyrolysis of biomass: A review. *Energy* **2019**, *170*, 326−337.
(178) Danish, M.; Ahmad, T. A review on utilization of wood biomass as a sustainable precursor for activated carbon production and application. *Renewable Sustainable Energy Rev.* **2018**, *87*, 1−21.
(179) Heidarinejad, Z.; Dehghani, M. H.; Heidari, M.; Javedan, G.; Ali, I.; Sillanpää, M. Methods for preparation and activation of activated carbon: a review. *Environ. Chem. Lett.* **2020**, *18* (2), 393−415.
(180) Thompson, E.; Danks, A. E.; Bourgeois, L.; Schnepp, Z. Iron-catalyzed graphitization of biomass. *Green Chem.* **2015**, *17* (1), 551−556.
(181) Dieguez-Alonso, A.; Anca-Couce, A.; Frišták, V.; Moreno-Jiménez, E.; Bacher, M.; Bucheli, T. D.; Cimò, G.; Conte, P.; Hagemann, N.; Haller, A.; et al. Designing biochar properties through the blending of biomass feedstock with metals: Impact on oxyanions adsorption behavior. *Chemosphere* **2019**, *214*, 743−753.
(182) Trubetskaya, A.; Larsen, F. H.; Shchukarev, A.; Ståhl, K.; Umeki, K. Potassium and soot interaction in fast biomass pyrolysis at high temperatures. *Fuel* **2018**, *225*, 89−94.
(183) Xu, Z.; Ma, J.; Shi, M.; Xie, Y.; Feng, C. Biomass based iron and nitrogen co-doped 3D porous carbon as an efficient oxygen reduction catalyst. *J. Colloid Interface Sci.* **2018**, *523*, 144−150.
(184) Wilson, F.; Tremain, P.; Moghtaderi, B. Characterization of Biochars Derived from Pyrolysis of Biomass and Calcium Oxide Mixtures. *Energy Fuels* **2018**, *32* (4), 4167−4177.
(185) Gargiulo, V.; Giudicianni, P.; Alfè, M.; Ragucci, R. Influence of possible interactions between biomass organic components and alkali metal ions on steam assisted pyrolysis: A case study on Arundo donax. *J. Anal. Appl. Pyrolysis* **2015**, *112*, 244−252.
(186) Santana, J. A., Jr.; Sousa, N. G.; Cardoso, C. R.; Carvalho, W. S.; Ataíde, C. H. Sodium, zinc and magnesium chlorides as additives for soybean hulls pyrolysis. *J. Therm. Anal. Calorim.* **2016**, *125*, 471−481.
(187) Liu, C.; Liu, X.; Bi, X. T.; Liu, Y.; Wang, C. Influence of inorganic additives on pyrolysis of pine bark. *Energy Fuels* **2011**, *25*, 1996−2003.
(188) Saddawi, A.; Jones, J. M.; Williams, A. Influence of alkali metals on the kinetics of the thermal decomposition of biomass. *Fuel Process. Technol.* **2012**, *104*, 189−197.
(189) Khelfa, A.; Bensakhria, A.; Weber, J.V. Investigations into the pyrolytic behaviour of birch wood and its main components: Primary degradation mechanisms, additivity and metallic salt effects. *J. Anal. Appl. Pyrolysis* **2013**, *101*, 111−121.
(190) Feng, D.; Sun, H.; Ma, Y.; Sun, S.; Zhao, Y.; Guo, D.; Chang, G.; Lai, X.; Wu, J.; Tan, H. Catalytic mechanism of K and Ca on the volatile−biochar interaction for rapid pyrolysis of biomass: experimental and simulation studies. *Energy Fuels* **2020**, *34*, 9741−9753.
(191) Martín-Lara, M. A.; Ronda, A.; Blázquez, G.; Pérez, A.; Calero, M. Pyrolysis kinetics of the lead-impregnated olivestone by non-isothermal thermogravimetry. *Process Saf. Environ. Prot.* **2018**, *113*, 448−458.
(192) Eibner, S.; Broust, F.; Blin, J.; Julbe, A. Catalytic effect of metal nitrate salts during pyrolysis of impregnated biomass. *J. Anal. Appl. Pyrolysis* **2015**, *113*, 143−152.
(193) Kumar, A.; Mylapilli, S. V. P.; Reddy, S. N. Thermogravimetric and kinetic studies of metal (Ru/Fe) impregnated banana pseudo-stem (Musa acuminate). *Bioresour. Technol.* **2019**, *285*, 121318.
(194) Safar, M.; Lin, B.-J.; Chen, W.-H.; Langauer, D.; Chang, J.-H.; Raclavska, H.; Pétrissans, A.; Rousset, P.; Pétrissans, M. Catalytic effects of potassium on biomass pyrolysis, combustion and torrefaction. *Appl. Energy* **2019**, *235*, 346−355.
(195) Zhang, X.; Li, J.; Yang, W.; Blasiak, W. Formation mechanism of levoglucosan and formaldehyde during cellulose pyrolysis. *Energy Fuels* **2011**, *25*, 3739−3746.
(196) Hosoya, T.; Sakaki, S. Levoglucosan formation from crystalline cellulose: importance of a hydrogen bonding network in the reaction. *ChemSusChem* **2013**, *6*, 2356−2368.
(197) Assary, R. S.; Curtiss, L. A. Thermochemistry and reaction barriers for the formation of levoglucosenone from cellobiose. *ChemCatChem* **2012**, *4*, 200−205.
(198) Mayes, H. B.; Broadbelt, L. J. Unraveling the reactions that unravel cellulose. *J. Phys. Chem. A* **2012**, *116*, 7098−7106.
(199) Agarwal, V.; Dauenhauer, P. J.; Huber, G. W.; Auerbach, S. M. Ab initio dynamics of cellulose pyrolysis: nascent decomposition pathways at 327 and 600°C. *J. Am. Chem. Soc.* **2012**, *134*, 14958−14972.
(200) Lu, Q.; Zhang, Y.; Dong, C-q.; Yang, Y-p.; Yu, H-z. The mechanism for the formation of levoglucosenone during pyrolysis of b-D-glucopyranose and cellobiose: A density functional theory study. *J. Anal. Appl. Pyrolysis* **2014**, *110*, 34−43.
(201) Zhang, M.; Geng, Z.; Yu, Y. Density functional theory (DFT) study on the pyrolysis of cellulose: the pyran ring breaking mechanism. *Comput. Theor. Chem.* **2015**, *1067*, 13−23.
(202) Mettler, M. S.; Paulsen, A. D.; Vlachos, D. G.; Dauenhauer, P. J. The chain length effect in pyrolysis: bridging the gap between glucose and cellulose. *Green Chem.* **2012**, *14*, 1284−1288.
(203) Poletto, M.; Ornaghi, H. L.; Zattera, A. J. Native cellulose: structure, characterization and thermal properties. *Materials* **2014**, *7*, 6105−6119.
(204) Chen, X.; Yu, J.; Zhang, Z. B.; Lu, C. H. Study on structure and thermal stability proper- ties of cellulose fibers from rice straw. *Carbohydr. Polym.* **2011**, *85*, 245−250.
(205) Lin, H.; Wang, S.; Zhang, L.; Ru, B.; Zhou, J.; Luo, Z. Structural evolution of chars from biomass components pyrolysis in a xenon lamp radiation reactor. *Chin. J. Chem. Eng.* **2017**, *25* (2), 232−237.
(206) Antal, M. J. Biomass Pyrolysis: A Review of the Literature Part 1—Carbohydrate Pyrolysis. In *Advances in Solar Energy*; Springer: Boston, MA, 1983; pp 61−111.
(207) Mukarakate, C.; Mittal, A.; Ciesielski, P. N.; Budhi, S.; Thompson, L.; Iisa, K.; Nimlos, N. R.; Donohoe, B. S. Influence of crystal allomorph and crystallinity on the products and behavior of cellulose during fast pyrolysis. *ACS Sustainable Chem. Eng.* **2016**, *4*, 4662−4674.
(208) Collard, F.-X.; Bensakhria, A.; Drobek, M.; Volle, G.; Blin, J. Influence of impregnated iron and nickel on the pyrolysis of cellulose. *Biomass Bioenergy* **2015**, *80*, 52−62.
(209) Zhao, S.; Liu, M.; Zhao, L.; Lu, J. Effects of organic and inorganic metal salts on thermogravimetric pyrolysis of biomass components. *Korean J. Chem. Eng.* **2017**, *34* (12), 3077−3084.

https://doi.org/10.1021/acs.energyfuels.0c04046
Energy Fuels 2021, 35, 5407−5478

(210) Wang, K.; Zhang, J.; Shanks, B. H.; Brown, R. C. The deleterious effect of inorganic salts on hydrocarbon yields from catalytic pyrolysis of lignocellulosic biomass and its mitigation. *Appl. Energy* **2015**, *148*, 115−120.
(211) Yu, Y.; Liu, D.; Wu, H. Formation and characteristics of reaction intermediates from the fast pyrolysis of NaCl- and MgCl2-loaded celluloses. *Energy Fuels* **2014**, *28*, 245−253.
(212) Liu, D.; Yu, Y.; Hayashi, J-i.; Moghtaderi, B.; Wu, H. Contribution of dehydration and depolymerization reactions during the fast pyrolysis of various salt-loaded celluloses at low temperatures. *Fuel* **2014**, *136*, 62−68.
(213) Zhu, C.; Maduskar, S.; Paulsen, A. D.; Dauenhauer, P. J. Alkaline-earth-metal-catalyzed thin-film pyrolysis of cellulose. *ChemCatChem* **2016**, *8*, 818−829.
(214) Marathe, P. S.; Oudenhoven, S. R. G.; Heerspink, P. W.; Kersten, S. R. A.; Westerhof, R. J. M. Fast pyrolysis of cellulose in vacuum: The effect of potassium salts on the primary reactions. *Chem. Eng. J.* **2017**, *329*, 187−197.
(215) Fu, X.; Wang, X.; Li, Y.; Xin, Y.; Li, S. Enhancing and upgrading bio-oil during catalytic pyrolysis of cellulose: The synergistic effect of potassium cation and different anions impregnation. *Fuel Process. Technol.* **2019**, *193*, 338−347.
(216) Richardson, Y.; Blin, J.; Volle, G.; Motuzas, J.; Julbe, A. In situ generation of Ni metal nanoparticles as catalyst for H2-rich syngas production from biomass gasification. *Appl. Catal., A* **2010**, *382* (2), 220−230.
(217) Villaescusa, I.; Fiol, N.; Martínez, M.1a; Miralles, N.; Poch, J.; Serarols, J. Removal of copper and nickel ions from aqueous solutions by grape stalks wastes. *Water Res.* **2004**, *38* (4), 992−1002.
(218) Räisänen, U.; Pitkänen, I.; Halttunen, H.; Hurtta, M. Formation of the main degradation compounds from arabinose, xylose, mannose and arabinitol during pyrolysis. *J. Therm. Anal. Calorim.* **2003**, *72* (2), 481−488.
(219) Wang, Y.; Mourant, D.; Hu, X.; Zhang, S.; Lievens, C.; Li, C. Z. Formation of coke during the pyrolysis of bio-oil. *Fuel* **2013**, *108*, 439−444.
(220) Gardiner, D. The pyrolysis of some hexoses and derived di-, tri-, and poly-saccharides. *J. Chem. Soc. C* **1966**, 1473−1476.
(221) Wang, S.; Ru, B.; Dai, G.; Sun, W.; Qiu, K.; Zhou, J. Pyrolysis mechanism study of minimally damaged hemicellulose polymers isolated from agricultural waste straw samples. *Bioresour. Technol.* **2015**, *190*, 211−218.
(222) Wang, S.; Ru, B.; Lin, H.; Sun, W. Pyrolysis behaviors of four O-acetyl-preserved hemicelluloses isolated from hardwoods and softwoods. *Fuel* **2015**, *150*, 243−251.
(223) Lu, Q.; Tian, H. Y.; Hu, B.; Jiang, X. Y.; Dong, C. Q.; Yang, Y. P. Pyrolysis mechanism of holocellulose-based monosaccharides: The formation of hydroxyacetaldehyde. *J. Anal. Appl. Pyrolysis* **2016**, *120*, 15−26.
(224) Huang, J.; He, C.; Pan, G.; Tong, H. A theoretical research on pyrolysis reactions mechanism of coumarone-contained lignin model compound. *Comput. Theor. Chem.* **2016**, *1091*, 92−98.
(225) Zhou, X.; Li, W.; Mabon, R.; Broadbelt, L. J. A mechanistic model of fast pyrolysis of Hemicellulose. *Energy Environ. Sci.* **2018**, *11*, 1240−1260.
(226) Huang, J.; Liu, C.; Tong, H.; Li, W.; Wu, D. Theoretical studies on pyrolysis mechanism of xylopyranose. *Comput. Theor. Chem.* **2012**, *1001*, 44−50.
(227) Sjostrom, E. *Wood Chemistry: Fundamentals and Applications*; Academic Press: San Diego, 1993.
(228) Asmadi, M.; Kawamoto, H.; Saka, S. Characteristics of softwood and hardwood pyrolysis in an ampoule reactor. *J. Anal. Appl. Pyrolysis* **2017**, *124*, 523−535.
(229) DeGroot, W. F. Preliminary investigation of the association of inorganic cations with carboxylic acid groups in wood. *Carbohydr. Res.* **1985**, *142*, 172−176.
(230) Nowakowski, D. J.; Jones, J. M. Uncatalysed and potassium-catalysed pyrolysis of the cell-wall constituents of biomass and their model compounds. *J. Anal. Appl. Pyrolysis* **2008**, *83*, 12−25.
(231) Collard, F.-X.; Blin, J.; Bensakhria, A.; Valette, J. Influence of impregnated metal on the pyrolysis conversion of biomass constituents. *J. Anal. Appl. Pyrolysis* **2012**, *95*, 213−226.
(232) Gargiulo, V.; Giudicianni, P.; Alfè, M.; Ragucci, R. About the influence of doping approach on the alkali metal catalyzed slow pyrolysis of xylan. *J. Chem.* **2019**, *2019*, 9392571.
(233) Rutkowski, P. Pyrolysis of cellulose, xylan and lignin with the K2CO3 and ZnCl2 addition for bio-oil production. *Fuel Process. Technol.* **2011**, *92*, 517−522.
(234) Case, P. A.; Truong, C.; Wheeler, M. C.; DeSisto, W. J. Calcium-catalyzed pyrolysis of lignocellulosic biomass components. *Bioresour. Technol.* **2015**, *192*, 247−252.
(235) Giudicianni, P.; Gargiulo, V.; Alfe, M.; Ragucci, R.; Ferreiro, A. I.; Rabaçal, M.; Costa, M. (2019). Slow pyrolysis of xylan as pentose model compound for hardwood hemicellulose: a study of the catalytic effect of Na ions. *J. Anal. Appl. Pyrolysis* **2019**, *137*, 266−275.
(236) Gargiulo, V.; Giudicianni, P.; Alfe, M.; Ragucci, R.; Ferreiro, A. I.; Rabaçal, M.; Costa, M. Experimental investigation on the effect of K+ ions on the slow pyrolysis of xylan. *Chem. Eng. Trans.* **2018**, *65*, 553−558.
(237) Jarvis, M. W.; Daily, J. W.; Carstensen, H.-H.; Dean, A. M.; Sharma, S.; Dayton, D. C.; Robichaud, D. J.; Nimlos, M. R. Direct detection of products from the pyrolysis of 2-phenethyl phenyl ether. *J. Phys. Chem. A* **2011**, *115*, 428−438.
(238) Elder, T.; Beste, A. Density functional theory study of the concerted pyrolysis mechanism for lignin models. *Energy Fuels* **2014**, *28*, 5229−5235.
(239) Huang, J.; Liu, C.; Wu, D.; Tong, H.; Ren, L. Density functional theory studies on pyrolysis mechanism of b-O-4 type lignin dimer model compound. *J. Anal. Appl. Pyrolysis* **2014**, *109*, 98−108.
(240) Kim, S.; Chmely, S. C.; Nimlos, M. R.; Bomble, Y. J.; Foust, T. D.; Paton, R. S.; Beckham, G. T. Computational study of bond dissociation enthalpies for a large range of native and modified lignins. *J. Phys. Chem. Lett.* **2011**, *2*, 2846−2852.
(241) Wang, M.; Liu, C. Theoretic studies on decomposition mechanism of o-methoxy phenethyl phenyl ether: primary and secondary reactions. *J. Anal. Appl. Pyrolysis* **2016**, *117*, 325−333.
(242) Parthasarathi, R.; Romero, R. A.; Redondo, A.; Gnanakaran, S. Theoretical study of the remarkably diverse linkages in lignin. *J. Phys. Chem. Lett.* **2011**, *2*, 2660−2666.
(243) Choi, Y. S.; Singh, R.; Zhang, J.; Balasubramanian, G.; Sturgeon, M. R.; Katahira, R.; Chupka, G.; Beckham, G. T.; Shanks, B. H. Pyrolysis reaction networks for lignin model compounds: unraveling thermal deconstruction of β-O-4 and α-O-4 compounds. *Green Chem.* **2016**, *18*, 1762−1773.
(244) Liu, C.; Deng, Y.; Wu, S.; Lei, M.; Liang, J. Experimental and theoretical analysis of the pyrolysis mechanism of a dimeric lignin model compound with α-O-4 linkage. *Bioresources* **2016**, *11*, 3626−3636.
(245) Huang, J.; He, C. Pyrolysis mechanism of α-O-4 linkage lignin dimer: a theoretical study. *J. Anal. Appl. Pyrolysis* **2015**, *113*, 655−664.
(246) Jiang, X.-Y.; Lu, Q.; Ye, X.-N.; Hu, B.; Dong, C.-Q. Experimental and theoretical studies on the pyrolysis mechanism of β-1-type lignin dimer model compound. *Bioresources* **2016**, *11*, 6232−6243.
(247) Elder, T. Bond dissociation enthalpies of a dibenzodioxocin lignin model compound. *Energy Fuels* **2013**, *27*, 4785−4790.
(248) Yang, J.; Wang, X.; Shen, B.; Hu, Z.; Xu, L.; Yang, S. Lignin from energy plant (Arundo donax): Pyrolysis kinetics, mechanism and pathway evaluation. *Renewable Energy* **2020**, *161*, 963−971.
(249) Trubetskaya, A.; Lange, H.; Wittgens, B.; Brunsvik, A.; Crestini, C.; Rova, U.; Christakopoulos, P.; Leahy, J. J.; Matsakas, L. Structural and thermal characterization of novel organosolv lignins from wood and herbaceous sources. *Processes* **2020**, *8* (7), 860.
(250) Wang, W.-L.; Ren, X.-Y.; Li, L.-F.; Chang, J.-M.; Cai, L.-P.; Geng, J. Catalytic effect of metal chlorides on analytical pyrolysis of alkali lignin. *Fuel Process. Technol.* **2015**, *134*, 345−351.
(251) Han, T.; Yang, W.; Jönsson, P. G. Pyrolysis and subsequent steam gasification of metal dry impregnated lignin for the production of

https://doi.org/10.1021/acs.energyfuels.0c04046
Energy Fuels 2021, 35, 5407−5478

H2-rich syngas and magnetic activated carbon. *Chem. Eng. J.* **2020**, *394*, 124902.
(252) Kleen, M.; Gellerstedt, G. Influence of inorganic species on the formation of polysaccharide and lignin degradation products in the analytical pyrolysis of pulps. *J. Anal. Appl. Pyrolysis* **1995**, *35*, 15−41.
(253) Sharma, K.; Khaire, K. C.; Thakur, A.; Moholkar, V. S.; Goyal, A. Acacia xylan as a substitute for commercially available xylan and its application in the production of xylooligosaccharides. *ACS Omega* **2020**, *5*, 13729−13738.
(254) Mukkamala, S.; Wheeler, M. C.; van Heiningen, A. R.; DeSisto, W. J. Formate-assisted fast pyrolysis of lignin. *Energy Fuels* **2012**, *26* (2), 1380−1384.
(255) Jakab, E.; Faix, O.; Till, F. Thermal decomposition of milled wood lignins studied by thermogravimetry/mass spectrometry. *J. Anal. Appl. Pyrolysis* **1997**, *40*−*41*, 171−186.
(256) Jiang, X. Y.; Lu, Q.; Hu, B.; Chen, D. Y.; Liu, J.; Dong, C. Q. Influence of inherent alkali metal chlorides on pyrolysis mechanism of a lignin model dimer based on DFT study. *J. Therm. Anal. Calorim.* **2019**, *137* (1), 151−160.
(257) Hwang, H.; Oh, S.; Cho, T.-S.; Choi, I.-G.; Choi, J. W. Fast pyrolysis of potassium impregnated poplar wood and characterization of its influence on the formation as well as properties of pyrolytic products. *Bioresour. Technol.* **2013**, *150*, 359−366.
(258) Kleinert, M.; Barth, T. Towards a lignincellulosic biorefinery: Direct one-step conversion of lignin to hydrogen-enriched biofuel. *Energy Fuels* **2008**, *22* (2), 1371−1379.
(259) Shah, M. H.; Deng, L.; Bennadji, H.; Fisher, E. M. Pyrolysis of potassium-doped wood at the centimeter and submillimeter scales. *Energy Fuels* **2015**, *29* (11), 7350−7357.
(260) Lu, Q.; Zhang, Z-x.; Wang, X.; Guo, H-q.; Cui, M-s.; Yang, Y-p. Catalytic fast pyrolysis of biomass impregnated with potassium phosphate in a hydrogen atmosphere for the production of phenol and activated carbon. *Front. Chem.* **2018**, *6*, 32.
(261) Mahadevan, R.; Adhikari, S.; Shakya, R.; Wang, K.; Dayton, D.; Lehrich, M. S.; Taylor, S. E. Effect of alkali and alkaline earth metals on in-situ catalytic fast pyrolysis of lignocellulosic biomass: a microreactor study. *Energy Fuels* **2016**, *30*, 3045−3056.
(262) Wang, Y.; Wu, H.; Sárossy, Z.; Dong, C.; Glarborg, P. Release and transformation of chlorine and potassium during pyrolysis of KCl doped biomass. *Fuel* **2017**, *197*, 422−432.
(263) Aho, A.; DeMartini, N.; Pranovich, A.; Krogell, J.; Kumar, N.; Eränen, K.; Holmbom, B.; Salmi, T.; Hupa, M.; Murzin, D. Y. Pyrolysis of pine and gasification of pine chars − Influence of organically bound metals. *Bioresour. Technol.* **2013**, *128*, 22−29.
(264) Chen, W.; Li, K.; Chen, Z.; Xia, M. W.; Chen, Y.; Yang, H.; Chen, X.; Chen, H. A new insight into chemical reactions between biomass and alkaline additives during pyrolysis process. *Proc. Combust. Inst.* **2020**, 1−10.
(265) Shen, Y.; Zhang, N.; Zhang, S. Catalytic pyrolysis of biomass with potassium compounds for Coproduction of high-quality biofuels and porous carbons. *Energy* **2020**, *190*, 116431.
(266) Liu, X.; Dong, Y.; Yin, H.; Zhang, G. Catalytic effect of MgCl2 on cotton stalk pyrolysis for chemical production at low temperature. *Can. J. Chem. Eng.* **2015**, *93*, 1343−1348.
(267) Carvalho, W. S.; Cunha, I. F.; Pereira, M. S.; Ataíde, C. H. Thermal decomposition profile and product selectivity of analytical pyrolysis of sweet sorghum bagasse: Effect of addition of inorganic salts. *Ind. Crops Prod.* **2015**, *74*, 372−380.
(268) Shi, L.; Yu, S.; Wang, F.-C.; Wang, J. Pyrolytic characteristics of rice straw and its constituents catalyzed by internal alkali and alkali earth metals. *Fuel* **2012**, *96*, 586−594.
(269) Case, P. A.; Wheeler, M. C.; DeSisto, W. J. Formate assisted pyrolysis of pine sawdust for in-situ oxygen removal and stabilization of bio-oil. *Bioresour. Technol.* **2014**, *173*, 177−184.
(270) Haddad, K.; Jeguirim, M.; Jellali, S.; Guizani, C.; Delmotte, L.; Bennici, S.; Limousy, L. Combined NMR structural characterization and thermogravimetric analyses for the assessment of the AAEM effect during lignocellulosic biomass pyrolysis. *Energy* **2017**, *134*, 10−23.
(271) Link, S.; Arvelakis, S.; Hupa, M.; Yrjas, P.; Külaots, I.; Paist, A. (2010). Reactivity of the biomass chars originating from reed, Douglas fir, and pine. *Energy Fuels* **2010**, *24*, 6533−6539.
(272) Trubetskaya, A. Fast Pyrolysis of Biomass at High Temperatures. Doctoral dissertation, Danmarks Tekniske Universitet, DTU, 2016.
(273) Liu, W. J.; Tian, K.; Jiang, H.; Zhang, X. S.; Ding, H. S.; Yu, H. Q. Selectively improving the bio-oil quality by catalytic fast pyrolysis of heavy-metal-polluted biomass: take copper (Cu) as an example. *Environ. Sci. Technol.* **2012**, *46* (14), 7849−7856.
(274) Al Chami, Z.; Amer, N.; Smets, K.; Yperman, J.; Carleer, R.; Dumontet, S.; Vangronsveld, J. Evaluation of flash and slow pyrolysis applied on heavy metal contaminated Sorghum bicolor shoots resulting from phytoremediation. *Biomass Bioenergy* **2014**, *63*, 268−279.
(275) Jiu, B. B.; Li, B. X.; Yu, Q. J. Effects of Pb on pyrolysis behavior of water hyacinth. *J. Anal. Appl. Pyrolysis* **2015**, *112*, 270−275.
(276) He, J.; Strezov, V.; Kan, T.; Weldekidan, H.; Asumadu-Sarkodie, S.; Kumar, R. Effect of temperature on heavy metal (loid) deportment during pyrolysis of Avicennia marina biomass obtained from phytoremediation. *Bioresour. Technol.* **2019**, *278*, 214−222.
(277) Zakzeski, J.; Bruijnincx, P. C. A.; Jongerius, A. L.; Weckhuysen, B. M. The catalytic valorization of lignin for the production of renewable chemicals. *Chem. Rev.* **2010**, *110*, 3552−3599.
(278) Skutil, K.; Czechowicz, D.; Taniewski, M. Nitrogen-rich natural gases as a potential direct feedstock for some novel methane transformation processes. Part 2: Non-oxidative processes. *Energy Fuels* **2009**, *23*, 4449−4459.
(279) Ramsurn, H.; Gupta, R. B. Production of biocrude from biomass by acidic subcritical water followed by alkaline supercritical water two-step liquefaction. *Energy Fuels* **2012**, *26* (4), 2365−2375.
(280) Okuno, T.; Sonoyama, N.; Hayashi, J-i.; Li, C.-Z.; Sathe, C.; Chiba, T. Primary release of alkali and alkaline earth metallic species during the pyrolysis of pulverized biomass. *Energy Fuels* **2005**, *19* (5), 2164−2171.
(281) Li, S.; Wang, C.; Luo, Z.; Zhu, X. Investigation on the catalytic behavior of alkali metals and alkaline earth metals on the biomass pyrolysis assisted with real-time monitoring. *Energy Fuels* **2020**, *34*, 12654−12664.
(282) Hu, S.; Han, H.; Syed-Hassan, S. S. A.; Zhang, Y.; Wang, Y.; Zhang, L.; He, L.; Su, S.; Jiang, L.; Cheng, J.; Xiang, J. Evolution of heavy components during sewage sludge pyrolysis: A study using an electrospray ionization Fourier transform ion cyclotron resonance mass spectrometry. *Fuel Process. Technol.* **2018**, *175*, 97−103.
(283) Zhang, M.; Li, M.; Wu, H. Ageing of bio-oil and its fractions in presence of surfactants. *Fuel* **2019**, *252*, 403−407.
(284) Xiong, Z.; Guo, J.; Han, H.; Xu, J.; Jiang, L.; Su, S.; Hu, S.; Wang, Y.; Xiang, J. Effects of AAEMs on formation of heavy components in bio-oil during pyrolysis at various temperatures and heating rates. *Fuel Process. Technol.* **2021**, *213*, 106690.
(285) Fahmi, R.; Bridgwater, A. V.; Donnison, I.; Yates, N.; Jones, J. M. The effect of lignin and inorganic species in biomass on pyrolysis oil yields, quality and stability. *Fuel* **2008**, *87*, 1230−1240.
(286) Abanades, S.; Flamant, G.; Gauthier, D. Kinetics of heavy metal vaporization from model wastes in fluidized bed. *Environ. Sci. Technol.* **2002**, *36*, 3879−3884.
(287) Björkman, E.; Strömberg, B. Release of Chlorine from Biomass and Model Compounds at Pyrolysis and Gasification Conditions. *Energy Fuels* **1997**, *11*, 1026−1032.
(288) Knudsen, J. N.; Jensen, P. A.; Dam-Johansen, K. Transformation and release to the gas phase of Cl, K, and S during combustion of annual biomass. *Energy Fuels* **2004**, *18*, 1385−1399.
(289) Jensen, P. A.; Frandsen, F. J.; Dam-Johansen, K.; Sander, B. Experimental investigation of the transformation and release to gas phase of potassium and chlorine during straw pyrolysis. *Energy Fuels* **2000**, *14*, 1280−1285.
(290) Zintl, F.; Strömberg, B., Björkman, E. *Release of Chlorine from Biomass at Gasification Conditions*. Biomass Energy Ind. 10th European Conference and Technology Exhibition, 1998, p 1608.

https://doi.org/10.1021/acs.energyfuels.0c04046
Energy Fuels 2021, 35, 5407−5478

(291) Hamilton, J. T. G.; McRoberts, W. C.; Keppler, F.; Kalin, R. M.; Haper, D. B. Chloride methylation by plant pectin: An efficient environmentally significant process. *Science* **2003**, *301*, 206−209.
(292) Egsgaard, H.; Ahrenfeldt, J.; Henriksen, U. B. On the Significance of Methyl Chloryde in Gasification Processes. *Proc. 18th European Biomass Conference and Exhibition*, 2010, pp 590−592.
(293) Saleh, S. B.; Flensborg, J. P.; Shoulaifar, T. K.; Sárossy, Z.; Hansen, B. B.; Egsgaard, H.; DeMartini, N.; Jensen, P. A.; Glarborg, P.; Dam-Johansen, K. Release of chlorine and sulfur during biomass torrefaction and pyrolysis. *Energy Fuels* **2014**, *28*, 3738−3746.
(294) Johansen, J. M.; Jakobsen, J. G.; Frandsen, F. J.; Glarborg, P. Release of K, Cl, and S during pyrolysis and combustion of high-chlorine biomass. *Energy Fuels* **2011**, *25*, 4961−4971.
(295) Dayton, D. C.; Jenkins, B. M.; Turn, S. Q.; Bakker, R. R.; Williams, R. B.; Belle-Oudry, D.; Hill, L. M. Release of inorganic constituents from leached biomass during thermal conversion. *Energy Fuels* **1999**, *13*, 860−870.
(296) Lang, T.; Jensen, A. D.; Jensen, P. A. Retention of organic elements during solid fuel pyrolysis with emphasis on the peculiar behaviour of nitrogen. *Energy Fuels* **2005**, *19*, 1631−1643.
(297) Van Lith, S. C.; Jensen, P. A.; Frandsen, F. J.; Glarborg, P. Release to the gas phase of inorganic elements during wood combustion. Part 2: influence of fuel composition. *Energy Fuels* **2008**, *22*, 1598−1609.
(298) Hamdan, H.; Muhid, M. N. M.; Endud, S.; Listiorini, E.; Ramli, Z. 29Si MAS NMR, XRD and FESEM studies of rice husk silica for the synthesis of zeolites. *J. Non-Cryst. Solids* **1997**, *211* (1−2), 126−131.
(299) Jing, L.; Yu-Zhao, M.; Zhi-Wei, L.; An-Xian, L. Preparation of transparent glass-ceramics with high crystallinity. *Chinese J. Nonferrous Metals* **2011**, *21*, 1450−6.
(300) Lehmann, J., Joseph, S., Eds.; *Biochar for Environmental Management: Science, Technology and Implementation*; Routledge, 2015.
(301) Tomczyk, A.; Sokołowska, Z.; Boguta, P. Biochar physicochemical properties: pyrolysis temperature and feedstock kind effects. *Rev. Environ. Sci. Bio/Technol.* **2020**, *19* (1), 191−215.
(302) Rodriguez Correa, C.; Hehr, T.; Voglhuber-Slavinsky, A.; Rauscher, Y.; Kruse, A. Pyrolysis vs. hydrothermal carbonization: Understanding the effect of biomass structural components and inorganic compounds on the char properties. *J. Anal. Appl. Pyrolysis* **2019**, *140*, 137−147.
(303) Ren, Q.; Zhao, C.; Wu, X.; Liang, C.; Chen, X.; Shen, J.; Tang, G.; Wang, Z. Effect of mineral matter on the formation of NOx precursors during biomass pyrolysis. *J. Anal. Appl. Pyrolysis* **2009**, *85*, 447−453.
(304) Ronsse, F.; VanHecke, S.; Dickinson, D.; Prins, W. Production and characterization of slow pyrolysis biochar: influence of feedstock type and pyrolysis conditions. *GCB Bioenergy* **2013**, *5*, 104−115.
(305) Ding, W.; Dong, X.; Ime, I. M.; Gao, B.; Ma, L. Q. Pyrolytic temperatures impact lead sorption mechanisms by bagasse biochars. *Chemosphere* **2014**, *105*, 68−74.
(306) Zhao, L.; Cao, X.; Zheng, W.; Wang, Q.; Yang, F. Endogenous minerals have influences on surface electrochemistry and ion exchange properties of biochar. *Chemosphere* **2015**, *136*, 133−139.
(307) Dahou, T.; Defoort, F.; Khiari, B.; Labaki, M.; Dupont, C.; Jeguirim, M. Role of inorganics on the biomass char gasification reactivity: A review involving reaction mechanisms and kinetics models. *Renewable Sustainable Energy Rev.* **2021**, *135*, 110136.
(308) Kirtania, K.; Axelsson, J.; Matsakas, L.; Christakopoulos, P.; Umeki, K.; Furusjö, E. Kinetic study of catalytic gasification of wood char impregnated with different alkali salts. *Energy* **2017**, *118*, 1055−1065.
(309) Dupont, C.; Jacob, S.; Marrakchy, K. O.; Hognon, C.; Grateau, M.; Labalette, F.; Da Silva Perez, D. How inorganic elements of biomass influence char steam gasification kinetics. *Energy* **2016**, *109*, 430−435.
(310) Tromp, P. J. J.; Cordfunke, E. H. P. A thermochemical study of the reactive intermediate in the alkali-catalyzed carbon gasification. I. X-ray diffraction results on the alkali-carbon interaction. *Thermochim. Acta* **1984**, *77*, 49−58.
(311) Gonzalez-Vazquez, M.P.; Garcia, R.; Gil, M.V.; Pevida, C.; Rubiera, F. Unconventional biomass fuels for steam gasification: kinetic analysis and effect of ash composition on reactivity. *Energy* **2018**, *155*, 426−437.
(312) Delannay, F.; Tysoe, W. T.; Heinemann, H.; Somorjai, G. A. The role of KOH in the steam gasification of graphite: identification of the reaction steps. *Carbon* **1984**, *22* (4−5), 401−407.
(313) Strandberg, A.; Holmgren, P.; Wagner, D. R.; Molinder, R.; Wiinikka, H.; Umeki, K.; Broström, M. Effects of pyrolysis conditions and ash formation on gasification rates of biomass char. *Energy Fuels* **2017**, *31*, 6507−6514.
(314) Zolin, A.; Jensen, A.; Jensen, P. A.; Frandsen, F.; Dam-Johansen, K. The influence of inorganic materials on the thermal deactivation of fuel chars. *Energy Fuels* **2001**, *15*, 1110−1122.
(315) Jones, J. M.; Williams, A.; Darvell, L. I.; Nawaz, M.; Baxter, X. The Role of Metals in Biomass Pyrolysis, Char Formation and Char Properties. In *Science in Thermal and Chemical Biomass Conversion*; CPL Press: Victoria, Canada, 2004.
(316) Wu, R.; Beutler, J.; Baxter, L. L. Non-catalytic ash effect on char reactivity. *Appl. Energy* **2020**, *260*, 114358.
(317) Demirbaş, A. Gaseous products from biomass by pyrolysis and gasification: effects of catalyst on hydrogen yield. *Energy Convers. Manage.* **2002**, *43*, 897−909.
(318) Wang, L.; Hustad, J. E.; Skreiberg, Ø.; Skjevrak, G.; Grønli, M. A critical review on additives to reduce ash related operation problems in biomass combustion applications. *Energy Procedia* **2012**, *20*, 20−29.
(319) Yao, X.; Zhao, Z.; Li, J.; Zhang, B.; Zhou, H.; Xu, K. Experimental investigation of physicochemical and slagging characteristics of inorganic constituents in ash residues from gasification of different herbaceous biomass. *Energy* **2020**, *198*, 117367.
(320) Burton, A.; Wu, H. Mechanistic investigation into bed agglomeration during biomass fast pyrolysis in a fluidized-bed reactor. *Energy Fuels* **2012**, *26*, 6979−6987.
(321) Bridgwater, A. V. Upgrading biomass fast pyrolysis liquids. *Environ. Prog. Sustainable Energy* **2012**, *31*, 261−268.
(322) Banks, S. Ash Control Methods to Limit Biomass Inorganic Content and Its Effect on Fast Pyrolysis Bio-Oil Stability. Doctoral dissertation, Aston University, 2014.
(323) Diebold, J. P. *A Review of the Chemical and Physical Mechanisms of the Storage Stability of Fast Pyrolysis Bio-Oils*; NREL/SR-570-27613; National Renewable Energy Laboratory: Golden, CO, 1999.
(324) Oasmaa, A.; Fonts, I.; Pelaez-Samaniego, M. R.; Garcia-Perez, M. E.; Garcia-Perez, M. Pyrolysis oil multiphase behavior and phase stability: a review. *Energy Fuels* **2016**, *30* (8), 6179−6200.
(325) Oasmaa, A.; Peacocke, C.; Gust, S.; Meier, D.; McLellan, R. Norms and standards for pyrolysis liquids. End-user requirements and specifications. *Energy Fuels* **2005**, *19* (5), 2155−2163.
(326) Niu, Y.; Tan, H.; Hui, S. Ash-related issues during biomass combustion: Alkali-induced slagging, silicate melt-induced slagging (ash fusion), agglomeration, corrosion, ash utilization, and related countermeasures. *Prog. Energy Combust. Sci.* **2016**, *52*, 1−61.
(327) Wenglarz, R. A. Deposition, Erosion and Corrosion Protection for Coal-Fired Gas Turbines. In *Turbo Expo: Power for Land, Sea, and Air*, Vol. *79436*; American Society of Mechanical Engineers, September 1985; p V002T03A004.
(328) Hoekstra, E.; Hogendoorn, K. J.; Wang, X.; Westerhof, R. J.; Kersten, S. R.; van Swaaij, W. P.; Groeneveld, M. J. Fast pyrolysis of biomass in a fluidized bed reactor: in situ filtering of the vapors. *Ind. Eng. Chem. Res.* **2009**, *48*, 4744−4756.
(329) Pyreg. https://www.pyreg.de/karbonisierung/?lang=en (accessed September 01, 2020).
(330) Cavaliere, A.; De Joannon, M. Mild combustion. *Prog. Energy Combust. Sci.* **2004**, *30*, 329−366.
(331) Mullen, C. A.; Boateng, A. A. Accumulation of inorganic impurities on HZSM-5 zeolites during catalytic fast pyrolysis of switchgrass. *Ind. Eng. Chem. Res.* **2013**, *52*, 17156−17161.
(332) Paasikallio, V.; Lindfors, C.; Kuoppala, E.; Solantausta, Y.; Oasmaa, A.; Lehto, J.; Lehtonen, J. Product quality and catalyst

https://doi.org/10.1021/acs.energyfuels.0c04046
Energy Fuels 2021, 35, 5407−5478

deactivation in a four day catalytic fast pyrolysis production run. *Green Chem.* **2014**, *16*, 3549−3559.
(333) Stefanidis, S. D.; Kalogiannis, K. G.; Pilavachi, P. A.; Fougret, C. M.; Jordan, E.; Lappas, A. A. Catalyst hydrothermal deactivation and metal contamination during the in situ catalytic pyrolysis of biomass. *Catal. Sci. Technol.* **2016**, *6*, 2807−2819.
(334) Iisa, K.; French, R. J.; Orton, K. A.; Yung, M. M.; Johnson, D. K.; ten Dam, J.; Watson, M. J.; Nimlos, M. R. In situ and ex situ catalytic pyrolysis of pine in a bench-scale fluidized bed reactor system. *Energy Fuels* **2016**, *30*, 2144−2157.
(335) Buss, W.; Graham, M. C.; Shepherd, J. G.; Mašek, O. Suitability of marginal biomass-derived biochars for soil amendment. *Sci. Total Environ.* **2016**, *547*, 314−322.
(336) Grottola, C. M.; Giudicianni, P.; Michel, J. B.; Ragucci, R. Torrefaction of woody waste for use as biofuel. *Energy Fuels* **2018**, *32*, 10266−10271.
(337) Lievens, C.; Yperman, J.; Vangronsveld, J.; Carleer, R. Study of the potential valorisation of heavy metal contaminated biomass via phytoremediation by fast pyrolysis: Part I. Influence of temperature, biomass species and solid heat carrier on the behaviour of heavy metals. *Fuel* **2008**, *87* (10−11), 1894−1905.
(338) Lievens, C.; Carleer, R.; Cornelissen, T.; Yperman, J. Fast pyrolysis of heavy metal contaminated willow: Influence of the plant part. *Fuel* **2009**, *88* (8), 1417−1425.
(339) Stals, M.; Thijssen, E.; Vangronsveld, J.; Carleer, R.; Schreurs, S.; Yperman, J. Flash pyrolysis of heavy metal contaminated biomass from phytoremediation: influence of temperature, entrained flow and wood/leaves blended pyrolysis on the behaviour of heavy metals. *J. Anal. Appl. Pyrolysis* **2010**, *87* (1), 1−7.
(340) Huang, H.; Yao, W.; Li, R.; Ali, A.; Du, J.; Guo, D.; Xiao, R.; Guo, Z.; Zhang, Z.; Awasthi, M. K. Effect of pyrolysis temperature on chemical form, behavior and environmental risk of Zn, Pb and Cd in biochar produced from phytoremediation residue. *Bioresour. Technol.* **2018**, *249*, 487−493.
(341) He, J.; Strezov, V.; Zhou, X.; Kumar, R.; Kan, T. Pyrolysis of heavy metal contaminated biomass pre-treated with ferric salts: product characterisation and heavy metal deportment. *Bioresour. Technol.* **2020**, *313*, 123641.
(342) Li, S.; Zhang, T.; Li, J.; Shi, L.; Zhu, X.; Lü, J.; Li, Y. Stabilization of Pb (II) accumulated in biomass through phosphate-pretreated pyrolysis at low temperatures. *J. Hazard. Mater.* **2017**, *324*, 464−471.
(343) Gonsalvesh, L.; Yperman, J.; Carleer, R.; Mench, M.; Herzig, R.; Vangronsveld, J. Valorisation of heavy metals enriched tobacco biomass through slow pyrolysis and steam activation. *J. Chem. Technol. Biotechnol.* **2016**, *91*, 1585−1595.
(344) Břendová, K.; Tlustoš, P.; Száková, J. Can biochar from contaminated biomass be applied into soil for remediation purposes? *Water, Air, Soil Pollut.* **2015**, *226*, 193.
(345) Wang, X.; Bai, S.; Jin, Q.; Li, S.; Li, Y.; Li, Y.; Tan, H. Soot formation during biomass pyrolysis: Effects of temperature, water-leaching, and gas-phase residence time. *J. Anal. Appl. Pyrolysis* **2018**, *134*, 484−494.
(346) McGrath, T.; Hoffman, J.; Wooten, J.; Hajaligol, M. The effect of inorganics on the formation of PAH during low temperature pyrolysis of cellulose. *Fuel Chemistry Division Preprints* **2002**, *47* (1), 418−419.
(347) McGrath, T. E.; Chan, W. G.; Hajaligol, M. R. Low temperature mechanism for the formation of polycyclic aromatic hydrocarbons from the pyrolysis of cellulose. *J. Anal. Appl. Pyrolysis* **2003**, *66*, 51−70.
(348) Gao, Q.; Budarin, V. L.; Cieplik, M.; Gronnow, M.; Jansson, S. PCDDs, PCDFs and PCNs in products of microwave-assisted pyrolysis of woody biomass−Distribution among solid, liquid and gaseous phases and effects of material composition. *Chemosphere* **2016**, *145*, 193−199.
(349) Hale, S. E.; Lehmann, J.; Rutherford, D.; Zimmerman, A. R.; Bachmann, R. T.; Shitumbanuma, V.; O'Toole, A.; Sundqvist, K. L.; Arp, H. P. H.; Cornelissen, G. Quantifying the total and bioavailable polycyclic aromatic hydrocarbons and dioxins in biochars. *Environ. Sci. Technol.* **2012**, *46*, 2830−2838.
(350) Gudka, B.; Jones, J. M.; Lea-Langton, A. R.; Williams, A.; Saddawi, A. A review of the mitigation of deposition and emission problems during biomass combustion through washing pre-treatment. *J. Energy Inst.* **2016**, *89*, 159−171.
(351) Peral, C. Biomass Pretreatment Strategies (Technologies, Environmental Performance, Economic Considerations, Industrial Implementation). In *Biotransformation of Agricultural Waste and By-Products*; Elsevier, 2016; pp 125−160.
(352) Kuzhiyil, N.; Dalluge, D.; Bai, X.; Kim, K. H.; Brown, R. C. Pyrolytic sugars from cellulosic biomass. *ChemSusChem* **2012**, *5*, 2228−2236.
(353) Dalluge, D. L.; Daugaard, T.; Johnston, P.; Kuzhiyil, N.; Wright, M. M.; Brown, R. C. Continuous production of sugars from pyrolysis of acid-infused lignocellulosic biomass. *Green Chem.* **2014**, *16*, 4144−4155.
(354) Lacey, J. A.; Aston, J. E.; Westover, T. L.; Cherry, R. S.; Thompson, D. N. Removal of introduced inorganic content from chipped forest residues via air classification. *Fuel* **2015**, *160*, 265−273.
(355) Thompson, V. S.; Lacey, J. A.; Hartley, D.; Jindra, M. A.; Aston, J. E.; Thompson, D. N. Application of air classification and formulation to manage feedstock cost, quality and availability for bioenergy. *Fuel* **2016**, *180*, 497−505.
(356) Hu, H.; Westover, T. L.; Cherry, R.; Aston, J. E.; Lacey, J. A.; Thompson, D. N. Process simulation and cost analysis for removing inorganics from wood chips using combined mechanical and chemical preprocessing. *BioEnergy Res.* **2017**, *10*, 237−247.
(357) Thompson, V. S.; Aston, J. E.; Lacey, J. A.; Thompson, D. N. Optimizing biomass feedstock blends with respect to cost, supply, and quality for catalyzed and uncatalyzed fast pyrolysis applications. *BioEnergy Res.* **2017**, *10*, 811−823.
(358) Ray, A. E.; Li, C.; Thompson, V. S.; Daubaras, D. L.; Nagle, N.; Hartley, D. S. *Biomass Blending and Densification: Impacts on Feedstock Supply and Biochemical Conversion Performance*; INL/MIS-16-38547-Revision-1; Idaho National Laboratory: Idaho Falls, ID, 2017.
(359) Edmunds, C. W.; Reyes Molina, E. A.; Andre, N.; Hamilton, C.; Park, S.; Fasina, O.; Adhikari, S.; Kelley, S. S.; Tumuluru, J. S.; Rials, T. G.; Labbe, N. Blended feedstocks for thermochemical conversion: biomass characterization and bio-oil production from switchgrass-pine residues blends. *Front. Energy Res.* **2018**, *6*, 79.
(360) Carpenter, D.; Westover, T.; Howe, D.; Deutch, S.; Starace, A.; Emerson, R.; Hernandez, S.; Santosa, D.; Lukins, C.; Kutnyakov, I. Catalytic hydroprocessing of fast pyrolysis oils: impact of biomass feedstock on process efficiency. *Biomass Bioenergy* **2017**, *96*, 142−151.
(361) Ren, X.; Meng, J.; Chang, J.; Kelley, S. S.; Jameel, H.; Park, S. Effect of blending ratio of loblolly pine wood and bark on the properties of pyrolysis bio-oils. *Fuel Process. Technol.* **2017**, *167*, 43−49.
(362) Casler, M. D.; Boe, A. R. Cultivar× environment interactions in switchgrass. *Crop Sci.* **2003**, *43*, 2226−2233.
(363) Jørgensen, U. Genotypic variation in dry matter accumulation and content of N, K and Cl in Miscanthus in Denmark. *Biomass Bioenergy* **1997**, *12* (3), 155−169.
(364) Lewandowski, I.; Clifton-Brown, J. C.; Andersson, B.; Basch, G.; Christian, D. G.; Jørgensen, U.; Jones, M. B.; Riche, A. B.; Schwarz, K. U.; Tayebi, K.; et al. Environment and harvest time affects the combustion qualities of Miscanthus genotypes. *J. Agron.* **2003**, *95* (5), 1274−1280.
(365) Ferreiro, A. I.; Segurado, R.; Costa, M. Modelling soot formation during biomass gasification. *Renewable Sustainable Energy Rev.* **2020**, *134*, 110380.
(366) Rabaçal, M.; Costa, M.; Vascellari, M.; Hasse, C. Kinetic modelling of sawdust and beech wood pyrolysis in drop tube reactors using advanced predictive models. *Chem. Eng. Trans.* **2014**, *37*, 79−84.
(367) Fletcher, T. H. Review of 30 Years of Research Using the Chemical Percolation Devolatilization Model. *Energy Fuels* **2019**, *33*, 12123−12153.
(368) Li, J.; Singer, S. L. An efficient coal pyrolysis model for detailed tar species vaporization. *Fuel Process. Technol.* **2018**, *171*, 248−257.

https://doi.org/10.1021/acs.energyfuels.0c04046
Energy Fuels 2021, 35, 5407−5478

(369) Grønli, M. G.; Várhegyi, G.; Di Blasi, C. Thermogravimetric Analysis and Devolatilization Kinetics of Wood. *Ind. Eng. Chem. Res.* **2002**, *41*, 4201−4208.
(370) Cai, J.; Wu, W.; Liu, R. An overview of distributed activation energy model and its application in the pyrolysis of lignocellulosic biomass. *Renewable Sustainable Energy Rev.* **2014**, *36*, 236−246.
(371) Ranzi, E.; Debiagi, P. E. A; Frassoldati, A. Mathematical Modeling of Fast Biomass Pyrolysis and Bio-Oil Formation. Note II: Secondary Gas-Phase Reactions and Bio-Oil Formation. *ACS Sustainable Chem. Eng.* **2017**, *5*, 2882−2896.
(372) Ranzi, E.; Debiagi, P. E. A; Frassoldati, A. Mathematical Modeling of Fast Biomass Pyrolysis and Bio-Oil Formation. Note I: Kinetic Mechanism of Biomass Pyrolysis. *ACS Sustainable Chem. Eng.* **2017**, *5*, 2867−2881.
(373) Soria, J.; Zeng, K.; Asensio, D.; Gauthier, D.; Flamant, G.; Mazza, G. Comprehensive CFD modelling of solar fast pyrolysis of beech wood pellets. *Fuel Process. Technol.* **2017**, *158*, 226−237.
(374) Mellin, P.; Kantarelis, E.; Yang, W. Computational fluid dynamics modeling of biomass fast pyrolysis in a fluidized bed reactor, using a comprehensive chemistry scheme. *Fuel* **2014**, *117*, 704−715.
(375) Dussan, K.; Dooley, S.; Monaghan, R. Integrating compositional features in model compounds for a kinetic mechanism of hemicellulose pyrolysis. *Chem. Eng. J.* **2017**, *328*, 943−961.
(376) Bach-Oller, A.; Furusjö, E.; Umeki, K. On the role of potassium as a tar and soot inhibitor in biomass gasification. *Appl. Energy* **2019**, *254*, 113488.
(377) Umeki, K.; Häggström, G.; Bach-Oller, A.; Kirtania, K.; Furusjö, E. Reduction of Tar and Soot Formation from Entrained-Flow Gasification of Woody Biomass by Alkali Impregnation. *Energy Fuels* **2017**, *31*, 5104−5110.
(378) Septien, S.; Valin, S.; Peyrot, M.; Spindler, B.; Salvador, S. Influence of steam on gasification of millimetric wood particles in a drop tube reactor: Experiments and modelling. *Fuel* **2013**, *103*, 1080−1089.
(379) Anca-Couce, A. Reaction mechanisms and multi-scale modelling of lignocellulosic biomass pyrolysis. *Prog. Energy Combust. Sci.* **2016**, *53*, 41−79.
(380) Guerrero, M. R. B.; Marques da Silva Paula, M.; Zaragoza, M. M.; Gutierrez, J. S.; Velderrain, V. G.; Ortiz, A. L.; Collins-Martinez, V. Thermogravimetric study on the pyrolysis kinetics of apple pomace as waste biomass. *Int. J. Hydrogen Energy* **2014**, *39*, 16619−16627.
(381) Bai, F.; Sun, Y.; Liu, Y.; Li, Q.; Guo, M. Thermal and kinetic characteristics of pyrolysis and combustion of three oil shales. *Energy Convers. Manage.* **2015**, *97*, 374−381.
(382) Ferreiro, A. I.; Rabaçal, M.; Costa, M. A combined genetic algorithm and least squares fitting procedure for the estimation of the kinetic parameters of the pyrolysis of agricultural residues. *Energy Convers. Manage.* **2016**, *125*, 290−300.
(383) Chen, D.; Zhang, Z.; Li, Z.; Lv, Z.; Cai, N. Optimizing in-situ char gasification kinetics in reduction zone of pulverized coal air-staged combustion. *Combust. Flame* **2018**, *194*, 52−71.
(384) Dussan, K.; Dooley, S.; Monaghan, R. F. D. A model of the chemical composition and pyrolysis kinetics of lignin. *Proc. Combust. Inst.* **2019**, *37*, 2697−2704.
(385) Jensen, A.; Dam-Johansen, K.; Wójtowicz, M. A.; Serio, M. A. TG-FTIR Study of the Influence of Potassium Chloride on Wheat Straw Pyrolysis. *Energy Fuels* **1998**, *12*, 929−938.
(386) Hao, Q.; Li, B.; Liu, L.; Zhang, Z.-B.; Dou, B.; Wang, C. Effect of potassium on pyrolysis of rice husk and its components. *J. Fuel Chem. Technol.* **2015**, *43*, 34−41.
(387) Ferreiro, A. I.; Costa, M.; Rabaçal, M.; Giudicianni, P.; Gargiulo, V.; Alfè, M.; Ragucci, R. Kinetic Modeling of the Catalytic Effects of Na + and K+ on the Slow Pyrolysis of Hemicellulose. *Proceedings of 9th European Combustion Meeting*, Lisboa, Portugal, 2019.
(388) Leng, E.; Wang, Y.; Gong, X.; Zhang, B.; Zhang, Y.; Xu, M. Effect of KCl and CaCl2 loading on the formation of reaction intermediates during cellulose fast pyrolysis. *Proc. Combust. Inst.* **2017**, *36*, 2263−2270.
(389) Trendewicz, A.; Evans, R.; Dutta, A.; Sykes, R.; Carpenter, D.; Braun, R. Evaluating the effect of potassium on cellulose pyrolysis reaction kinetics. *Biomass Bioenergy* **2015**, *74*, 15−25.
(390) Trubetskaya, A.; Surup, G.; Shapiro, A.; Bates, R. B. Modeling the influence of potassium content and heating rate on biomass pyrolysis. *Appl. Energy* **2017**, *194*, 199−211.
(391) Trubetskaya, A.; Timko, M. T.; Umeki, K. Prediction of fast pyrolysis products yields using lignocellulosic compounds and ash contents. *Appl. Energy* **2020**, *257*, 113897.
(392) Debiagi, P. E. A.; Gentile, G.; Pelucchi, M.; Frassoldati, A.; Cuoci, A.; Faravelli, T.; Ranzi, E. Detailed kinetic mechanism of gas-phase reactions of volatiles released from biomass pyrolysis. *Biomass Bioenergy* **2016**, *93*, 60−71.
(393) Jeong, K.; Jeong, H. J.; Lee, G.; Kim, S. H.; Kim, K. H.; Yoo, C. G. Catalytic Effect of Alkali and Alkaline Earth Metals in Lignin Pyrolysis: A Density Functional Theory Study. *Energy Fuels* **2020**, *34* (8), 9734−9740.
(394) Umeki, K.; Moilanen, A.; Gómez-Barea, A.; Konttinen, J. A model of biomass char gasification describing the change in catalytic activity of ash. *Chem. Eng. J.* **2012**, *207*, 616−624.
(395) Fatehi, H.; Costa, M.; Bai, X. S. Numerical study on K/S/Cl release during devolatilization of pulverized biomass at high temperature. *Proc. Combust. Inst.* **2020**, na DOI: 10.1016/j.proci.2020.06.079.
(396) Keown, D. M.; Favas, G.; Hayashi, J. I.; Li, C. Z. Volatilisation of alkali and alkaline earth metallic species during the pyrolysis of biomass: Differences between sugar cane bagasse and cane trash. *Bioresour. Technol.* **2005**, *96*, 1570−1577.
(397) Zhao, H. B.; Song, Q.; Wu, X. Y.; Yao, Q. Study on the Transformation of Inherent Potassium during the Fast-Pyrolysis Process of Rice Straw. *Energy Fuels* **2015**, *29*, 6404−6411.
(398) Glarborg, P.; Marshall, P. Mechanism and modeling of the formation of gaseous alkali sulfates. *Combust. Flame* **2005**, *141* (1−2), 22−39.
(399) Glarborg, P. Hidden interactions-Trace species governing combustion and emissions. *Proc. Combust. Inst.* **2007**, *31*, 77−98.
(400) Niu, Y.; Tan, H.; Hui, S. Ash-related issues during biomass combustion: Alkali-induced slagging, silicate melt-induced slagging (ash fusion), agglomeration, corrosion, ash utilization, and related countermeasures. *Prog. Energy Combust. Sci.* **2016**, *52*, 1−61.
(401) Van Lith, S. C.; Alonso-Ramírez, V.; Jensen, P. A.; Frandsen, F. J.; Glarborg, P. Release to the gas phase of inorganic elements during wood combustion. Part 1: Development and evaluation of quantification methods. *Energy Fuels* **2006**, *20*, 964−978.

https://doi.org/10.1021/acs.energyfuels.0c04046
Energy Fuels 2021, 35, 5407−5478